FABRICATION AND CHARACTERIZATION OF SHAPE MEMORY POLYMERS AT SMALL-SCALES

A Dissertation
Presented to
The Academic Faculty

by

Edem Wornyo

In Partial Fulfillment
of the Requirements for the Degree
Doctor of Philososphy in the
School of Electrical and Computer Engineering

Georgia Institute of Technology
December 2008

FABRICATION AND CHARACTERIZATION OF SHAPE MEMORY POLYMERS AT SMALL-SCALES

Approved by:

Dr. Ken Gall, Advisor
School of Materials Science and Engineering/Mechanical Engineering
Georgia Institute of Technology

Dr. Levent Degertekin
School of Electrical and Computer Engineering/Mechanical Engineering
Georgia Institute of Technology

Dr. Gary S. May, Advisor
School of Electrical and Computer Engineering
Georgia Institute of Technology

Dr. Oliver Brand
School of Electrical and Computer Engineering
Georgia Institute of Technology

Dr. Dr. Linda Milor
School of Electrical and Computer Engineering
Georgia Institute of Technology

Date Approved: October 31, 2008

To ,

My dear brother, ERIC KAFUI WORNYO (Jun 23 1984–September 22 2007), an energetic and promising final year student of North Georgia College and State University. He passed on in Dahlonega, near Atlanta, Georgia. May his gentle soul rest in the abode of the Lord

Fofo, wo luvɔ ne dzudzɔ le Mawu fe fiadufe me.

,

ACKNOWLEDGEMENTS

I would like to express my heartfelt appreciation to Dr. Ken Gall for accepting me into his group, and Dr. Gary S. May for agreeing to co-advise me despite his many responsibilities as chair of the School of Electrical and Computer Engineering. Both of you have been being great role models for me. My advisors should take same for their support which enabled me to complete this program. I am heavily indebted to them. I again would like to thank my committee members, Dr. Linda Milor, Dr. Degertekin, and Dr. Brand for all their help in the dissertation process.

I am also very grateful to the staff of the Microelectronics Research Center, especially Gary Spinner, Harrington, Eric Woods, Vinny Nguyen, Charlie Suh, William Kimes, and Christina Scelsi for their help at the Microelectronics Research Center (MiRC) cleanroom. I thank my collaborators Dr. William King, Dr. Fuzheng Yang and Dr. Ravi Doraiswami. I also would like to thank Mr. David Cowan and Dr. Michael Best for providing the platform for me to use my skills in areas such as health delivery and international development.

This work will not have been completed without the support of my group members in the Advanced Materials Laboratory of the School of Materials Science and Engineering and the Intelligent Semiconductor Manufacturing Group of the School of Electrical and Computer Engineering. For this, I say thanks.

My appreciation further goes to the National Science Foundation (NSF) and the Steve Chaddick Chair in Electrical and Computer Engineering for sponsoring this work.

I also thank all staff of the School of Electrical and Computer Engineering, all staff of the School of Material Science and Engineering. I render my sincere thanks to the many supporters and teachers over the years, and people who have encouraged me throughout this long journey. Indeed, I met many people who have influenced my life positively in many ways.

My parents Torgbui Butuvor II and Mrs. Georgina Attopley-Wornyo for their encouragement and support. I would but say I am forever grateful. I thank my uncle Mr. Godwin Yao Dogbey for his mentoring over the years. I also want to thank my wife Sena. My siblings Priscilla Yayra Ekui Wornyo and Dela Wornyo should accept my gratitude for their moral support. I cannot leave you out, little ones Eyram Ekui Wornyo and Kafui Amey Wornyo for your infectious and encouraging smiles.

Above all, I give praise and honor to the Almighty Maker of Heaven and Earth, the Author and Finisher for his guidance, protection, knowledge and encouragement from time immemorial. Without His Grace, nothing is possible. It is Him who has made this journey possible. He Has delivered me–the meaning of my name Edem.

TABLE OF CONTENTS

LIST OF TABLES

LIST OF FIGURES

LIST OF SYMBOLS OR ABBREVIATIONS

100tBA	100% of tBA.
AFM	atomic force microscopy.
BCB	benzocyclobutene.
BPA	bisphenol A dimethacrylate.
DEGDMA	diethylene glycol dimethacrylate.
DMA	dynamic mechanical analysis.
DSC	differential scanning calorimetry.
GAs	genetic algorithms.
H	hardness.
h	depth or displacement.
i	indenter.
m	material.
MLP	multilayer perceptron.
P	Force.
PC	polycarbonate.
S	stiffness.
SMA	shape memory alloy.
SMM	shape memory material.
tBA	*tert*-butyl acrylate.
wt%	weight percent.

SUMMARY

The objective of this research is to thoroughly investigate the shape memory effect in polymers, characterize, and optimize these polymers for applications in information storage systems. Previous research effort in this field concentrated on shape memory metals for biomedical applications such as stents. Minimal work has been done on shape memory polymers; and the available work on shape memory polymers has not characterized the behaviors of this category of polymers fully. Copolymer shape memory materials based on diethylene glycol dimethacrylate (DEGDMA) crosslinker, and *tert* butyl acrylate (tBA) monomer are designed. The design encompasses a careful control of the backbone chemistry of the materials. Characterization methods such as dynamic mechanical analysis (DMA), differential scanning calorimetry (DSC); and novel nanoscale techniques such as atomic force microscopy (AFM), and nanoindentation are applied to this system of materials. Designed experiments are conducted on the materials to optimize spin coating conditions for thin films. Furthermore, the recovery, a key for the use of these polymeric materials for information storage, is examined in detail with respect to temperature. In sum, the overarching objectives of the proposed research are to: (i) Design shape memory polymers based on polyethylene glycol dimethacrylate (PEGDMA) and diethylene glycol dimethacrylate (DEGDMA) crosslinkers, 2-hydroxyethyl methacrylate (HEMA) and *tert*-butyl acrylate monomer (tBA). (ii) Utilize dynamic mechanical analysis (DMA) to comprehend the thermomechanical properties of shape memory polymers based on DEGDMA and tBA. (iii) Utilize nanoindentation and atomic force microscopy (AFM) to understand the nanoscale behavior of these SMPs, and explore the strain storage and recovery of the polymers from a deformed state. (iv) Study spin coating conditions on thin film quality with designed experiments. (iv) Apply neural networks and genetic algorithms to optimize these systems.

CHAPTER I

RESEARCH OBJECTIVES

The confluence of the micro-/nano-electronics and biomedical industries is driving various material innovations, particularly in miniaturized polymers [2, 31]. Due to the ease of processing and cheaper cost of polymers compared to their metallic counterparts, they have become central to the microelectronics industry [14], as these materials are finding applications in sensors [32], lithography [4], and biomedical devices [19, 21, 23]. This onus on polymers requires that the materials possess different properties in order to reduce the cost of production, decrease the scale of devices, and offer devices with new functional properties. Many researchers have worked on modifying existing polymers by the addition or removal of tailored functional groups to make the polymers "smart" hence enhancing the utility of the materials [12, 17, 22]. Recently, the Semiconductor Industry Association (SIA) developed a framework for the continued maintenance of the semiconductor industry's progress through Moore's Law. Since the proclamation of Moore's Law, which states that the number of devices on a chip doubles every 18 months, microelectronics has grown exponentially up to now.

According to the SIA's National Technology Roadmap for Semiconductors, nanotechnology will require devices of dimensions on the order of 50 nm by the year 2012. This requirement calls for the development of new resist technologies to keep up with miniaturization, and maintain Moore's Law. Moreover, devices on a miniaturized scale may not have the same behavior as devices on the microscale/macroscale. As a result, novel nanoscale techniques such as nanoindentation and atomic force microscopy are indispensable for understanding behavior of materials at these scales.

Since the invention of the first shape memory material, Nickel-Titanium about half a century ago [15], shape memory materials have elicited enormous interest, and have already grown into a multi-billion dollar industry [3, 5, 6, 11].

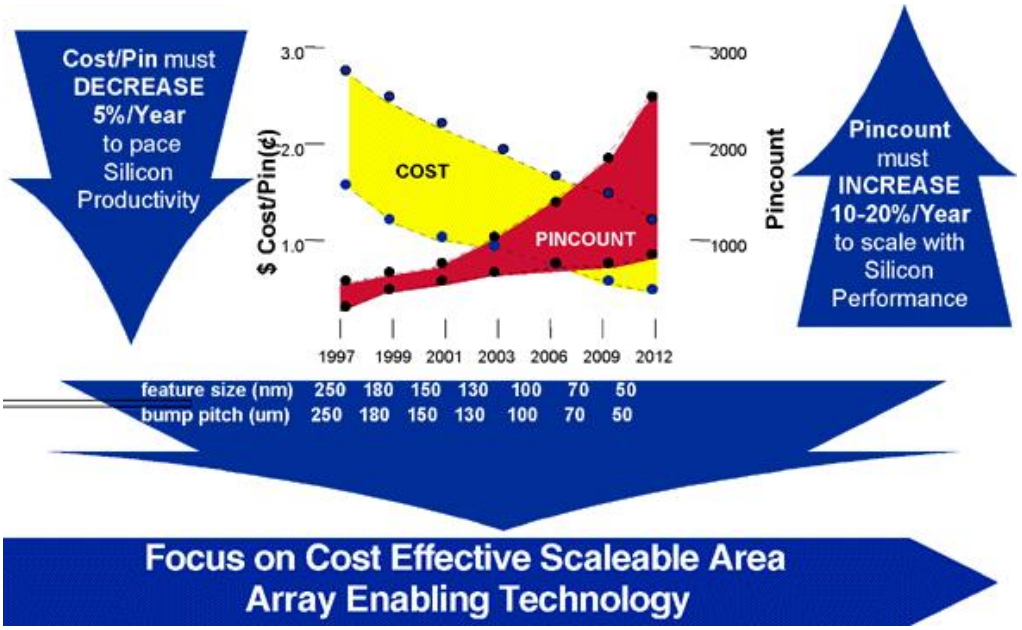

Figure 1.1: SIA's International Technology Roadmap for Semiconductors (ITRS) [13]

Storage of information has seen a drastic transformation within the past half century. The advent of new information storage integration technologies has led to the reduction of information storage media. For example, $100\mu m^2$ space suffices for storing a printed page. A small magnetic disk suffices for storing books in an entire library. Advent of novel technologies in semiconductors, tribology, and giant magnetoresistance has led to these possibilities in storage. It is also known that magnetic storage has a limit [38] [30].

At very small scales, the particle size of magnetic domains decreases. Temperature fluctuations lead to a reduction in signal strength at these small scales. The phenomenon further leads to randomization of the magnetic domains. This leads to data erasure. This effect is known as the superparamagnetic limit. In magnetic media, the maximum storage density is $100Gbitin.^2$.

Researchers have developed other technologies such as optical holography, higher coercivity materials, and isolation of individual magnetic nanodomains, among others, to solve this superparamagnetic problem. As a result of these difficulties, the Millipede project, developed by researchers at IBM has shown a lot of promise. The approach was based on indentation of polymers at small scales using the atomic force microscope (AFM). Vettiger

and coworkers have shown that a unit area of polymer can hold more information compared to the same unit area of magnetic and holographic media. This finding has spurred a lot of interest in investigating the use of polymers for information storage [38]. However, the polymer used by these researchers was polymethyl methacrylate (PMMA). The continuous writing, reading, and erasing of information from the PMMA led to a breakdown of polymer. This breakdown resulted in ineligible data after many cycles. Here, we introduce a new class of polymers–shape memory polymers- capable of withstanding many cycles of writing, reading, and erasing.

Shape memory polymers are a class of elastomer-like polymers that possess the ability to recover their original shape from a deformed shape, upon the application of an external stimulus such as light, magnetic field, and heat [20, 24]. The deformation could be molding, indentation, twisting, among others.

The objective of the research is to explore the nanoscale characteristics of shape memory polymers. We consider factors such as the effect of crosslink density on the nanoindentation behavior of polymer networks exhibiting shape memory. We determine baseline polymer properties using bulk dynamic mechanical analysis and tensile testing. Small-scale deformation and recovery properties in the polymers are explored using nanoindentation and atomic force microscopy. Besides material investigations, statistically designed experiments are utilized to optimize various experimental variables. Neural networks have been shown to possess better accuracy and predictive capabilities compared to their empirical counterparts. Research has also confirmed that a small number of experimental points suffice for generalization in training neural networks. Although extensive research has been performed in the past two decades on shape memory polymers in general, just a few researchers examined shape memory polymers based on DEGDMA and tBA. Earlier work by researchers focused on shape memory polyurethane. Most of these researchers investigated the shape fixity, recoverability, and creep [35–37]. None of the previous work exploited the influence of a gradual increase of crosslinking on the thermomechanical properties of shape memory polymers. Our approach fills in the aforementioned gaps and critically examines the behavior of these polymers at minuscule scales. Probing the characteristics of materials at these scales

is necessary to understand the deformation of materials; and knowledge of failure mechanisms increases reliability and decreases failures at these scales. Furthermore, the literature contains little information on optimization of processing conditions of thin films of these copolymers. The literature also has limited work on optimization and modeling of polymers using neural networks and genetic algorithms [10, 27] [9] [1] [16, 18, 25, 26, 28, 29, 33, 34, 39] [16, 18, 25, 26, 28, 29, 33, 34, 39] [38]. In light of this, we investigate the influence of various processing parameters on the mechanical properties of these polymers. This work provides a framework for the utility of the polymers on the nanoscale to satisfy the growing demands of nanotechnology.

In summary, the objectives of this research are to:

1. Design of shape memory polymers based on diethylene glycol dimethacrylate (DEGDMA) crosslinker, and *tert*-butyl acrylate monomer (tBA).

2. Utilize dynamic mechanical analysis (DMA) to comprehend the thermomechanical properties of shape memory polymers based on DEGDMA and tBA.

3. Utilize nanoindentation to understand the nanoscale behavior of these SMPs, and explore the recovery of the polymers from a deformed state.

4. Study spin coating conditions on thin film quality with designed experiments.

5. Model and optimize spin coating conditions of these thin films using neural networks and genetic algorithms.

We selected DEGDMA and tBA, as these acrylates have been photopolymerized, and explored for applications in bioengineering [7]. In addition, since the basic characteristics of these materials are not well understood especially at the nanoscale we expect that the exploration of this research will form a framework for the utility of these polymers for nanotechnology applications in microelectronics, aerospace and defense, and biomedical engineering. A few research labs have started using these materials for applications such as nanoimprint lithography [8], and as sutures in biomedical applications. We expect that our work will form the basis for future work on incorporating these materials into devices.

The core of this research is on the application of shape memory polymers as information storage media. Prior work by researchers at IBM (Millipede project) investigated the use of polymers for information storage. The results of the study indicated a great promise for the use of polymers as potential candidates to replace or supplement the status quo, the magnetic storage devices currently available. The research showed that a unit area of a polymer can store more information compared to either a magnetic or a optical media. However, volatility of data, ease of writing, and other factors remain a challenge in the use of polymers for storage applications. Our aim is to investigate various shape memory materials to resolve some of the issues mentioned above to make polymers attractive as potential candidates for storage applications. In addition, the current research also utilizes designed experiments, neural networks, and genetic algorithms for optimizing processing conditions for these acrylates. The use of neural networks rather than empirical statistical modeling techniques is due to the limited accuracy of statistical models. Notwithstanding the simplicity of statistical techniques, neural networks are intrinsically capable of modeling non-linear and complex processes with better accuracy. It has also been proved that neural networks provide better prediction error and model generalization. Neural networks also provide superior model generalization taking into account manufacturing variations and parameter indeterminacy. We examine the dependence of nanomechanical properties such as hardness and modulus on processing conditions. These investigations are critical for the use of these materials at the nanoscale for applications in nanotechnology.

1.1 Outline of Thesis

The manuscript is organized as follows: the origin and history of the problem is expounded in Chapter II, with explanations of shape memory polymers, and characterization methods used in this research and general outline of the problem. Chapter III discusses characterization techniques used in this research. Chapter IV addresses nanoindentation of shape memory polymer networks while Chapter V covers nanoscale indent formation and recovery of shape memory polymer networks. Designed experiments and neural network analysis is performed in Chapter VI, while neural network modeling is carried out in Chapter VII. Conclusions

and future work are discussed in Chapter VIII.

REFERENCES

[1] Akita, S., Nakayama, Y., Mizooka, S., Takano, Y., Okawa, T., Miyatake, Y., Yamanaka, S., Tsuji, M., and Nosaka, T., "Nanotweezers consisting of carbon nanotubes operating in an atomic force microscope," *Applied Physics Letters*, vol. 79, pp. 1691–1691, 2001.

[2] Armstrong, W. D. and Lilholt, H., "The time dependant, super-viscoelastic behavior of niti shape memory alloy fiber reinforced polymer matrix composites," *Materials Science and Engineering B-Solid State Materials for Advanced Technology*, vol. 68, no. 3, pp. 149–155, 2000. The time dependant, super-viscoelastic behavior of NiTi shape memory alloy fiber reinforced polymer matrix composites.

[3] Ballandras, S., Calin, M., Zissi, S., Bertsch, A., Andre, J. C., Bourjault, A., and Hauden, D., "Miniaturized shape memory alloy actuators fabricated using microstereophotolithography," *Journal De Physique Iii*, vol. 6, no. 12, pp. 1759–1774, 1996. Miniaturized shape memory alloy actuators fabricated using microstereophotolithography.

[4] Beake, B. D., Chen, S., Hull, J. B., and Gao, F., "Nanoindentation behavior of clay/poly(ethylene oxide) nanocomposites," *Journal of Nanoscience and Nanotechnology*, vol. 2, no. 1, pp. 73–79, 2002. article.

[5] Bidaux, J. E., Bataillard, L., Manson, J. A., and Gotthardt, R., "Phase-transformation behavior of thin shape-memory alloy wires embedded in a polymer matrix composite," *Journal De Physique Iv*, vol. 3, no. C7, pp. 561–564, 1993. article Part 1.

[6] Bidaux, J. E., Yu, W. J., Gotthardt, R., and Manson, A. E., "Modeling of the martensitic-transformation in shape-memory alloy composites," *Journal De Physique*

Iv, vol. 5, no. C2, pp. 543–548, 1995. article.

[7] Bowman, C. N., Carver, A. L., Kennett, S. N., Williams, M. M., and Peppas, N. A., "Polymers for information storage systems. iii. crosslinked structure of polydimethacrylates," *Polymer*, vol. 31, no. 1, pp. 135–9, 1990. article.

[8] Chou, S. Y., Krauss, P. R., and Renstrom, P. J., "Imprint of sub-25 nm vias and trenches in polymers," *Applied Physics Letters*, vol. 67, no. 21, pp. 3114–3116, 1995. article.

[9] Cleon, D. E. and May, G. S., "Neural network control of variable-frequency microwave processing of polymer dielectric curing," *IEEE Transactions on Electronic Packaging Manufacturing*, pp. 1521 – 334X, 2008. article.

[10] Davis, C., Harry, J., Cupta, M., Joseph, P., Kohl, P., and May, G., "Neural network modeling of acid-catalyzed degradation of photosensitive polycarbonates," *Proceedings of the International Symposium and Exhibition on Advanced Packaging Materials Processes, Properties and Interfaces*, vol. 2007, pp. 115 –, 2007. article.

[11] F. El Feninat, G. L. M. F. D. M., "Shape memory materials for biomedical applications," *Advanced Engineering Materials*, vol. 4, no. 3, pp. 91–104, 2002. article 10.1002/1527-2648(200203)4:3<91::AID-ADEM91>3.0.CO;2-B.

[12] Feng, W., Brash, J. L., and Zhu, S., "Non-biofouling materials prepared by atom transfer radical polymerization grafting of 2-methacryloloxyethyl phosphorylcholine: Separate effects of graft density and chain length on protein repulsion," *Biomaterials*, vol. 27, no. 6, pp. 847–855, 2006. article.

[13] Frear, D., "Materials issues in area-array microelectronic packaging," *JOM Journal of the Minerals, Metals and Materials Society*, vol. 51, no. 3, pp. 22–27, 1999.

[14] Gall, K., Kreiner, P., Turner, D., and Hulse, M., "Shape-memory polymers for microelectromechanical systems," *Journal of Microelectromechanical Systems*, vol. 13, no. 3, pp. 472–483, 2004. article.

[15] Ham-Su, R., Healey, J., Underhill, R., Farrell, S., Cheng, L., Hyatt, C., Rogge, R., and Gharghouri, M., "Fabrication of magnetic shape memory alloy/polymer composites," *Proceedings of SPIE*, vol. 5761, p. 490, 2005.

[16] HAN, S., CAI, L., ROHATGI, A., and MAY, G., "Optimizing the growth of pecvd silicon nitride films for solar cell applications using neural networks and genetic algorithms," *Intelligent Engineering Systems Through Artificial Neural Networks: Proceedings of the 1997 Artificial Neural Networks in Engineering Conference (Annie'97)*, 1996.

[17] Kallrot, M., Edlund, U., and Albertsson, A. C., "Surface functionalization of degradable polymers by covalent grafting," *Biomaterials*, vol. 27, no. 9, pp. 1788–1796, 2006. article 05509548592 Compilation and indexing terms, Copyright 2005 Elsevier Engineering Information, Inc. 0142-9612 Covalent Solvent free Vapor-phase grafting.

[18] Kim, T. S. and May, G. S., "Intelligent control of via formation by photosensitive bcb formcm-l/d applications," *Semiconductor Manufacturing, IEEE Transactions on*, vol. 12, no. 4, pp. 503–515, 1999.

[19] Larraz, E., Elvira, C., and San Roman, J., "Design and properties of novel self-curing acrylic formulations for application in intervertebral disks restoration," *Biomacromolecules*, vol. 6, no. 4, pp. 2058 – 2066, 2005. article.

[20] Lendlein, A., Jiang, H. Y., Junger, O., and Langer, R., "Light-induced shape-memory polymers," *Nature*, vol. 434, no. 7035, pp. 879–882, 2005. article.

[21] Lendlein, A. and Kelch, S., "Degradable, multifunctional polymeric biomaterials with shape-memory," 2005.

[22] Lu, D., Liu, Z., Zhang, M., Wang, X., and Liu, Z., "Dextran-grafted-pnipaam as an artificial chaperone for protein refolding," *Biochemical Engineering Journal*, vol. 27, no. 3, pp. 336–343, 2006. article 05459460055 Compilation and indexing terms, Copyright 2005 Elsevier Engineering Information, Inc. 1369-703X Grafting ratio Cerium nitrate Protein aggregation.

[23] Mallikarjuna, N. N. and Aminabhavi, T. M., "Versatile conjugated polymer actuators in biomedical applications," *Polymer News*, vol. 30, no. 6, pp. 195 – 196, 2005. article Electrical energy;Dielectric elastomers;Biomedical actuators;Nitinol;.

[24] Mohr, R., Kratz, K., Weigel, T., Lucka-Gabor, M., Moneke, M., and Lendlein, A., "Initiation of shape-memory effect by inductive heating of magnetic nanoparticles in thermoplastic polymers," *PNAS*, vol. 103, no. 10, pp. 3540–3545, 2006. article.

[25] Pratap, R. J., Lee, J. H., Pinel, S., May, G. S., Laskar, J., and Tentzeris, E. M., "Millimeter wave rf front end design using neuro-genetic algorithms," *Electronic Components and Technology, 2005. ECTC'05. Proceedings*, pp. 1802–1806.

[26] Pratap, R. J., Staiculescu, D., Pinel, S., Laskar, J., and May, G. S., "Modeling and sensitivity analysis of circuit parameters for flip-chip interconnects using neural networks," *IEEE Transactions on Advanced Packaging*, vol. 28, no. 1, pp. 71–78, 2005. article.

[27] Pratap, R. J., Sen, P., Davis, C. E., Mukhophdhyay, R., May, G. S., and Laskar, J., "Neurogenetic design centering," *IEEE Transactions on Semiconductor Manufacturing*, vol. 19, no. 2, pp. 173 – 181, 2006. article.

[28] Setia, R. and May, G. S., "Run-to-run failure detection and diagnosis using neural networks and dempster-shafer theory: an application to excimer laser ablation," *IEEE Transactions on Electronics Packaging Manufacturing*, vol. 29, no. 1, pp. 42–9, 2006. article.

[29] Setia, R. and May, G. S., "Run-to-run failure detection and diagnosis using neural networks and dempster??Dgshafer theory: An application to excimer laser ablation," *Electronics Packaging Manufacturing, IEEE Transactions on [see also Components, Packaging and Manufacturing Technology, Part C: Manufacturing, IEEE Transactions on]*, vol. 29, no. 1, pp. 42–49, 2006.

[30] Shaw, G., Trethewey, J., Johnson, A., Drugan, W., and Crone, W., "Thermomechanical high-density data storage in a metallic material via the shape-memory effect," *Advanced Materials*, vol. 17, no. 9, pp. 1123–1127, 2005.

[31] Shmulewitz, A., Langer, R., and Patton, J., "Convergence in biomedical technology," *Nature Biotechnology*, vol. 24, no. 3, pp. 277–280, 2006. article.

[32] Small, W. I., Metzger, M. F., Wilson, T. S., and Maitland, D. J., "Laser-activated shape memory polymer microactuator for thrombus removal following ischemic stroke: preliminary in vitro analysis," *Selected Topics in Quantum Electronics, IEEE Journal of*, vol. 11, no. 4, pp. 892–901, 2005. article 1077-260X.

[33] Tae Seon, K. and May, G. S., "Optimization of via formation in photosensitive dielectric layers using neural networks and genetic algorithms," *IEEE Transactions on Electronics Packaging Manufacturing*, vol. 22, no. 2, pp. 128–36, 1999. article.

[34] Thongvigitmanee, T. and May, G. S., "Modeling and optimization of integral capacitor fabrication usingneural networks," *Electronics Manufacturing Technology Symposium, 2000. Twenty-Sixth IEEE/CPMT International*, pp. 47–54, 2000.

[35] Tobushi, H., Hashimoto, T., Ito, N., Hayashi, S., and Yamada, E., "Shape fixity and shape recovery in a film of shape memory polymer of polyurethane series," *Journal of Intelligent Material Systems and Structures*, vol. 9, no. 2, pp. 127–136, 1998. article.

[36] Tobushi, H., Ito, N., Takata, K., and Hayashi, S., "Thermomechanical constitutive modeling of polyurethane-series shape memory polymer," 2000.

[37] Tobushi, H., Shimada, D., Hayashi, S., and Endo, M., "Shape fixity and shape recovery of polyurethane shape-memory polymer foams," *Proceedings of the Institution of Mechanical Engineers Part L-Journal of Materials-Design and Applications*, vol. 217, no. L2, pp. 135–143, 2003. article.

[38] Vettiger, P., Cross, G., Despont, M., Drechsler, U., Durig, U., Gotsmann, B., Haberle, W., Lantz, M. A., Rothuizen, H. E., Stutz, R., and Binnig,

G. K., "The "millipede" - nanotechnology entering data storage," *IEEE Transactions on Nanotechnology*, vol. 1, no. 1, pp. 39–55, 2002. article.

[39] YUN, I. and MAY, G. S., "Passive circuit model parameter extraction using genetic algorithms," *Electronic Components and Technology Conference, 1999. 1999 Proceedings. 49th*, pp. 1021–1024, 1999.

CHAPTER II

ORIGIN AND HISTORY OF THE PROBLEM

In this chapter, the underlying principle of polymers is discussed. Further, the shape memory principle and a few previous shape memory material systems are discussed. The principle behind the first types of shape memory materials—shape memory metallic alloys is presented. In addition, information storage in various media is discussed.

2.1 Polymer

Polymers are large molecules made of smaller units. The large molecule is called a macromolecule. The name polymer emanates from Greek: "poly" means many, "mer" means part. Thus, a monomer is the fundamental building block of a polymer. A polymer may consist of two parts, in which case the molecule is a dimer. A polymer that has a few molecules is called an oligomer. Polymers occur in nature. Natural rubber is a polymer that has been used extensively for many products, such as tires through the process of vulcanization, rubber bands, among others. Other naturally occurring polymers include the deoxyribonucleic acid (DNA)—the purveyor of genetic information. The process of converting a monomer into a polymer is termed polymerization.

Figure 2.1 shows a cross-linked network of polymers in which there are bonds between polymer molecules. As the degree of crosslinking increases in a polymer, the polymer chains are hindered from flowing and this leads to thermoset behavior. Figure 2.2 illustrates a type of polymer called thermoplastic. These are linear or branched chains of polymers that have the ability to flow when heated.

2.2 Time-Temperature Effects

A polymer may be represented by a time-temperature superposition in which modulus is plotted against time shift, (t/a), where a is the horizontal shift on a logarithmic scale [20, 32].

The Deborah number, De, is a parameter which defines the viscoelastic behavior of a

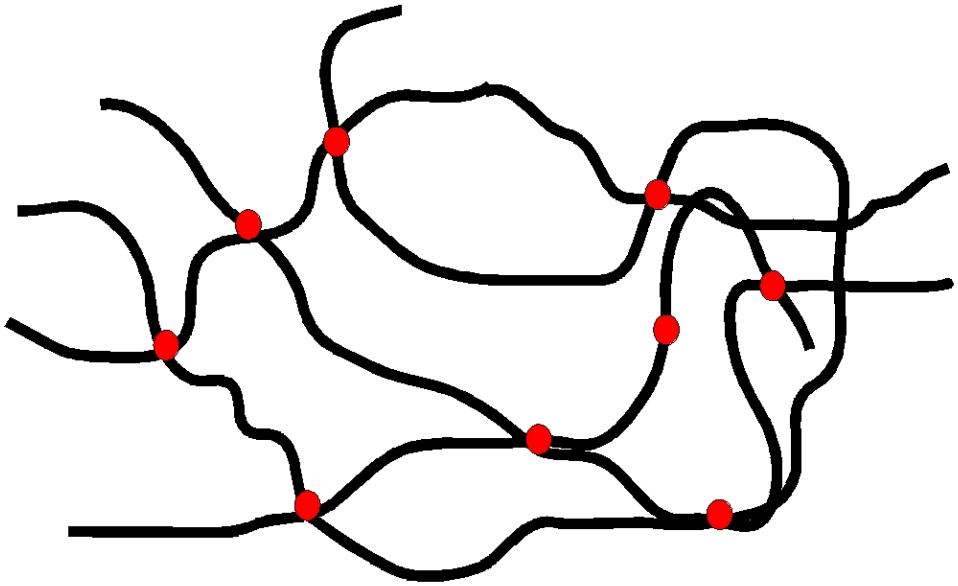

1

Figure 2.1: Crosslinked network.

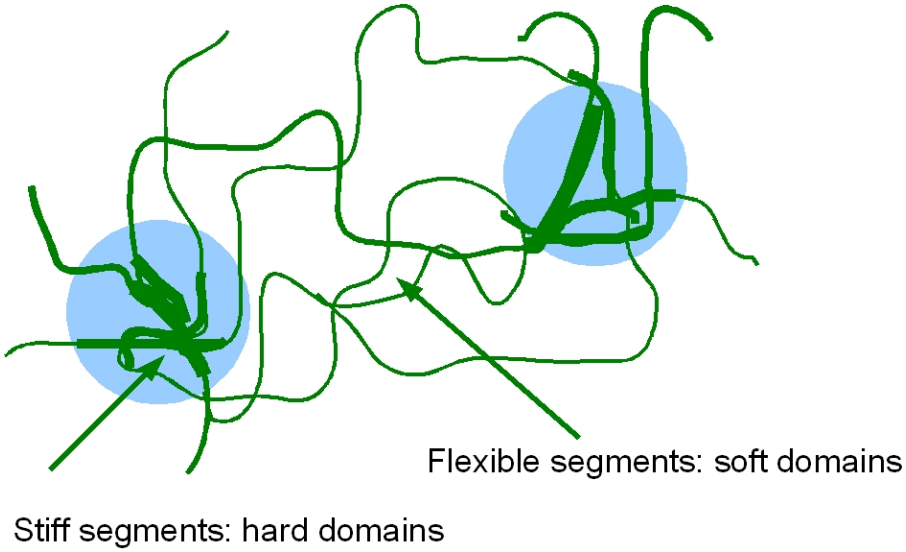

2

Figure 2.2: A schematic of a thermoplastic network

material. It is expressed by the dimensional quantity

$$De = \frac{\lambda}{t} \tag{2.1}$$

where λ is the relaxation time of the material.

The name, Deborah number, was first used by Marcus Reiner. Reiner derived the name from the Bible scripture, "The mountains melted from before the LORD, even that Sinai from before the LORD God of Israel" (Judges 5:5, KJV). Thus, even a mountain will flow if one waits for a long time. In polymers, a polymeric material with a high molecular weight will have a high Deborah number. However, after a long period of time its De will vanish and the material will begin to flow.

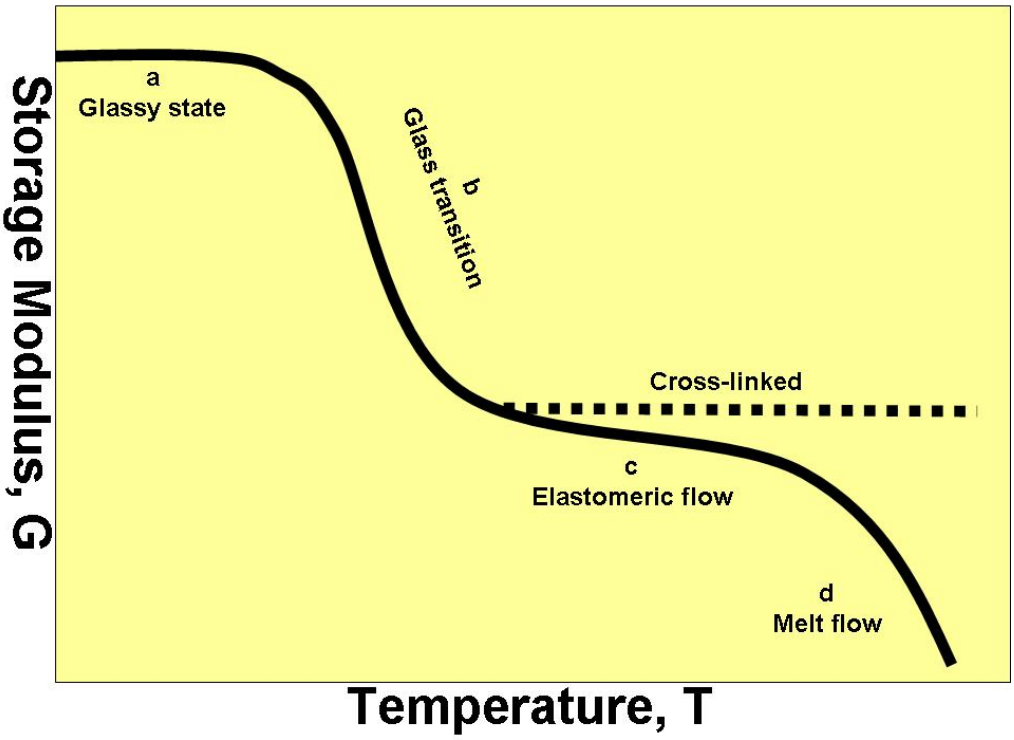

Figure 2.3: Typical thermomechanical curve of a polymer. For a cross-linked polymer, the three regions of interest are the glassy regime, transition regime, and the rubbery regime. The glass transition temperature is defined as the temperature at the midpoint of the transition region or the temperature at the peak of the tan delta (the ratio of the loss- to the storage-modulus) curve.

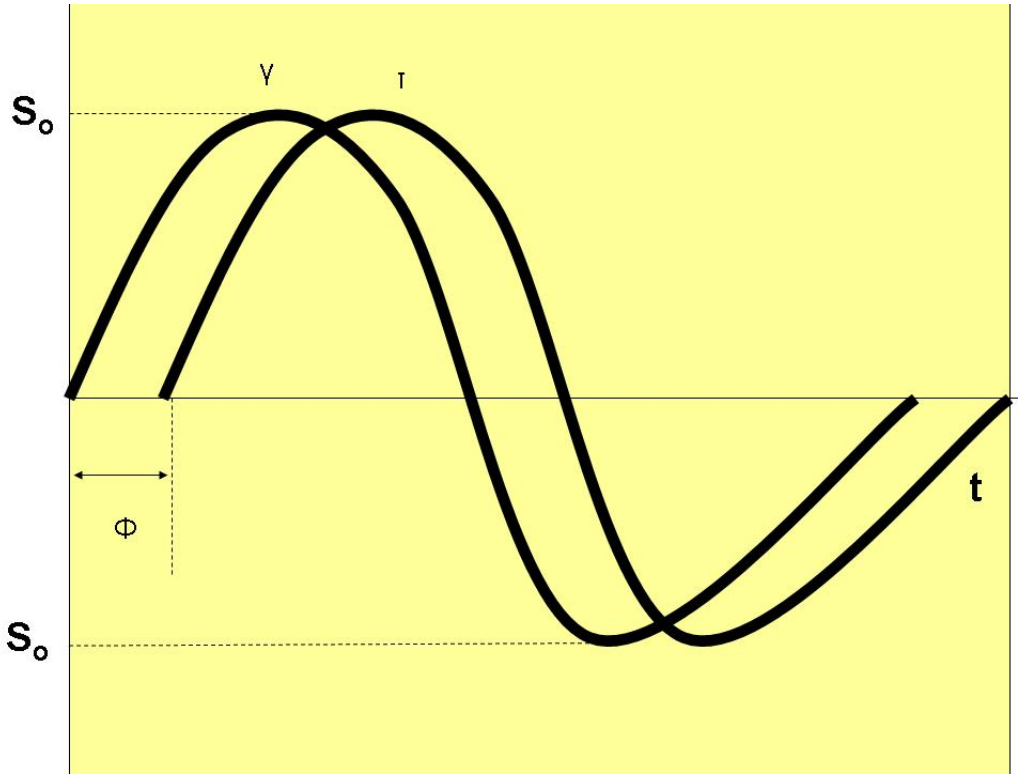

Figure 2.4: Stress-strain relationship for a material

2.2.1 Oscilatory (Periodic) Stresses

If a material is subjected to periodic oscillatory stresses at a frequency λ as shown in Figure 2.4, dynamic properties of the material can be derived. There is a direct transformation between frequency and time, so the properties of the material can be estimated across a large time range. Assuming that a sinusoidal signal

$$S^* = S_o sin(\omega t) \tag{2.2}$$

is applied to a material, where S^* is dynamic stress, and t is time.

The resulting periodic strain, γ^*, with an angle shift of $0^o < \phi < 90^o$ may occur. The periodic strain, γ^*, may be expressed as

$$\gamma^* = \gamma_o sin(\omega t + \phi) \tag{2.3}$$

For an elastic solid ϕ=0, which means that the strain and stress are in phase; a viscous liquid is represented by ϕ=90 (phase shift of 90 degrees) and the stress is proportional to

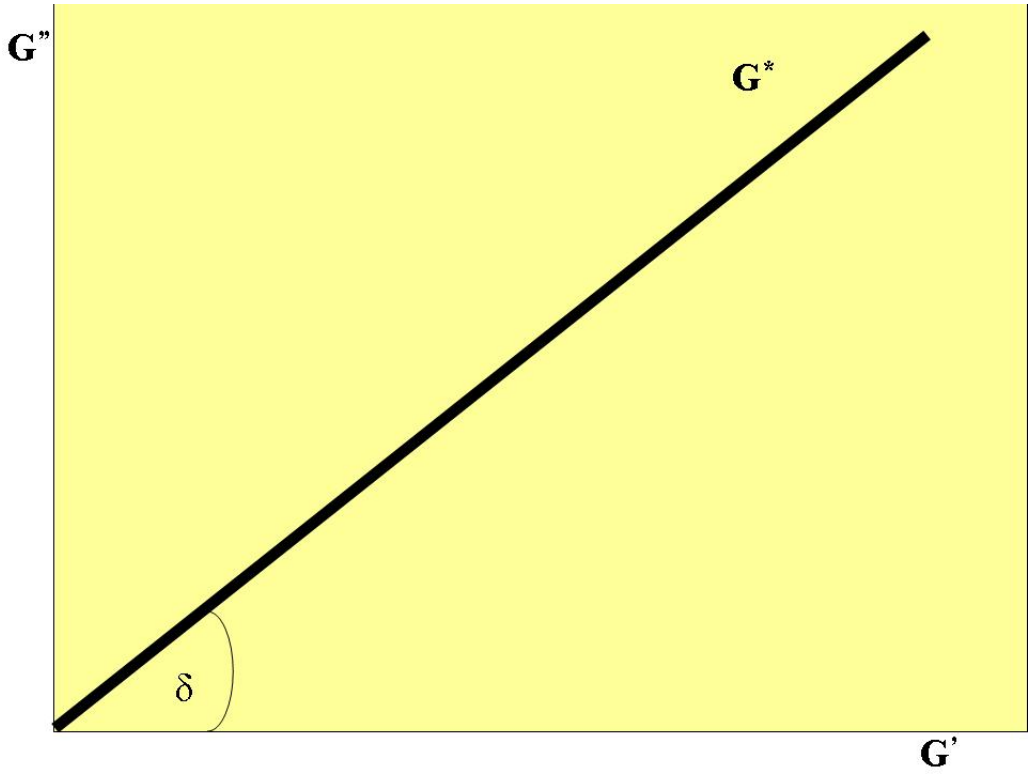

Figure 2.5: The relationship between $tan\delta$, the storage-,the loss-, and the complex-modulus

the rate of strain.

2.2.2 Storage- and Loss-Modulus

The dynamic characteristics of a material may be expressed as a complex quantity consisting of a real part called the storage modulus, $G^{'}$, and an imaginary part named the loss modulus, $G^{“}$:

$$\frac{S^*}{\gamma^*} = G^* = G^{'} + jG^{“} \tag{2.4}$$

where, $j = \sqrt{-1}$

Alternatively, we can express the above equation in polar coordinates

$$\frac{S^*}{\gamma^*} = G^* == |G^*| \angle tan^{-1}(\frac{G^{“}}{G^{'}}) \tag{2.5}$$

The ratio of the storage modulus to the loss modulus is called the loss factor or $tan\delta$ and is given by

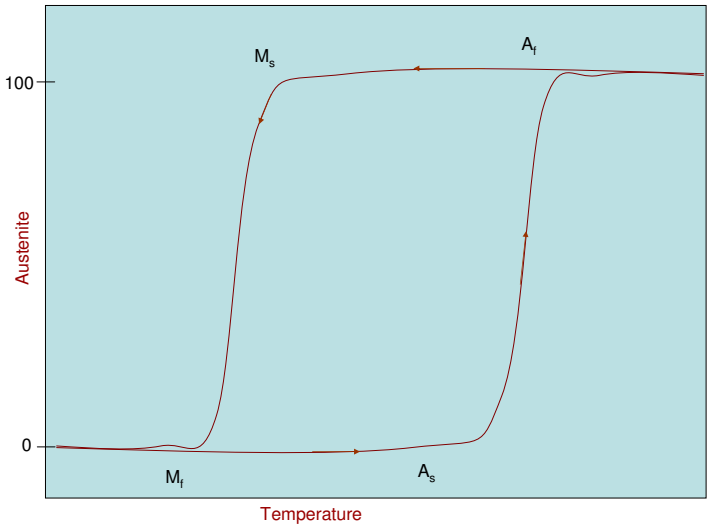

Figure 2.6: Shape memory in an alloy showing martensite-austenite transformation

$$tan\delta = \frac{G^{\text{“}}}{G'} \tag{2.6}$$

2.3 Shape Memory Materials

Since the accidental discovery of shape memory in nickel-titanium (Nitinol) by the Naval Ordnance Laboratory in 1968, research on shape memory materials has gained worldwide attention for the past half century. In general terms, a shape memory material possesses the ability to recover its shape from a deformed state. Shape memory has been reported in ceramics [40], metal alloys [1], gels [17], and polymers [14, 15]. We describe briefly the shape memory effect in metal alloys, as a prelude to shape memory polymers.

2.3.1 Shape Memory Alloys

Shape memory in alloys results from enthalpic changes i.e martensite-austenite phase changes as illustrated in 2.6. Several alloys have been reported to possess shape memory, including binary materials such as NiTi, CuZn, AuCd and InTi. Ternary systems, such as NiTiCu and CuZnAl have also been reported in the literature to possess shape memory [12].

Shape memory alloys based on Nitinol(NiTi) has been used extensively in industrial

applications such as orthodontic wires, flexible aircraft wings, actuators, and MEMS, among others [3, 13, 26]. The limitations of Nitinol's application is due to the high production costs [26], as a result of the requirement for high temperatures during processing [28].

2.4 Shape Memory Polymers

Shape memory polymers (SMPs)have been the center of intensive research since the first report more than three decades ago. Figure 2.9 illustrates the principle behind shape memory in materials. The shape memory effect may be demonstrated in a polymeric material by deforming the material at a temperature, T_d, above the glass transition temperature, T_g; storage of the material in the pre-set form is done at a temperature, T_s, below T_g. Regaining of the original shape is performed by heating the polymer to a temperature beyond T_g [15]. Figure 2.9 illustrates the rudiments of shape recovery of a shape memory polymer. Rubber is a naturally occuring shape memory polymer capable of assuming many shapes before returning to its original shape [12]. In thermoplastics, the shape memory effect is dependent on the presence of a soft phase and a hard phase in the polymer mixture [25]. In thermosets, chemical crosslinks facilitate shape memory. The soft phase establishes the shape memory characteristics of the material, while the hard phase determines the structural properties of the material [9]. Crosslinking is a way to achieve shape memory by undergoing isomerization when irradiated with light. Azobenzene is an example of a crosslinking agents for polymer fabrics. Azobenzene undergoes a cis-trans transformation when irradiated with ultraviolet light leading to the shape change. In contrast, ordinary polymers cannot exhibit shape memory properties The shape memory effect in polymers is different from that of ceramics and metals due to the lower stresses and larger recoverable strains exhibited by polymers [11]. Owing to their ease of manufacturability, and cheaper cost compared to their metallic shape alloy counterparts, shape memory polymers are finding many applications, including biomedical devices [25, 27, 36], microsystems [9], aerospace and defense [34], and robotics [11]. disadvantage of shape memory polymers have a lower recovery stress (0.98–2.94 MPa) when compared to their metallic alloy counterparts (147–294 MPa). One of the earlier forms of shape memory polymers, covalently cross-linked polyethylene has been utilized

as heat-shrink tubing material and anti-corrosive coating for pipe lines, and insulation for electric wires [23]. In these applications, the permanent shape of the material is determined by covalent crosslinks, while the melting temperature of the polyethylene crystallites enable the shape switching process.

2.4.1 Characteristics of Shape Memory Polymers

In ordinary polymers, the molecules are frozen in the glassy state, while in the rubbery state the molecules are free to rotate. Polymers exist in two phases depending on the temperature; the glassy state at lower temperatures, and a rubbery state at higher temperatures as depicted in Figure 2.3. As is evident in Figure 2.3, the glassy modulus in polymers is at least two orders of magnitude greater than the rubbery modulus. Since the polymer molecules in the rubbery state have a lower modulus, the molecules are pliable to large deformation loads. As a result, in the rubbery regime, the stored elastic energy is insufficient to cause a reverse transformation upon load removal [37]. Thus, ordinary polymers cannot recover completely from a deformed state. It is noted in the figure that for a cross-linked polymer, only three regions are present: there is a region after the transition which is flat [32]. A shape memory polymer differs from ordinary polymers due to the former's ability to recover its original shape from a deformed state [37]. Entropy transformations provide the shape memory in polymers, as opposed to the case in alloys where shape memory is dictated by austenitic-maretensitic phase transformations. Polymer networks exhibit phase transformations, with a maximum entropyand low internal energy at a temperature greater than a critical temperature, T_{crit} (T_{crit} may be the glass transition temperature, T_g, or the melting temperature,T_m) [24]. At T_{crit}, a polymeric chains between crosslink points of the materials are free to rotate and deform. The rotations are about the the bacbone bonds. exhibits ""superelasticity"

2.4.1.1 Acrylate Shape Memory Polymers

Polymer materials based on acrylates have been studied for many years [4, 7, 8, 16, 19, 33]. The interest in acrylates stem from properties such as light weight, high optical transmittance, low production cost, among others. For example, polymethyl methycralyte (PMMA)

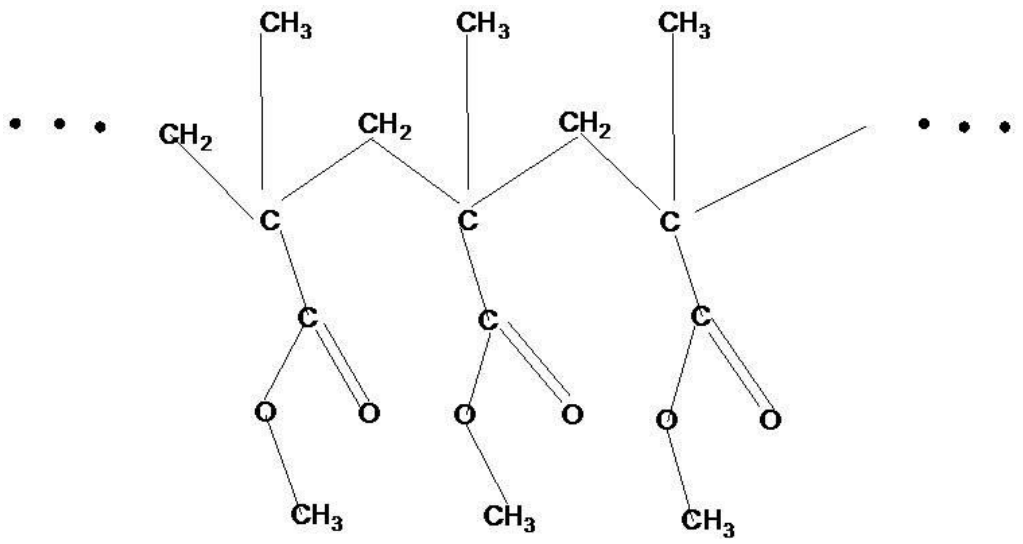

Figure 2.7: PMMA structure

has served a myriad of industries, such as its use in microelectronics as photoresist. Gall and collaborators studied the shape memory properties of tert-butyl acrylate monomer crosslinked with diethyleneglycol diacrylate crosslinker. The glass transition temperature of the materials was 65°C. The polymers demonstrated 100% strain recovery at low and high temperatures to strains of 80%. Kagami, Jiang, and Osada investigated shape memory in copolymerized stearyl acrylate and methyl acrylate. Reversible order-disorder transition of crystalline aggregates of stearyl moieties is responsible for shape memory in this case. Lendlein and coworkeres [22] demonstrated light activation of shape memory polymers based on n-butylacrylate grafted on hydroxyethyl methacrylate (HEMA) and ethyleneglycol-1-acrylate-2CA (HEA-CA) with poly (propylene glycol)-dimethacralyte as crosslinker. Photoreversible crosslinks acting as molecular switches are responsible for the temporary shape when irradiated with UV light at a wavelength $\lambda \succ > 260$ nm . The material recovers when exposed to light at a wavelength of $\lambda \prec 260$ nm. The shape transformation is illustrated by Figure 2.8. Strain-recovery rate in photoresponsive shape memory polymers is lower than that in thermoresponsive shape memory polymers. the lower strain-recovery in photoresponsive shape memory polymers is because the new chemical points formed as a result of irradiation leads to elastic contraction of the stretched segments. In thermoresponsive polymers, freezing of the stretched chains account for shape-fixation. The advantage of

photoresponsive shape memory polymers is the remote activation of the device without any temperature interference.

In order to fully comprehend the suitability of these materials for the aforementioned applications—especially at the nanoscale—and assure reliability, characterization methods such as nanoindentation are necessary—especially for small scale applications. Recently, Willet prepared shape memory polymers from a starch-poly methyl acrylate graft copolymers palsticized with urea and water at humidities higher than 50%. Size reductions were observed in the polymers at humidities of 75%. The urea/starch ratio controlled rge equilibrium mloisture content in the films. He found no shrinkage dependence on realtive humidity above 75%. Kelch and collaborators synthesized shape memory polymer networks from oligo[(epsilon-hydroxycaproate)-co-glycolate]dimethacrylate via photopolymerization. The materials had hydrolytic degradation properties making them suitable for applications in biomedical devices.

2.4.1.2 Shape Memory Review

The past decade has seen much focused research in the development of many shape memory polymers. Notable among these researchers include Langer and Kelch. Most recently, these researchers explored light for the activation of SMPs. SMPs may be classified according to the form of activation. Kim et al. investigated the thermal shape memory effect in segmented polyurethane (PU) prepared from 4,4'-diphenylmethane diisocyanate, and 1,4-butanediol. They explored the effects of soft segment molecular weight, soft content, and maximum strain on the recovery. It was observed that the shape memory properties of the materials are dependent on the thermomechanical properties of the materials. These workers obtained almost 100 % shape recovery of the materials. Most recently, Shmidt explored the electromagnetic activation of shape memory polymers. Yakacki et al. investigated the cyclotoxicity and thermomechanical properties of shape memory polymers. The work reported small changes in the glass transition temperature of the polymer networks under gamma irradiation [38]. These polymers are for biomedical applications.

Ferninat and coworkers investigated the use of shape memory polymers for applications

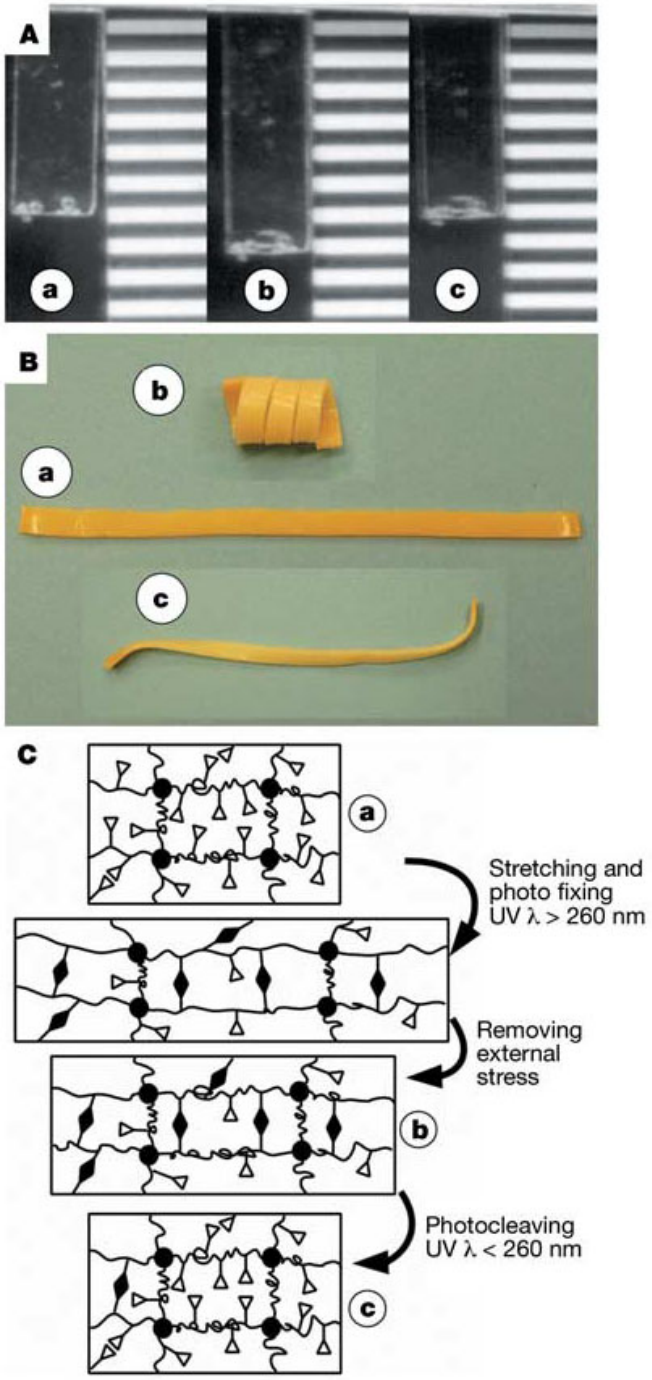

Figure 2.8: Schematic of shape memory in photoresponsive polymers. i, A film of grafted polymer BHCA(10,2,1). a, Original shape (6 cm ə 1.2 cm ə 0.05 cm); b, temporary shape; c, recovered original shape. ii, An IPN polymer film. a, Original shape (8 cm ə 0.4 cm ə 0.05 cm); b, corkscrew spiral temporary shape; c, recovered shape obtained by irradiation with UV light of l , 260 nm for 60 min. iii, Molecular mechanism of shape-memory effect of the grafted polymer network: the chromophores are covalently grafted onto the permanent polymer network , forming photoreversible crosslinks; fixity and recovery of the temporary shape are realized by UV light irradiation of suitable wavelengths [21]

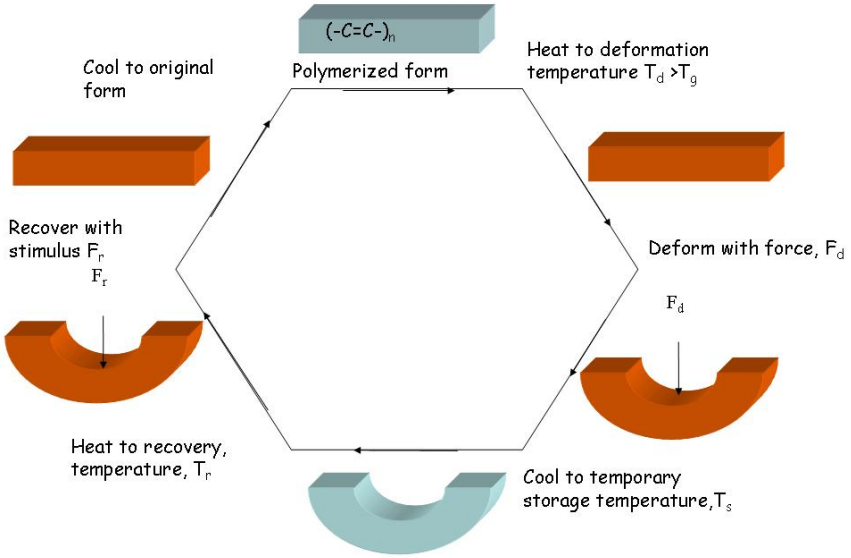

Figure 2.9: Schematic of the shape memory principle

in biomedical engineering.

2.4.1.3 Tensile Shape Recovery

An important property of shape memory polymers is the ability of the polymeric material to recover from an imposed strain. This property is mostly measured by using a tensile tester to monitor the properties of the material as the material is subjected to an applied strain. Strain shape recovery may be defined as

$$R_r(N) = \frac{\epsilon_m - \epsilon_p(N)}{\epsilon_m - \epsilon_p(N-1)} \tag{2.7}$$

Here, N is the cycle number. The percentage of recovered strain is the ratio of the recovered strain to the applied strain when a sample is heated beyond the storage temperature, T_s.

$$\%Strain recovery = \frac{\epsilon_m - \epsilon_p}{\epsilon_m - \epsilon_p} x100\% \tag{2.8}$$

$$\%Strain fixity = \frac{\epsilon_u}{\epsilon_m} x100\% \tag{2.9}$$

2.5 Information Storage

Traditional information storage systems have been based on magnetic materials–an example is the hard dsik drives used in modern computers. The storage usually involve high-speed, solid-state electronic materials. Information storage using magnetic media is based on the giant magentoresistance effect, which is seen in alternating ferromagnetic and nonmagnetic metal structures. The information is stored in bits in a magnetic read/write head in nanometer size layers. When an external electric field is applied, the layers align with themselves as the resistance between layers decrease. In the absence of an applied electric field, the direction of magnetization is anti-parallel as a result of weak coupling between layers. Though magnetic storage technologies have persisted for many years, the information storage limit for magnetic media is the superparamagnetic limit (60ŋ-100 Gb/in^2). Recently, optical storage has received so much attention due to the potential of optical holograms as storage media. Optical storage have limits of 100 Gb/in^2. Polymers as information storage media have been demonstrated through the IBM Millipede project. Binnig and coworkers studied the use of PMMA as an information storage media. A group of researchers at IBM demonstrated that for a given unit area of a polymeric material, more bits of information can be stored compared to either the optical storage or magnetic storage media. Polymeric storage media reached a storage limit of 1 Tb/in^2. In the millipede data storage system, PMMA is used as the material and AFM tips are used to write information in the PMMA film. The process is a form of thermomechanical data storage system. Figure 2.10 depicts the thermomechanical information storage in a film of PMMA. The left figure illustrates the predecessor which used thicker bulk polycarbonate layers [35].

2.5.1 Atomic Force Microscopy (AFM)

The atomic force microscope (AFM) or the scanning force microscope (SFM) is an important tool in nanometer science. It has better resolution than the scanning electron microscope (SEM). It is a scanning technique based on atomic scale manipulation of a material at extremely small scales. The procedure uses a tip of radius 10 nm located on a cantilever to produce sharp images of the surface of a material. Since its invention in 1986 by Binnig and

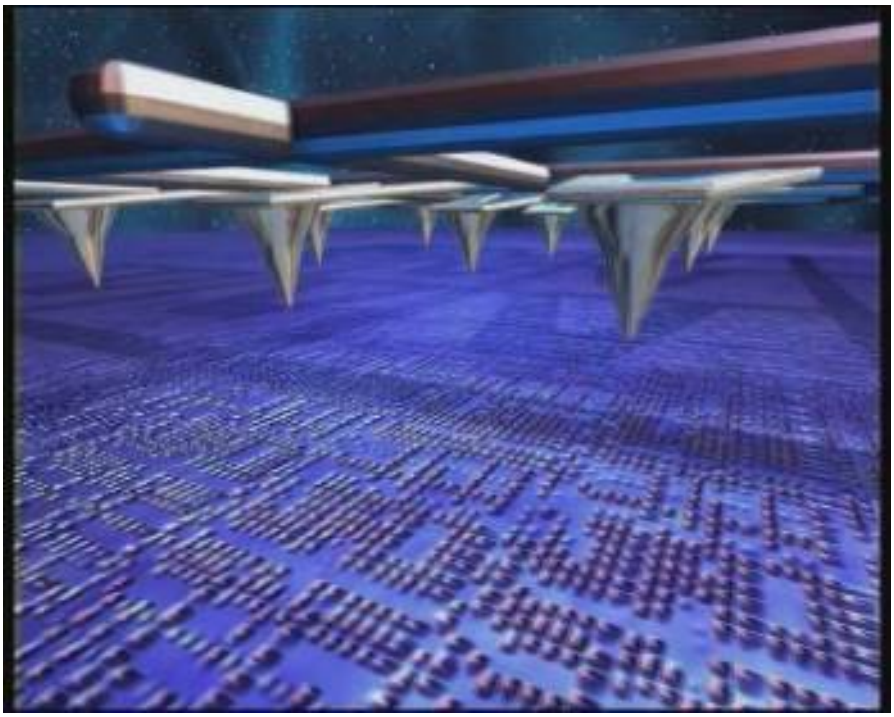

Figure 2.10: Thermomechanical storage system using PMMA as the storage media [IBM Corp].

coworkers [5, 6], the AFM has been used in many areas including individual atom manipulation [2, 31], nanoimaging [29], semiconductor manufacturing [18], biomedical engineering [30], polymer characterization [10] and nanoindentation [39], among others.

2.5.1.1 Basic AFM Theory

Figure 4.15 shows an atomic force microscope.

The atomic force microscope comprises a small-scale cantilever with a sharp probe tip (on the order of 25 nm), as shown above. The material under study is probed with the tip of the AFM. As the tip approaches the material surface, deflection occurs due to interaction between the tip and the material.

There are two main modes of operation of an AFM. These are the contact (static) mode and the dynamic mode. External oscillation of the cantilever at a frequency close to its fundamental resonance frequency is used. Tip-sample interaction results in changes in oscillation amplitude, phase and resonance frequency. Dynamic mode operation may be frequency or amplitude modulation. Changes in the oscillation frequency of the tip gives

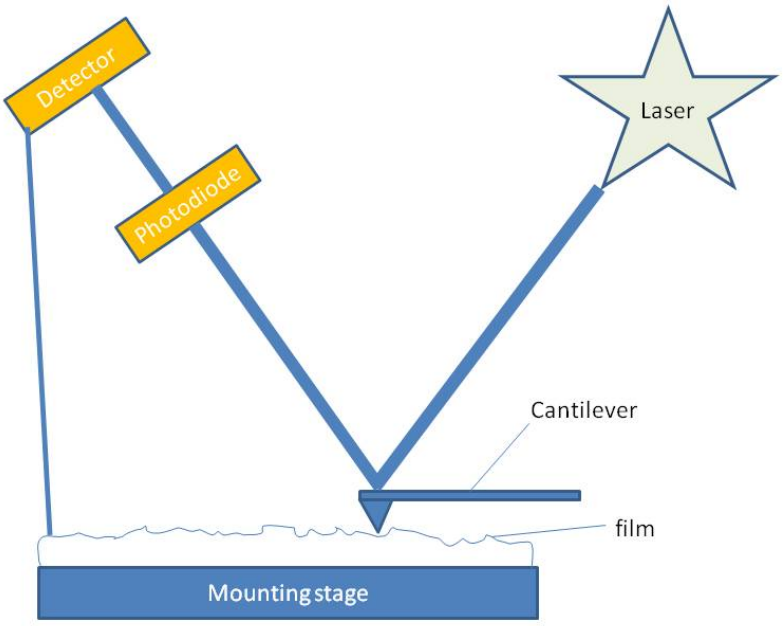

Figure 2.11: A schematic of an atomic force microscope

sample-tip interaction information. Changes in the phase (amplitude) of oscillation gives sample-tip information.

2.5.2 Dynamic Mechanical Analysis (DMA)

Dynamic mechanical analysis is a technique for the determination of the thermomechanical properties of materials, especially polymers. In this technique, a sinusoidal signal is applied to a material and the displacement is monitored. Some of the properties obtainable from a DMA thermogram are the glass transition temperature, T_g, the loss modulus, and the storage modulus. The relationship between the complex modulus, G^* can be expressed as

$$G^* = G_s + jG_l \tag{2.10}$$

$$tan\delta = \frac{G_l}{G_s} \tag{2.11}$$

The glass transition temperature is determined from the peak of $tan\delta$. Tan delta is the ratio of the storage to the loss modulus of the material. T_g can be defined in many ways. However, we define T_g in this work to be the peak of the $tan\delta$. The peak of the $tan\delta$ peak defines the heterogeneity of the specimen.

2.6 Summary

The current chapter reviews concepts that are important to shape memory polymers. It covers topics such as the definition of polymers and dynamic mechanical analysis.

The next chapter discusses nanoindentation. The chapter reviews literature on nanoindentation in general, and shape memory polymers in particular.

REFERENCES

[1] Armstrong, W. D. and Lilholt, H., "The time dependant, super-viscoelastic behavior of niti shape memory alloy fiber reinforced polymer matrix composites," *Materials Science and Engineering B-Solid State Materials for Advanced Technology*, vol. 68, no. 3, pp. 149–155, 2000. The time dependant, super-viscoelastic behavior of NiTi shape memory alloy fiber reinforced polymer matrix composites.

[2] Bartels, L., Meyer, G., and Rieder, K. H., "Basic steps of lateral manipulation of single atoms and diatomic clusters with a scanning tunneling microscope tip," *Physical Review Letters*, vol. 79, no. 4, pp. 697–700, 1997.

[3] Benard, W. L., Kahn, H., Heuer, A. H., and Huff, M. A., "Thin-film shape-memory alloy actuated micropumps," *Journal of Microelectromechanical Systems*, vol. 7, no. 2, pp. 245–251, 1998. article.

[4] Berkowicz, B. D. and Peppas, N. A., "Characterization of surgical adhesives from uv-polymerized poly(peg dimethacrylate-co-2-hydroxyethyl methacrylate) copolymers," *Journal of Applied Polymer Science*, vol. 56, no. 6, pp. 715 –, 1995. article.

[5] Binnig, G., Quate, C. F., and Gerber, C., "Atomic force microscope," *Physical Review Letters*, vol. 56, no. 9, pp. 930–933, 1986.

[6] Binnig, G. K., "Atomic-force microscopy," *Physica Scripta*, vol. 19, pp. 53–54, 1987.

[7] Bowman, C. N., Carver, A. L., Kennett, S. N., Williams, M. M., and Peppas, N. A., "Polymers for information storage systems. iii. crosslinked structure of polydimethacrylates," *Polymer*, vol. 31, no. 1, pp. 135–9, 1990. article.

[8] Bowman, C. N. and Peppas, N. A., "Polymers for information storage systems. ii. polymerization kinetics for preparation of highly crosslinked polydimethacrylates," *Journal of Applied Polymer Science*, vol. 42, no. 7, pp. 2013–2018, 1991. article.

[9] Cheung, E., Karagozler, M. E., Park, S., Kim, B., and Sitti, M., "A new endoscopic microcapsule robot using beetle inspired microfibrillar adhesives," *Proceedings, 2005 IEEE/ASME International Conference on Advanced Intelligent Mechatronics*, pp. 551 – 557, 2005. article.

[10] Clifford, C. A. and Seah, M. P., "Quantification issues in the identification of nanoscale regions of homopolymers using modulus measurement via afm nanoindentation," *Applied Surface Science*, vol. 252, no. 5, pp. 1915–1933, 2005. article.

[11] Duncheon, C., "Robots will be of service with muscles, not motors," *Industrial Robot-an International Journal*, vol. 32, no. 6, pp. 452–455, 2005. article.

[12] F. El Feninat, G. L. M. F. D. M., "Shape memory materials for biomedical applications," *Advanced Engineering Materials*, vol. 4, no. 3, pp. 91–104, 2002. article 10.1002/1527-2648(200203)4:3<91::AID-ADEM91>3.0.CO;2-B.

[13] Fischer, H., Vogel, B., and Welle, A., "Applications of shape memory alloys in medical instruments," *Minimally Invasive Therapy & Allied Technologies*, vol. 13, no. 4, pp. 248–253, 2004. article.

[14] Gall, K., Kreiner, P., Turner, D., and Hulse, M., "Shape-memory polymers for microelectromechanical systems," *Journal of Microelectromechanical Systems*, vol. 13, no. 3, pp. 472–483, 2004. article.

[15] Gall, K., Kreiner, P., Turner, D., and Hulse, M., "Shape-memory polymers for microelectromechanical systems," *Microelectromechanical Systems, Journal of*, vol. 13, no. 3, pp. 472–483, 2004.

[16] Gall, K., "Shape memory polymers for biomedical applications," *Advanced Materials and Processes*, vol. 163, no. 7, pp. 46 –, 2005. article Shape memory polymers;Biomedical applications;.

[17] Goto, H., Zhang, H. Q., and Yashima, E., "Chiral stimuli-responsive gels: Helicity induction in poly(phenylacetylene) gels bearing a carboxyl group with chiral amines," *Journal of the American Chemical Society*, vol. 125, no. 9, pp. 2516–2523, 2003. article.

[18] Guerry, A., Gondran, C., and Miller, K., "Sidewall roughness measurement: a comparison of in- and off-line afm techniques," in *Proc. IEEE Conference and Workshop Advanced Semiconductor Manufacturing ASMC '04*, pp. 221–226, 4–6 May 2004.

[19] Kagami, Y., Gong, J. P., and Osada, Y., "Shape memory behaviors of crosslinked copolymers containing stearyl acrylate," *Macromolecular Rapid Communications*, vol. 17, no. 8, pp. 539–543, 1996. article.

[20] Kumar, A. S., *Fundamentals of polymer engineering.* New York :: Marcel Dekker, 2003. book Plastics engineering ; 66 Plastics engineering (Marcel Dekker, Inc.) ; 66.

[21] Lendlein, A., Jiang, H., Junger, O., and Langer, R., "Light-induced shape-memory polymers," *Nature*, vol. 434, no. 7035, pp. 879–882, 2005.

[22] Lendlein, A., Jiang, H. Y., Junger, O., and Langer, R., "Light-induced shape-memory polymers," *Nature*, vol. 434, no. 7035, pp. 879–882, 2005. <Go to ISI>://000228327600036.

[23] Lendlein, A. and Kelch, S., "Degradable, multifunctional polymeric biomaterials with shape-memory," 2005.

[24] Liu, C., Qin, H., and Mather, P., "Review of progress in shape-memory polymers," *Journal of Materials Chemistry*, vol. 17, no. 16, pp. 1543–1558, 2007.

[25] Liu, Y. P., Gall, K., Dunn, M. L., Greenberg, A. R., and Diani, J., "Thermomechanics of shape memory polymers: Uniaxial experiments and constitutive modeling," *International Journal of Plasticity*, vol. 22, no. 2, pp. 279–313, 2006. article.

[26] Mertmann, M., "Non-medical applications of nitinol," *Minimally Invasive Therapy & Allied Technologies*, vol. 13, no. 4, pp. 254–260, 2004. article.

[27] Metzger, M. F., Wilson, T. S., Schumann, D., Matthews, D. L., and Maitland, D. J., "Mechanical properties of mechanical actuator for treating ischemic stroke," *Biomedical Microdevices*, vol. 4, no. 2, pp. 89–96, 2002. article.

[28] Morgan, N. B., "Medical shape memory alloy applications - the market and its products," *Materials Science and Engineering a-Structural Materials Properties Microstructure and Processing*, vol. 378, no. 1-2, pp. 16–23, 2004. article Sp. Iss. SI.

[29] Neubauer, G., Dass, M., and Johnson, T., "Imaging vlsi cross sections by atomic force microscopy," in *Proc. 30th Annual International Reliability Physics Symposium 1992*, pp. 299–303, 31 March–2 April 1992.

[30] Nishi, D., Arai, T., Inoue, K., and Takubo, T., "Measurement of the mechanical properties of living cell using micro hand and developed afm system," in *Proc. IEEE/RSJ International Conference on Intelligent Robots and Systems (IROS 2005)*, pp. 990–995, 2–6 Aug. 2005.

[31] Oyabu, N., Custance, ., Yi, I., Sugawara, Y., and Morita, S., "Mechanical vertical manipulation of selected single atoms by soft nanoindentation using near contact atomic force microscopy," *Physical Review Letters*, vol. 90, no. 17, pp. 176102–176102, 2003.

[32] Ram, A., *Fundamentals of polymer engineering.* New York :: Plenum Press, 1997. book.

[33] Richardson, H., Sferrazza, M., and Keddie, J. L., "Influence of the glass transition on solvent loss from spin-cast glassy polymer thin films," *European Physical Journal E*, vol. 12, no. SUPPL 1, pp. 75 – 79, 2003. article Solvent loss;Energy barriers;Glassy thin films;.

[34] Toensmeier, P. A., "Shape memory polymers reshape product design," *Plastics Engineering*, pp. 10–11, 2005. article.

[35] Vettiger, P., Cross, G., Despont, M., Drechsler, U., Durig, U., Gotsmann, B., Haberle, W., Lantz, M. A., Rothuizen, H. E., Stutz, R., and Binnig, G. K., "The "millipede" - nanotechnology entering data storage," *IEEE Transactions on Nanotechnology*, vol. 1, no. 1, pp. 39–55, 2002. article.

[36] Wache, H. M., Tartakowska, D. J., Hentrich, A., and Wagner, M. H., "Development of a polymer stent with shape memory effect as a drug delivery system," *Journal of Materials Science: Materials in Medicine*, vol. 14, no. 2, pp. 109–112, 2003. article.

[37] Wei, Z. G., Sandstrom, R., and Miyazaki, S., "Shape memory materials and hybrid composites for smart systems - part ii shape-memory hybrid composites," *Journal of Materials Science*, vol. 33, no. 15, pp. 3763–3783, 1998. article.

[38] Yakacki, C., Lyons, M., Rech, B., Gall, K., and Shandas, R., "Cytotoxicity and thermomechanical behavior of biomedical shape-memory polymer networks cytotoxicity and thermomechanical behavior of biomedical shape-memory polymer networks post-sterilization," *Biomedical Materials*, vol. 3, p. 015010, 2008.

[39] Yang, F., Wornyo, E., Gall, K., and King, W., "Nanoscale indent formation in shape memory polymers using a heated probe tip," *Nanotechnology*, vol. 18, no. 285302, p. 285302, 2007.

[40] Yang, L., Liu, W., Chen, W., Wang, Y., Cao, X., and Ren, X., "Electro-shape-memory effect in Mn-doped (Pb, Sr) TiO3 ceramics," *Materials Science & Engineering A*, vol. 438, pp. 176–180, 2006.

CHAPTER III

NANOINDENTATION

In order to increase reliability of materials in complex biomedical and microelectronics systems on the nanoscale, it is necessary to understand the properties of materials at these scales. Traditional tensile testing methods are limited in assessing the deformation of small volumes of materials on a substrate.Figure 3.1 shows a picture of a nanoindenter in the Advanced Materials Laboratory at Georgia Tech. Figure 3.2 features the Hysitron Triboindenter at the Microelectronics Research Center at Georgia Tech.

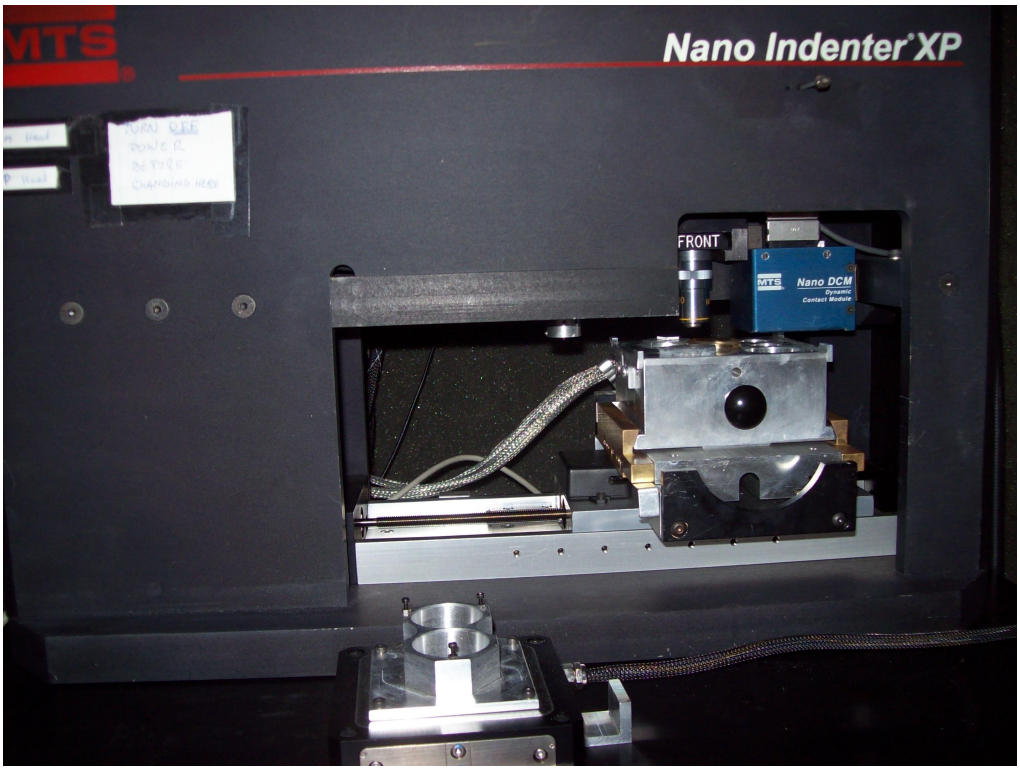

Figure 3.1: A picture of an MTS nanoindenter in our laboratory at Georgia Tech

Nanoindentation is a depth sensing instrumentation technique that is used to probe nanometer features of materials, for the determination of visco-elastic properties such as hardness and elastic modulus. In 3.3, the material surface is penetrated with an indenter

Figure 3.2: The Hysitron triboindenter at the Microelectronics Research Center at Georgia Tech

tip of load Pmax leading to a penetration depth, h, of the tip into the surface. Instrument controls continuously monitor and record the load and the corresponding depth with time. As the load is withdrawn from the material, the material begins to recover from the imposed deformation. However, plastic deformation limits full recovery of the material. The resulting load-displacement curve is illustrated in 3.4. The probe that is embedded into the material may be flat, spherical, pyramidal and conical, in geometry. This technique may also be used for the study of data storage in polymers [6–10, 14], biological samples [15, 16], metals [20], and ceramics [11]. Although there has been some study on polymers, it was not until recently that this method has been applied to the determination of the mechanical properties of polymers. The challenges of this method stem from the indentation size effect (ISE)–the increase of the modulus as the penetration depth reduces [13].

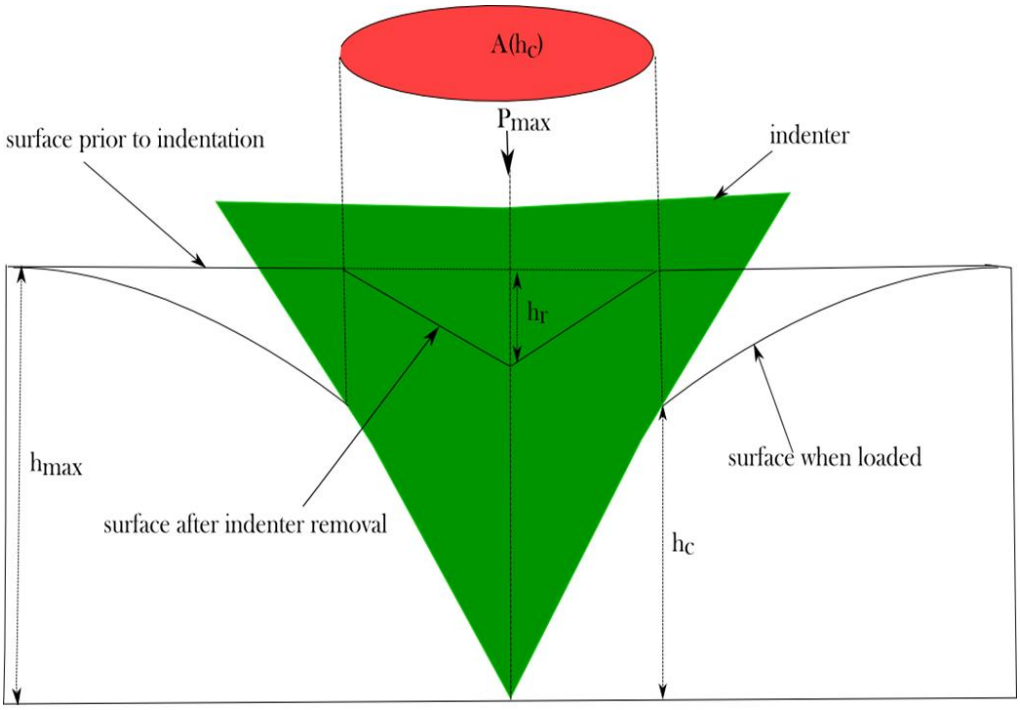

Figure 3.3: Illustration of an indenter tip in contact with a material. The relevant parameters are shown in this figure.

A graphical description of the nanoindentation experiment is shown in Fig. 3.4.

Materials may be identified as plastic, elastoplastic or elastic from the nanoindentation plots. A plastic material does not recover upon the application of an external load-the

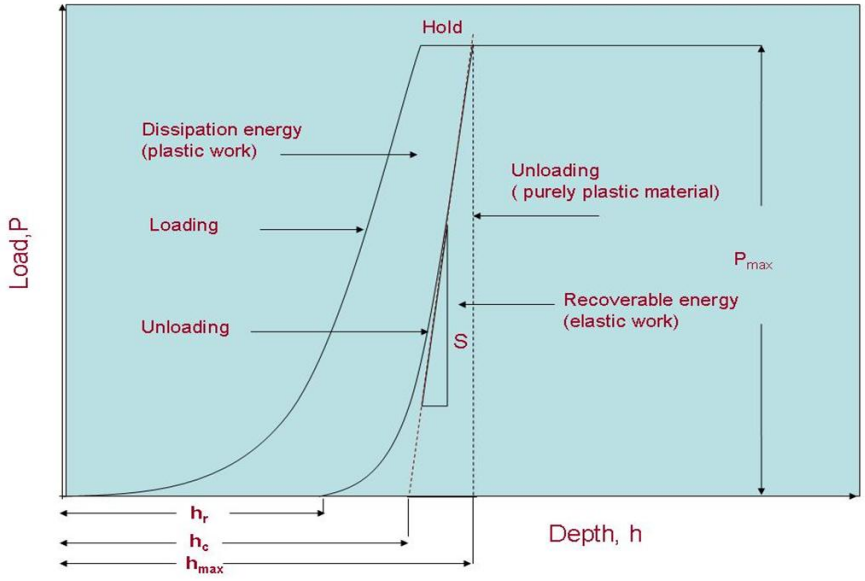

Figure 3.4: Typical load displacement curve of a nanoindentation experiment.

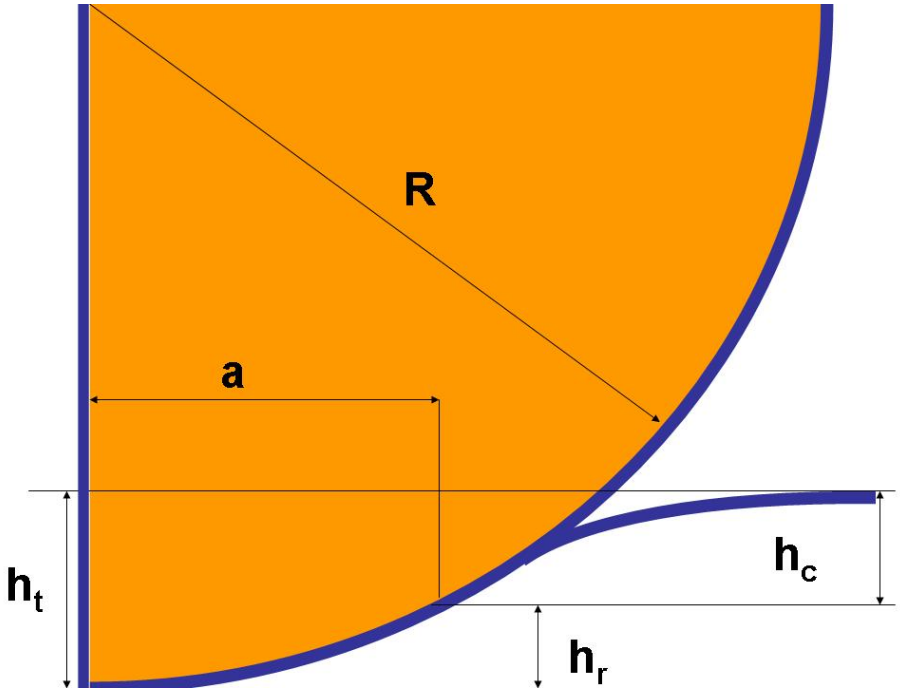

Figure 3.5: Contact depth

unloading and loading curves follow different paths. For elastic deformation, the loading and unloading curves follow the same path, whereas elastoplastic materials show some elastic behavior and plastic behavior.

Elastic contact analysis is a nannoindentation data analysis technique in which the unloading data is taken to be purely elastic at contact. The analysis is based on Hertz's contact theory of lenses proposed in the early 1880s. Many researchers have worked on the contact problem for many years. Some of the methods are named after the researchers who developed them: Sneddon, Nix-Doerner, Oliver-Pharr, Field-Swain, etc. However, Oliver-Pharr method has become dominant as the method of choice for nanoindentation analysis.

Initial work on nanoindentation was done at the Baikov Institute of Metallurgy in the 1970s. The analysis was based on the premise of purely elastic unloading.

3.1 Spherical Indenter

At low loads during nanoindentation with a spherical indenter, a material may have an initial elastic response at low loads. At higher loads, elastic and plastic deformations are present in the material. At full load, P_{max}, the surface of the material deforms to a maximum depth, h_{max}. In the absence of reverse plasticity, there is elastic deformation and the material has a residual depth of h_r. Assuming that the maximum load P_{max} is reapplied, the reloading will be elastic. The distance through which P_{max} moves is $h_c = h_t - h_r$ as evident in Figures 3.3 and 3.4. The elastic deformation may then be expressed as

$$P = \frac{4}{3} E^* R^{\frac{1}{2}} h_c^{\frac{3}{2}} \tag{3.1}$$

If the radius of the indenter and the material are R_1 and R_2 respectively, then the resultant radius may be expressed as

$$\frac{1}{R} = \frac{1}{R_1} + \frac{1}{R_2} \tag{3.2}$$

The nanoindentation parameters may be extracted via the Oliver-Pharr [12] model from an experimental plot akin to Figure 3.4. The gradient of the initial portion of the unloading stiffness curve gives the visco-elastic parameters of the material [1, 13]. Mathematically, the

stiffness, S is given as

$$S = \frac{dP}{dh} \tag{3.3}$$

A challenge of indentation is the determination of the contact area, A. In contrast to indentation at the macroscale and microscale, the size of the residual impression is difficult to determine by optical means [3, 13]. Thus, the penetration depth is used in conjunction with a knowledge of the indenter geometry to estimate the contact area, A. According to Oliver and Pharr [12], the determination of A may be done by estimating the contact depth, h_c from the equation

$$h_c = h_{max} - \epsilon \frac{P_{max}}{S} \tag{3.4}$$

for a geometrical constant ϵ. The effective elastic modulus, E_r, is expressed mathematically as

$$\frac{1}{E_r} = \frac{1-\nu^2}{E} + \frac{1-\nu_i^2}{E_i} \tag{3.5}$$

where E and ν are the elastic modulus and the Poisson's ratio, respectively, of the material, and the subscript i refers to the indenter. The relationship between the stiffness, S, and the reduced modulus is

$$S = 2aE_r = \frac{2\beta E_r \sqrt{A}}{\sqrt{\pi}} \tag{3.6}$$

In order to accurately measure the parameters above, several issues must be tackled. The indenter tip calibration is of import as there may be imperfections on the tip, caused by many factors [1]. The tip calibration may be accomplished by using fused silica due to consistency of modulus with indentation depth [12].

3.2 Nix Nanoindentation Analysis

Before the proposition of the Oliver-Pharr analysis of nanoindentation data, other researchers such as Doerner and Nix proposed methods of analyzing nanoindentation data to extract material parameters. According to Doerner and Nix, an indenter may be assumed to be a

flat punch for a small change in contact area. The contact area was measured in brass by transmission electron microscopy (TEM).

3.3 Dynamic Nanoindentation

The above methods of nanoindentation described are based on quasi-static indentation–the deformation of the material is assumed to be non-time dependent. However, materials such as polymers have been shown to have time dependent deformation (viscoelastic). Corrections have been made to the above equations by many researchers. Notwithstanding these efforts, the viscoelastic nature of polymers demand a measurement method that will take into account the time dependence. Dynamic nanoindentation is a technique that measures the modulus as a complex value, and thus leading to a modulus which depends on frequency. The measurement is very similar to dynamic mechanical analysis (DMA) described earlier.

3.4 Errors in Nanoindentation Tests

As we have seen in sections 3.1, the extraction of hardness and modulus depend on the area function. In indentation studies, the area function is determined from the area of the residual impression in the material. Usually the contact area at full load is taken to be the size of the residual impression. This assumption does not take into account the elastic recovery (if elastic recovery is considered, then these two areas will not be the same). In some cases, imaging of residual impressions is performed to determine the area function–this is usually cumbersome. Thus, the measurement of the loading and unloading load-depth curves provide information for the calculation of the area function. The calculation of the area function from the load-depth curves result in errors. Some of these errors arise from the non-ideality of the indentation tip, pile-up and sink-in of material around the tip. Many researchers have examined the effects of these phenomena on nanoindentation data. Instrument manufacturers have deviced means of reducing some of these errors. Here, we examine some of the most common sources of error in nanoindentation.

3.4.1 Thermal Drift

Elasto-plastic behavior, which does not factor time dependence, is assumed in a nanoindentation experiment. Drift may either be creep due to plastic flow or thermal expansion/contraction of the instrument. Creep is seen in nanoindentation when a material deforms continuously when the load had been held at its maximum. Creep may be in the form of dislocation glide, dislocation creep, diffusion creep, and grain boundary slipping. Thermal drift may be computed at a constant load, as a change in depth with time. A study by Feng and Ngan [2] concluded that thermal drift becomes negligible, if the total time of unloading,

$$t_h \approx \frac{S}{\left|\dot{P}\right|} h_p \tag{3.7}$$

here, S is the contact stiffness, $\dot{P}$ the unloading rate, and h_p is the plastic depth.

3.5 Basic Properties

Xu *et al* recently used nanoindentation to measure the mechanical properties of a silicone elastomer. In this experiment, the hardness dependence on the annealing temperature for bio-applications was investigated [18]. In an effort to determine the mechanical properties of poly(lactic acid)(PLA), Wright-Charlesworth *et al* utilized nanoindentation to determine the effect of processing methods and other factors on material characteristics [17]. Gregory and Spearing [4] investigated the dependence of modulus and hardness on manufacturing methods. In this investigation, Gregory and Spearing compared and contrasted the mechanical properties of *in situ* and neat composite materials (IM7/977-3 and AS4/APC-2). They found out that there was a conspicuous increment in the modulus and hardness of the *in situ* polymers. Gregory and Spearing further employed finite element methods for the minimization of the polymer deformation. In a recent publication using nanoindentation, Yu *et al* [19] found that the elastic modulus and hardness of a dielectric material for microelectronic applications, hydrogen methyl silsesquioxane (HMSQ) matrix with a poly (amidoamine)(PAMAM) template, decreased with an increase in the PAMAM concentration. Ho and Marcolongo [5] found enhancements in the Young's and bending moduli of

poly (methyl methacrylate)(PMMA) matrix when the latter was coupled with silane and two other acrylate agents, using the nanoindentation technique.

REFERENCES

[1] Briscoe, B. J., Fiori, L., and Pelillo, E., "Nano-indentation of polymeric surfaces," *Journal of Physics D-Applied Physics*, vol. 31, no. 19, pp. 2395–2405, 1998. article.

[2] Feng, G. and Ngan, A., "Creep and strain burst in indium and aluminium during nanoindentation," *Scripta Materialia*, vol. 45, no. 8, pp. 971–976, 2001.

[3] Fischer-Cripps, A. C., *Nanoindentation*. New York: Springer, 2002. book With 87 figures.

[4] Gregory, J. R. and Spearing, S. M., "Nanoindentation of neat and in situ polymers in polymer-matrix composites," *Composites Science and Technology*, pp. 595–607, 2005. article.

[5] Ho, E. and Marcolongo, M., "Effect of coupling agents on the local mechanical properties of bioactive dental composites by the nano-indentation technique," *Dental Materials*, vol. 21, no. 7, pp. 656–664, 2005. article.

[6] Li, X. D. and Bhushan, B., "Micro/nanomechanical characterization of ceramic films for microdevices," *Thin Solid Films*, vol. 340, no. 1-2, pp. 210–217, 1999. article.

[7] Li, X. D. and Bhushan, B., "Micro/nanomechanical and tribological studies of bulk and thin-film materials used in magnetic recording heads," *Thin Solid Films*, vol. 398, pp. 313–319, 2001. article.

[8] Li, X. D., Bhushan, B., Takashima, K., Baek, C. W., and Kim, Y. K., "Mechanical characterization of micro/nanoscale structures for mems/nems applications using nanoindentation techniques," *Ultramicroscopy*, vol. 97, no. 1-4, pp. 481–494, 2003. article.

[9] Li, X. D. and Nardi, P., "Micro/nanomechanical characterization of a natural nanocomposite material - the shell of pectinidae," *Nanotechnology*, vol. 15, no. 1, pp. 211–217, 2004. article.

[10] Li, X. D., Zhang, L. M., and Gao, H. S., "Micro/nanomechanical characterization of a single decagonal alconi quasicrystal," *Journal of Physics D-Applied Physics*, vol. 37, no. 5, pp. 753–757, 2004. article.

[11] Loubet, J. L., Georges, J. M., Marchesini, O., and Meille, G., "Vickers indentation curves of magnesium-oxide (mgo)," *Journal of Tribology-Transactions of the ASME*, vol. 106, no. 1, pp. 43–48, 1984. article.

[12] Oliver, W. C. and Pharr, G. M., "An improved technique for determining hardness and elastic-modulus using load and displacement sensing indentation experiments," *Journal of Materials Research*, vol. 7, no. 6, pp. 1564–1583, 1992. article.

[13] VanLandingham, M. R., Villarrubia, J. S., Guthrie, W. F., and Meyers, G. F., "Nanoindentation of polymers: An overview," *Macromolecular Symposia*, vol. 167, pp. 15–43, 2001. article.

[14] Vettiger, P., Cross, G., Despont, M., Drechsler, U., Durig, U., Gotsmann, B., Haberle, W., Lantz, M. A., Rothuizen, H. E., Stutz, R., and Binnig, G. K., "The "millipede" - nanotechnology entering data storage," *IEEE Transactions on Nanotechnology*, vol. 1, no. 1, pp. 39–55, 2002. article.

[15] Wei, G. H., Bhushan, B., Ferrell, N., and Hansford, D., "Microfabrication and nanomechanical characterization of polymer microelectromechanical system for biological applications," *Journal of Vacuum Science and Technology A*, vol. 23, no. 4, pp. 811–819, 2005. article.

[16] Wei, G. H., Bhushan, B., and Torgerson, P. M., "Nanomechanical characterization of human hair using nanoindentation and sem," *Ultramicroscopy*, vol. 105, no. 1-4, pp. 248–266, 2005. article.

[17] Wright-Charlesworth, D. D., Miller, D. M., Miskioglu, I., and King, J. A., "Nanoindentation of injection molded pla and self-reinforced composite pla after in vitro conditioning for three months," *Journal of Biomedical Materials Research Part A*, vol. 74A, no. 3, pp. 388–396, 2005. article.

[18] Xu, W. H., Xiao, Z. Y., and Zhang, T. Y., "Mechanical properties of silicone elastomer on temperature in biomaterial application," *Materials Letters*, vol. 59, no. 17, pp. 2153–2155, 2005. article.

[19] Yu, S. Z., Wong, T. K. S., Hu, X., Wei, J., and Yong, M. S., "Structural, electrical and mechanical properties of templated silsesquioxane porous films," *Microelectronic Engineering*, vol. 77, no. 2, pp. 125–131, 2005. article.

[20] Zhang, S., Sun, D., Fu, Y. Q., and Du, H. J., "Recent advances of superhard nanocomposite coatings: a review," *Surface & Coatings Technology*, vol. 167, no. 2-3, pp. 113–119, 2003. article.

CHAPTER IV

NANOINDENTATION OF SHAPE MEMORY POLYMER NETWORKS

4.1 Introduction

The convergence of micro-/nano-electromechanical systems (MEMS/NEMS) and biomedical industries is driving various material innovations, particularly in miniaturized polymer based devices . Polymers are used extensively in the microelectronics industry [1–6], as sensing materials , lithography tools , and biomedical devices. This onus on polymers requires that the materials possess different properties in order to reduce the cost of production, decrease the scale of devices, and offer devices with new functional properties. Many researchers have modified existing polymers by the addition or removal of tailored functional groups to make the polymers smart, hence enhancing the material utility. Shape memory polymers are a class of elastomer-like polymers that possess the ability to recover their original shape from a deformed shape upon the application of an external stimulus such as light, magnetic field, or heat.

Although the shape memory effect is inherent to many chemically or physically crosslinked polymers, only polymers with elastomer type structures and tunable thermal transitions in the appropriate temperature range are useful shape memory polymers. In order to fully comprehend the suitability of shape memory polymers for various miniaturized biomedical and microsystems applications, it is necessary to characterize and understand their deformation and recovery response at sample surfaces and in small volumes of material.

4.2 Materials and Methods

Shape memory polymers based on a diethylene glycol dimethacrylate (DEGDMA) crosslinker, a polyethylene glycol dimethacrylate (PEGDMA) crosslinker with a molecular weight of 550, a *tert*-butyl acrylate (tBA) monomer, and the photoinitiator, 2,2-dimethoxy-2-phenyl acetophenone (DMPA) were designed. The chemicals are shown in Figures 4.1–4.2.

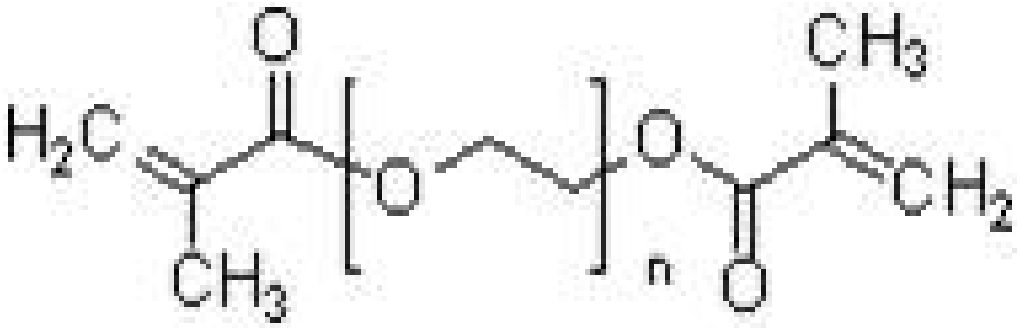

Figure 4.1: Structure of polyethylene glycol dimethacrylate

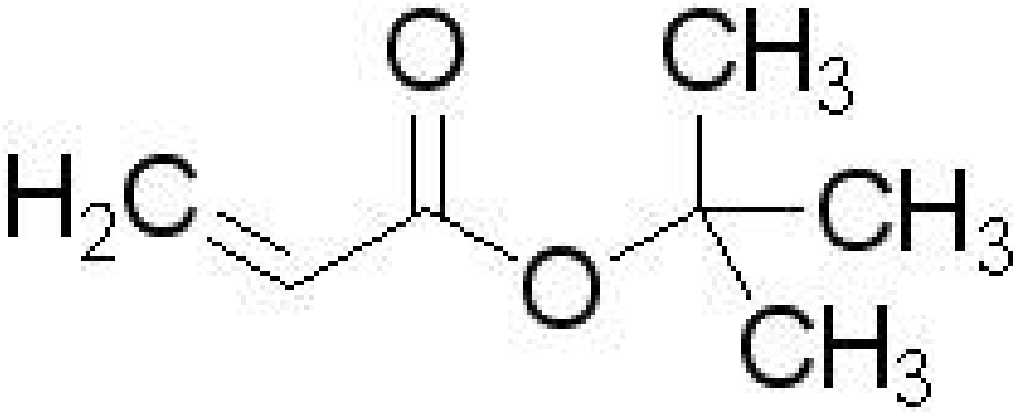

Figure 4.2: Structure of the tert-butyl acrylate monomer

All chemicals were used as received (Sigma-Aldrich, St. Louis, MO). Weight percentages of the cross-linker and monomer from 0 to 100 were prepared with 1 wt% photoinitiator added to each mixture in glass vials. A magnetic stirrer was used to mix the mixtures thoroughly. Microscope glass slides, coated with Rain-X, were made into molds of dimensions 75 mm x 25 mm x 1 mm and 75 mm x 75 mm x 1 mm for dynamic mechanical analysis (DMA) and tensile testing samples; similar molds were made with a spacer of 300 μm for atomic force microscopy (AFM) and nanoindentation experiments. The mixtures were pipetted into the molds and ultraviolet (UV) polymerized (B100AP Blak Ray, UVP, Upland, CA) at an intensity of 10 mW/cm^2 for 10 minutes. In order to determine the thermomechanical properties of these polymers, samples of dimension 25 mm x 4 mm x 1 mm were cut for DMA using a laser cutter. TA Instruments DMA Q 800 (TA Instruments Inc., Newcastle, DE) was used to obtain the dynamic mechanical properties of the co-polymers in tensile mode. Heating and cooling rates of 3 ^{o}C/min, and a sampling rate of 1 Hz were used for all DMA tests. In order to obtain information on the variation of the glass transition temperature, five independent DMA runs were performed and the average and standard deviation calculated. Four samples of dimensions 3 mm x 3 mm were cut out from the center of the samples and affixed to atomic force microscopy (AFM) discs with superglue. The average surface roughness at room temperature of the samples polymerized against a glass slide was 7$\pm$3 nm, as measured with the AFM in contact mode. Quasi-static nanoindentation was carried out on the samples using a nanoindenter (Triboscope-Hysitron, Inc., Minneapolis, MN) with a Berkovich tip (a three-sided pyramidal diamond tip). The instrument is enclosed in an environmental isolation chamber in order to reduce external interferences. A peak load of 5 mN with a loading/unloading rate of 500μN/s, and a hold time of 2 s at the maximum load was used. A maximum drift rate of 20 nm/s was set for the experiment. Four 3 x 3 arrays of indents were performed on each material sample. The indentations were performed in the central regions of the polymer samples to eliminate edge effects. Load-depth curves were analyzed for each of the 36 indents using the Oliver-Pharr model to determine the reduced modulus (Er) and the hardness (H) of the DEGDMA-co-tBA samples. Er was extracted from the 20% to 95% of the incipient unloading curve, while H was derived from Equations 1 to

3. Further, the results from the four 3 x 3 arrays were averaged, and the mean and standard deviation found for each wt% crosslinker. The dissipation energy was calculated from the area enclosed by the loading and unloading curves for each wt% crosslinker using MATLAB. Standard ASTM samples were laser-cut for tensile testing. The edges of the laser-cut samples were trimmed with sandpaper. The samples were then tested with a 2 kN load cell using an MTS Insight 2(MTS Systems, Eden Prairie, Mn) tensile tester at an applied displacement rate of 3 mm/s. An average of five results for each crosslinker concentration was taken. The indented samples were transferred to the AFM (Asylum Research,Santa Barbara, CA) for the measurement of indent profile during heated recovery. The indents were first located and imaged, and a scan of the surface profile was then performed as a function of increasing temperature at a rate of 1 ℃/min from room temperature to a temperature above the T_g of the material until the indents were fully recovered. The topography of indents at each temperature was analyzed with the Asylum Research software. The difference in height between the highest crest and the lowest trough was recorded as the peak-to-peak height of the indents. Table 1 depicts the nomenclature of material mixtures used in the present experiment.

4.3 Results and Discussion

Dynamic mechanical analysis (DMA) thermograms measured for the DEGDMA-co-tBA samples in tensile mode is shown in Figure 4.3. The figure demonstrates that the glass transition temperature, T_g, and rubbery modulus, E_r,of the material vary appreciably with crosslinker percentage, while the glassy modulus remains relatively constant within experimental error (more detailed glassy modulus data to be shown in latter graphs). The storage modulus in Figure 4.3 is approximately 3 MPa at temperatures less than T_g and then proceed through a transition to the rubbery regime above T_g. A controlled variation in T_g and E_r is fundamental to the use of a polymer network in shape memory applications. It is evident from Figure 4.3 that a rubbery plateau is absent for the thermoplastic material, 100tBA, as it has no chemical or significant physical crosslinks. Instead of a rubbery plateau, the material flows after going through the glass transition, characteristic of a single-phase

	Concentration of constituents (wt%)			ß Erubbery (GPa)		**Crosslink**
Material name	DEGDMA	PEGDMA550	tBA	@448 K	density (nm-3)	spacing(nm)
100tBA	0	0	**100**	NA	NA	NA
10DEG90tBA	**10**	0	**90**	2.5	0.135	1.95
20DEG80tBA	**20**	0	**80**	6	0.323	1.46
50DEG50tBA	**50**	0	**50**	14	0.755	1.09
100DEG	**100**	0	0	NA	9.63*	0.47
25DEG25PEG50tBA	**25**	**25**	**50**	11.5	0.62	1.17

Table 1: Nomenclature and crosslink density/spacing for all materials in the present experiment are displayed here

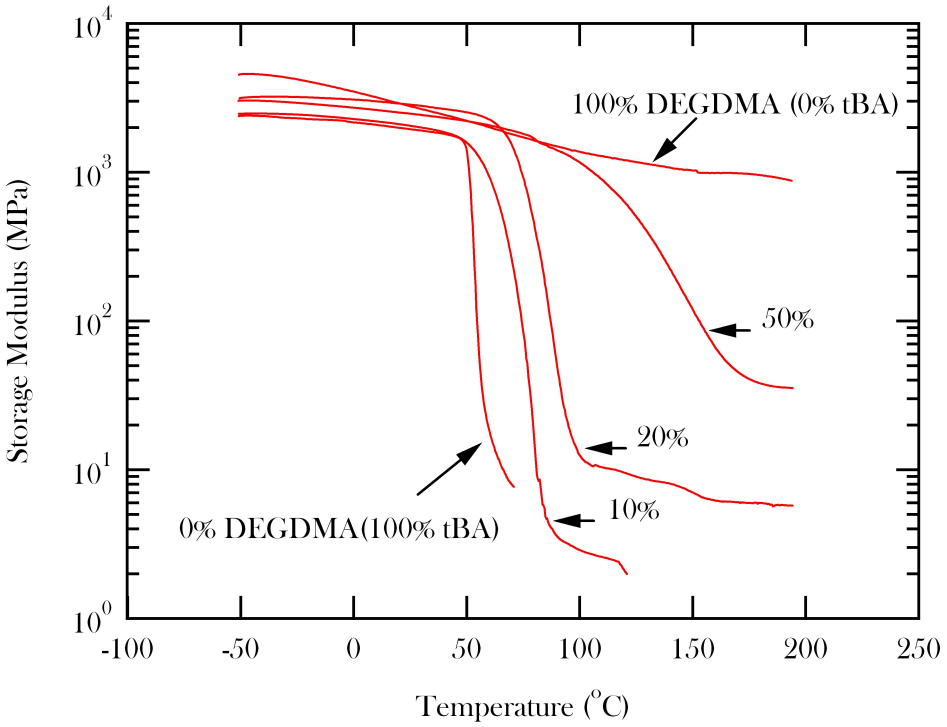

Figure 4.3: Dynamic mechanical analysis thermograms for the materials used in this section.

amorphous thermoplastic.

It is also observed in Figure 4.3 that there is no transition to a rubbery state for 100DEG. The lack of glass transition for the highly crosslinked 100DEG is due to the significant density of crosslinking imparted by the short di-functional DEGDMA molecules, as evident in Table 1. Such a heavily crosslinked network is relatively immobile at all temperatures since chemical netpoints are in close vicinity. In between these extremes, the addition of the di-functional crosslinking agent to the linear tBA material results in a systematic increase in the glass transition temperature. For the short DEGDMA crosslinker, the increase in T_g comes principally from the local restriction to coordinated conformational motions at network points. As the density of network points increases, the effective volume of material restricted from coordinated conformational motion increases, and the material gradually loses the ability to create appreciable free volume with a temperature change, and its glass transition disappears. It is important to note that T_g of all the polymers (those with a definable T_g) are above ambient temperature (25 °C) as illustrated in Figure 4.5. In addition

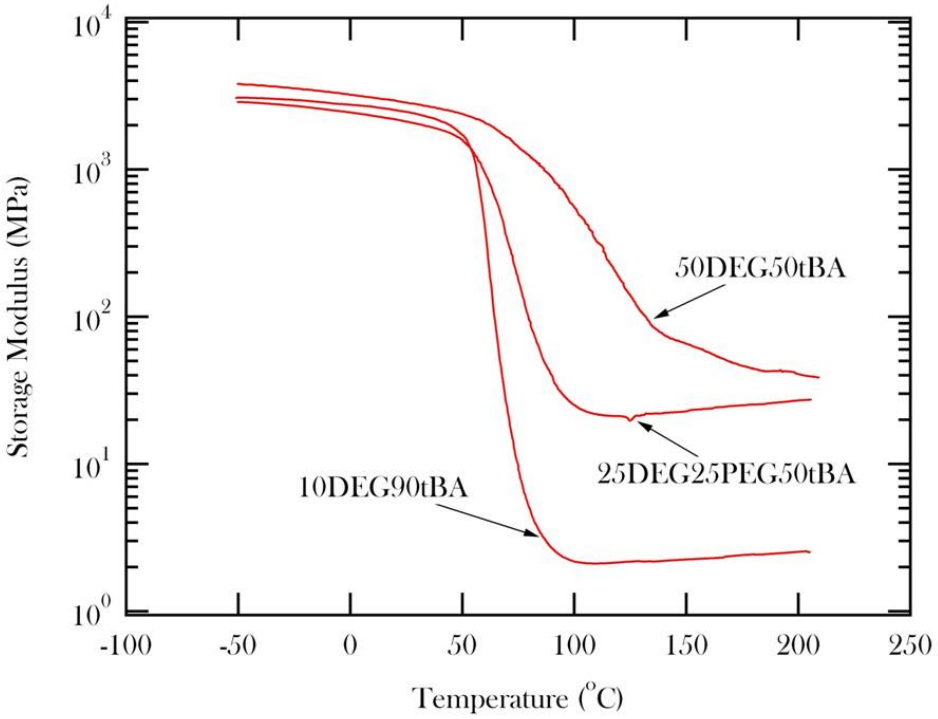

Figure 4.4: Comparison of the thermomechanical characteristics of 10DEG90tBA, 50DEG50tBA and 25DEG25PEG50tBA. It is realized that 10DEG90tBA and 25DEG25PEG50tBA have similar Tgs, and the rubbery modulus of 25DEG25PEG50tBA and 50DEG50tBA are in close proximity.

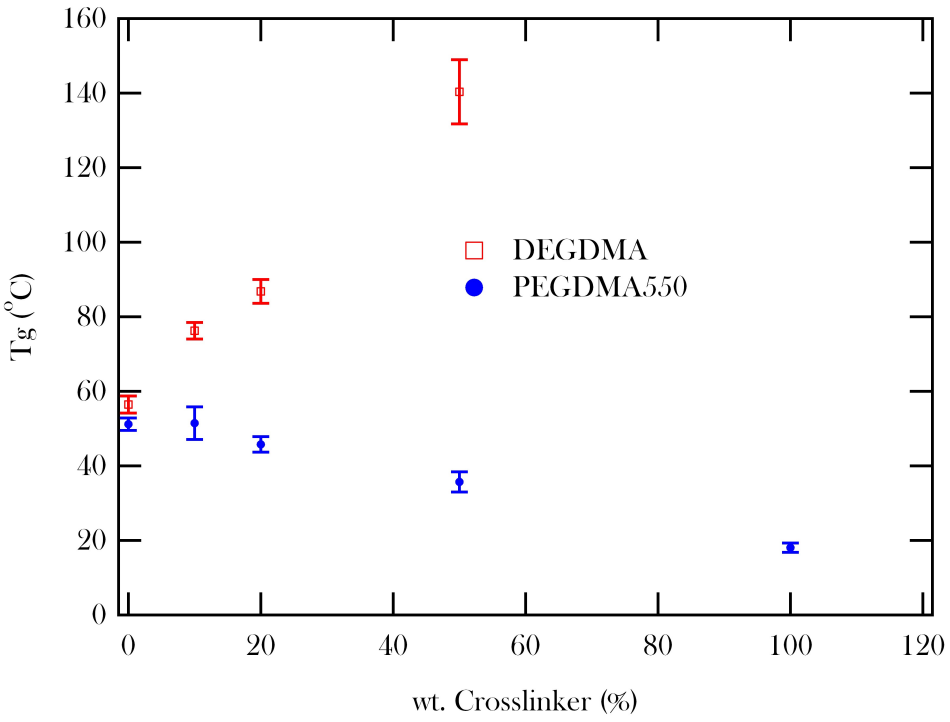

Figure 4.5: Comparison of the thermomechanical characteristics of 10DEG90tBA, 50DEG50tBA and 25DEG25PEG50tBA. It is realized that 10DEG90tBA and 25DEG25PEG50tBA have similar T_gs, and the rubbery modulus of 25DEG25PEG50tBA and 50DEG50tBA are in close proximity.

to a shift in the glass transition temperature, increased DEGDMA crosslinker concentration results in an increase in the rubbery modulus plateau (4.3). The increase in rubbery modulus is driven by an average shortening of the elastically active chain length between chemical netpoints. From the theory of rubbery elasticity, $E_r = 3kT\nu_e$ where k is the Boltzmann's constant, T is the temperature corresponding to the DMA rubbery modulus, and ν_e is the crosslink density. Table 1 is a compilation of ν_e for the various wt% crosslinkers used in the present study. The table also includes a calculation of the crosslink spacing between molecules for all materials with a definable rubbery modulus, based on the premise of uniform crosslink distribution. According to , estimation of crosslink parameters from the rubbery modulus of highly crosslinked materials is not recommended. It should be noted here that the crosslink spacing and density for 100DEG was estimated from a molecular size of 4.7 Å, as reported in . It is evident from the table that the crosslink spacing decreases with an increase in wt% crosslinker, as expected for the DEGDMA-co-tBA series of materials.

The results in Figure 4.3 represent the influence of increasing crosslinking in tBA without a significant co-polymer effect, due to the short length of the DEGDMA crosslinking molecules. The pure crosslinking effect leads to both an increase in glass transition temperature and rubbery modulus with increasing cross linker addition. It is possible to counterbalance the cross linking effect with a co-polymer effect by lengthening the cross linker through the use of PEGDMA 550. By replacing a fraction of the DEGDMA, with PEGDMA, the rubbery modulus will remain relatively constant, while the T_g will decrease relative to use of pure DEGDMA due to the lower glass transition temperature of PEGDMA. The aforementioned effect allows one to separate the effects of glass transition and rubbery modulus on nanomechanical properties, since these two effects are convoluted in the materials in 4.3. In Figure4.3 we present a representative storage modulus curve for a new material, 25DEG25PEG50tBA, where 25% of the DEGDMA has been replaced by 25% PEGDMA. This new material has a glass transition onset similar to the 10DEG90tBA material (see Figure 4.4 for averaged T_g data), but a rubbery modulus plateau approaching the 50DEG50tBA material. Comparison amongst these three materials allows evaluation of the relative role of T_g versus E_r during interpretation of nanoindentation results.

In nanoindentation, an accurate extraction of the area function is central to determining nanoscale material parameters such as hardness and reduced modulus. As a result, the selection of a standard material for the calibration of the indenter tip is paramount . The use of the fused silica (quartz) calibration standard, often used for hard materials, has been shown to provide inadequate results for polymers . The researchers in proposed the use of a standard with properties close to that of the materials under study, hence our choice of PC whose properties are in the vicinity of the polymers used here. displays load-depth curves of the standard materials considered in this research. Generally, the steeper the slope of the unloading portions of an indentation curve, the stiffer the material. Material hardness can be inferred from the load depth curve through a steeper loading curve and a small residual depth at the point of unloading. It is seen from this figure that quartz is the stiffest, whereas PMMA and PC have similar stiffness. PC was chosen over PMMA as the nanoindentation data of PC does not change appreciably with loading rate at room temperature . Moreover, PC's hardness and modulus are within the vicinity of the polymer networks used in this investigation, which are slightly softer than PMMA. Figure 4.7 displays the area function for a perfect uncompensated Berkovich tip, along with area functions based on elastic modulus fits to quartz and PC standards. In particular, these results illustrate the possible margins of error which may be incurred as a result of assuming a perfect tip, and choosing a standard calibration material with nanomechanical properties different from the materials under study.

Berkovich indentation load-depth curves representing various wt% DEGDMA-co-tBA samples at a maximum load of 5 mN are presented in Figure 4.8. Results from studies at different indentation depths and loads will be presented in future work. Based on analysis of multiple load-depth curves, the nanomechanical properties of the networks demonstrate a statistically significant dependence on crosslink density at ambient temperature. At elevated temperatures, the networks would possess an even more significant difference in nanomechanical properties due to their differences in glass transition temperatures, an effect that is sometimes overlooked in indentation studies on various polymers. In Figure 4.9, we compare the load-depth curves of 10DEG90tBA, 50DEG50tBA, and 25DEG25PEG50tBA. There is also a difference in the nanomechanical properties of the materials in Figure 4.9,

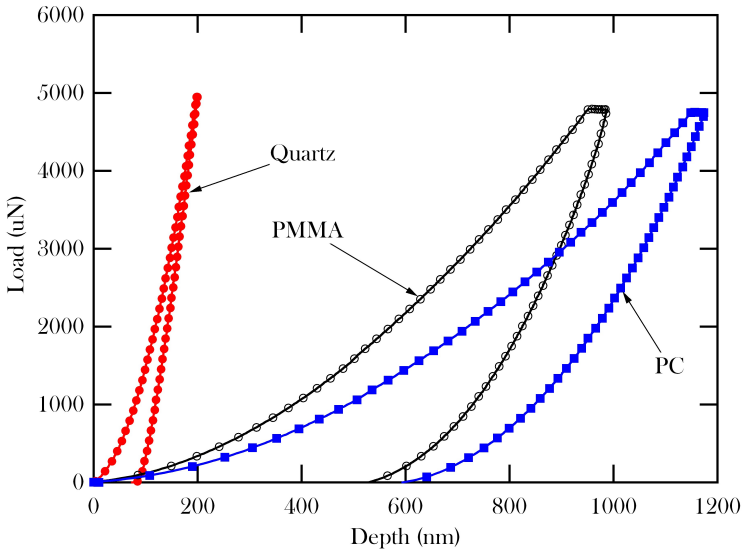

Figure 4.6: Standard materials used for calculating the area function of the Berkovich tip. Polycarbonate (PC) has a modulus in the vicinity of that of the DEGDMA-co-tBA polymers and was chosen as the standard for the calculation.

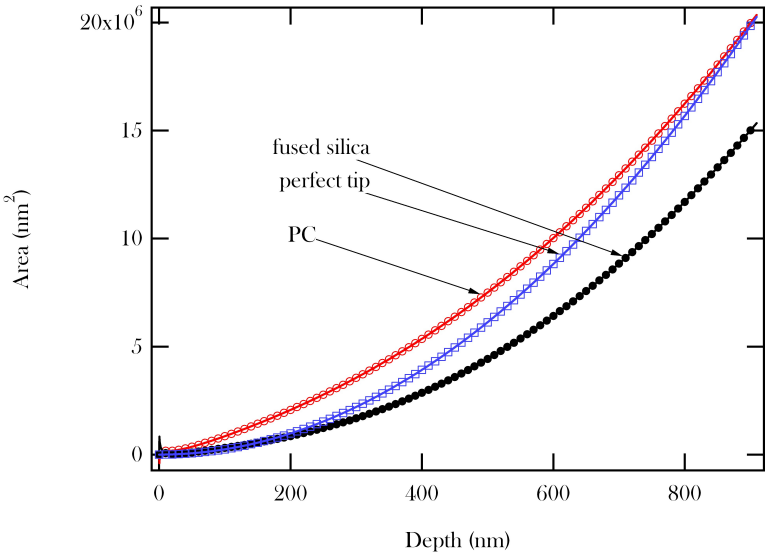

Figure 4.7: Plots of calculated area functions based on the assumption of a perfect Berkovich tip, quartz and PC. The area function is pivotal in the determination of material properties such as elastic modulus and hardness.

which have controlled differences in E_r and T_g. From the data in Figure 4.8, one would generally conclude that the materials become harder at ambient temperature (load depth curves shift left and/or intersect at shallower depths at zero load) as crosslinking density is increased. However, relating this increase to fundamental properties of the polymer networks (E_r and T_g) is difficult since both E_r and T_g increase with increasing DEGDMA crosslinker concentration. The results in Figure 4.9 help to separate out the effects of E_r and T_g on nanoindentation response. In particular, Figure 4.9 indicates that the glass transition temperature is more significant than the rubbery modulus as a predictor of the materials response to nanoindentation in the glassy state. The drop in the glass transition temperature of the 25DEG25PEG50tBA (see 4.5) results in considerable drop in hardness compared to the 50DEG50tBA even though these two materials have comparable crosslink density measured through rubbery modulus. Moreover, the hardness (vis-a-vis max and min penetration depths) of the 25DEG25PEG50tBA material is slightly lower than the 10DEG90tBA despite the higher crosslink density and rubbery modulus in the former material (both have a similar glass transition). This quantitative trend will be clearer in subsequent data analysis, although it is insightful to consider qualitative trends in the load depth curves since these interpretations do not involve the assumptions inherent to quantitative analysis.

We have performed subsequent analysis on the load depth curves shown in Figure 4.8 and 4.9 to quantify various trends in indentation data, and provide statistical information. The analysis includes all data from duplicate experiments to quantify statistical variability. The indentation hardness, calculated from Equations 1 to 3, as a function of crosslink density is shown in Figure 4.11 while the modulus as a function of cross linker is shown in 4.10. The error bars in Figures 4.11 and 4.10 represent one standard deviation from the dataset mean. The inherent variations in both the hardness and modulus data can be partially driven by inhomogeneities in the material structure, due to material preparation. Previous work elucidates the effects of material preparation on the mechanical properties of polymers. The data in Table 1 shows that the maximum crosslink spacing is less than 2 nm. Given the radius of the Berkovich tip (150 nm) and the depth of penetration into the surface (1000 nm) the stress zone beneath the nanoindenter tip samples a statistically significant

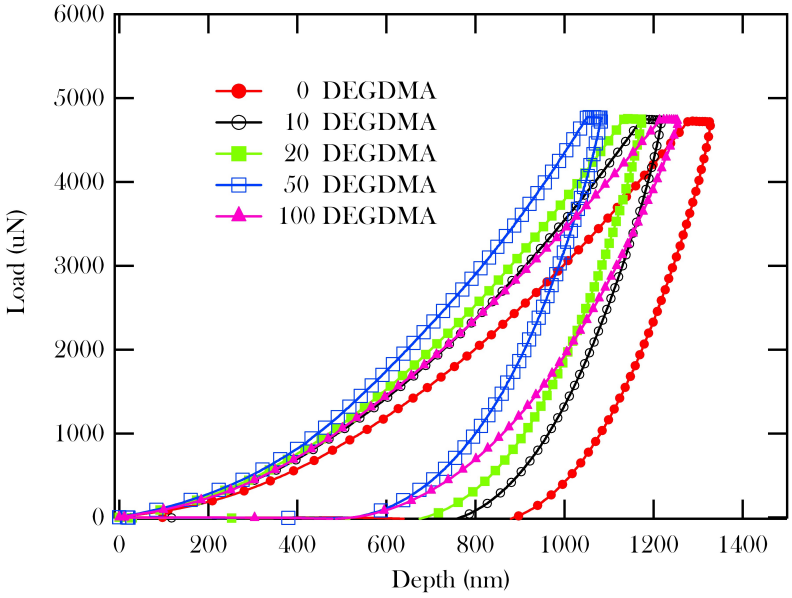

Figure 4.8: Representative load-depth plots of indentations at a maximum load of 5 mN on the DEGDMA-co-tBA samples.

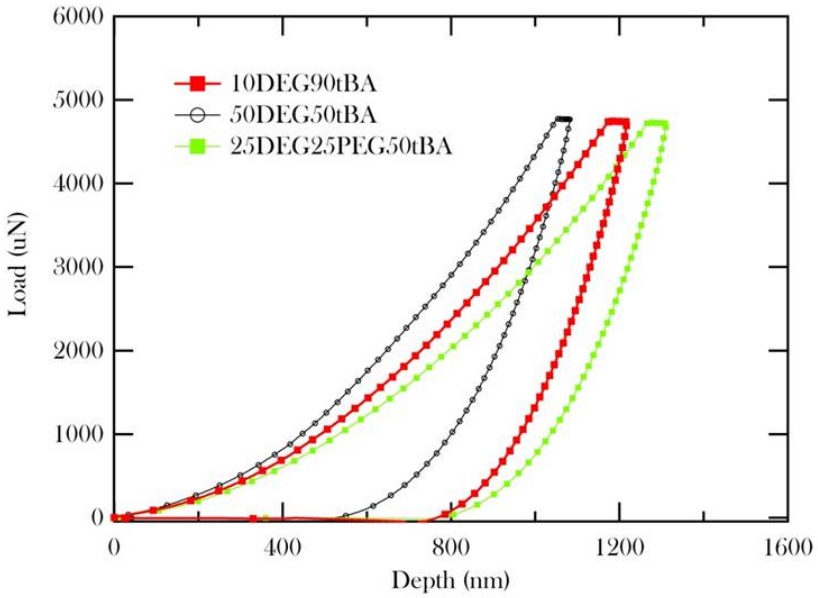

Figure 4.9: Juxtaposition of the nanoindentation curves of 10DEG90tBA, 50DEG50tBA and 25DEG25PEG50tBA.

fraction of crosslinks at maximum load, a region that likely characterizes a representative volume element for this material. Aside from material and surface factors, measurement uncertainty can be derived from the incipient unloading part of the indentation curve . One possible explanation for the uncertainty in the slope determination is the creep-viscoelastic properties inherent in polymers at the start of unloading. Similar patterns have been reported in the literature . A trapezoidal loading-unloading curve was used to minimize this effect, as prescribed in .

Given experimental error, statistically significant trends exist in ambient temperature hardness, but not modulus, as a function of pure (DEGDMA) cross-linking. The elastic moduli extracted from nanoindentation are juxtaposed with measurements of modulus from tensile tests in 4.10. While the ambient temperature nanoindentation modulus does not follow any statistically significant behavior with respect to increasing crosslink density, there is a slight trend of increasing modulus with increasing crosslink density in the tensile modulus data. Interestingly, the scatter in modulus data is significant for both the tensile and nanoindentation tests, although both techniques provide values that are in general agreement.

It is observed that as the crosslink density increases (crosslink spacing decreases), the hardness of the materials increases (Figure 4.10). This finding is due to the fact that for smaller crosslink spacing, the chains are restricted from conformational motion due to the increasingly immobile network (a phenomenon that also increases T_g). In order to achieve large strain deformation required for a permanent impression below the glass transition temperature, the polymer chains must experience conformational motion, which is more difficult for higher cross linked materials based on the measured increase in glass transition temperature. Consequently, the smallest crosslink spacing for 100DEG renders it the hardest of the materials in the present investigation, while the uncrosslinked material, 100tBA, is the softest.

From the DEGDMA data in Figure 4.11, it is clear that increasing cross-link density increases hardness, but it is unclear how to relate this increase to fundamental polymer properties since glass transition and rubbery modulus of the DEGDMA networks both increase with increasing cross linker. Both rubbery modulus and glass transition temperature could

potentially influence hardness data since both are linked to the ability of the materials to undergo conformation motion at a given temperature and stress, and both can be signatures of changes in crosslink density. Consistent with representative load-depth curves, the hardness of the 25DEG25PEG50tBA materials is significantly lower than the 50DEG50tBA and slightly lower than the 10DEG50tBA material (Figure 4.11). This important trend highlights the importance of T_g relative to the testing temperature, which is apparently more significant than the rubbery modulus in indentation response below glass transition. Consequently, the increase in hardness observed in Figure 4.11 scales more with T_g with increasing DEGDMA rather than just cross-link density itself (measured via rubbery modulus). In fact, increasing cross link density and rubbery modulus without influencing T_g has little effect on hardness (compare 10DEG50tBA and 25DEG25PEG50tBA which have similar T_g but much different rubbery modulus). This hypothesis is consistent with the flow behavior of glassy polymers below their glass transition temperature, where the slope of the hardening modulus during flow is more dependent on the vicinity to T_g rather than factors that control entropic elasticity and conformational stiffness.

The enclosed area between the loading and unloading curves is defined as the energy of dissipation , and is shown in Figure 4.12 as a function of cross-linker fraction. Once again, the error bars are within one standard deviation of the mean. The energy dissipation is another tool that can be used to compare the different materials. Since the materials used in this study show elasto-plastic characteristics as depicted in Figures 4.8 and 4.9, it is expected that some energy will be dissipated as a result of the plastic deformation. It is evident from Figure 4.12 that there is an inverse correlation between the dissipation energy and the wt% of crosslinking. As a result, the recoverable energy increases with increasing crosslinking. This finding may be explained in terms of the formidable opposition offered to conformational motions by the crosslinker molecules . Of course, the energy dissipation is strongly dependent on the vicinity of the polymer to its glass transition temperature, where it shows maximum loss during cyclic loading and unloading. Consequently, the change in dissipation with increasing crosslinking can also be linked to the change in the glass transition temperature of the network.

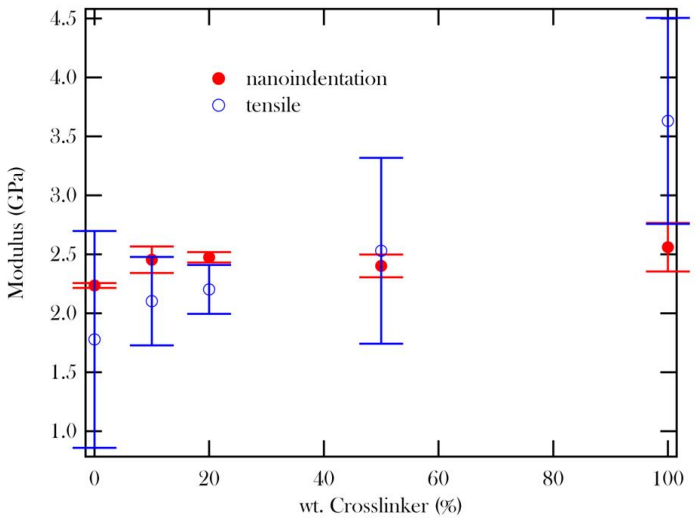

Figure 4.10: Modulus as a function of weight percent crosslinker. Statistical distribution of the nanoindentation and tensile modulus as a function of the weight percent of DEGDMA crosslinker within one standard deviation from the mean.

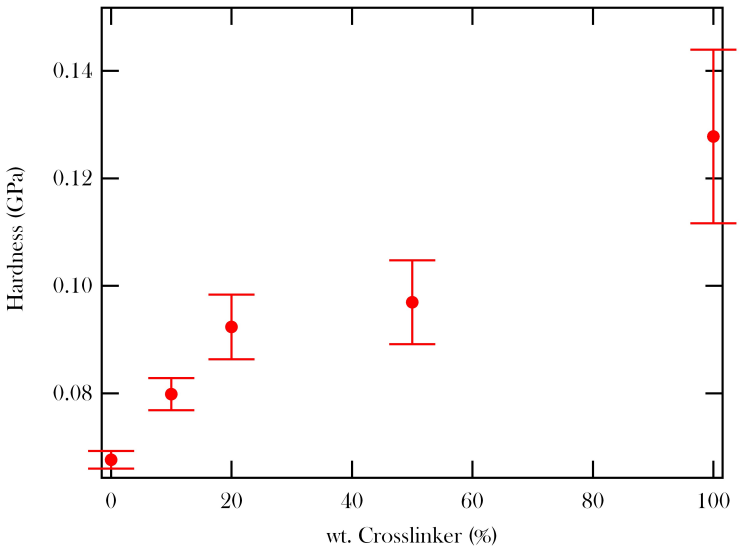

Figure 4.11: Hardness as a function of weight percent crosslinker within one standard deviation from the mean.

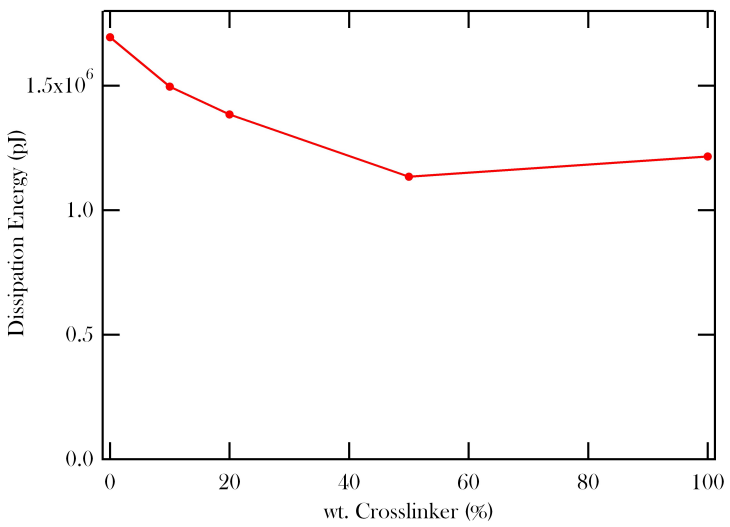

Figure 4.12: Dissipation energy as a function of crosslink wt%.The error bars are within a standard deviation from the mean.

The present results highlight the importance of considering differences in glass transition temperature relative to testing temperature when evaluating nanoindentation data. It is obvious that indentation response as a function of temperature will depend very strongly on the overall location of the testing temperature with respect to the glass transition (glassy, viscoelastic, versus rubbery). However, the results here indicate that below the glass transition temperature, hardness (not modulus) depends on vicinity to the glass transition temperature. This effect can cause a limitation when probing polymer structure or chemistry effects in polymers that have varying glass transition accompanying their structural changes or a glass transition temperature that varies with film thickness or near the material surface. Or, conversely, this effect may be useful for estimating changes in transition temperature in small volumes of material that can not have transition temperatures measured using conventional methods.

Recovery of the indents created at ambient temperature was studied for a constant heating rate using atomic force microscopy. Representative tapping mode AFM topographical scans of the indents are presented in Figure 4.15 for 100DEG and 50DEG50tBA. Similar images were obtained for all materials. Figure 4.16 displays the indent peak-to-peak height sweeps and normalized peak-to-peak heights with respect to the initial room temperature

indent height. Figure 4.17 presents the measured and normalized recovery volume as a function of temperature for the DEGDMA crosslinked material. The scans show recovery as the temperature is ramped. At temperatures in proximity to or in excess of T_g, the stored intermolecular forces between crosslinks act through an increase in free volume, allowing a reduction in stored entropy culminating in the recovery of the deformed material. The recovery occurs at lower temperatures for materials with less cross-linking density and lower glass transition temperature, as expected based on results herein. Within measurement resolution, the materials recover all the imposed permanent deformation at a temperature in the vicinity of their T_g.

A similar recovery pattern is observed in Figure 4.15, for the 10DEG90tBA, 50DEG50tBA, and 25DEG25PEG50tBA materials. Here, higher temperatures are required to recover the impressions in the 50DEG50tBA material relative to the other two due to its higher glass transition temperature. The similarity between the recovery profile of the 10DEG90tBA and the 25DEG25PEG50tBA indicate that the rubbery modulus is not strongly influencing the free strain recovery, even though the higher rubbery modulus does provide additional entropic driving force during recovery. The additional entropic driving force present during free recovery is apparently not significant enough to alter free strain recovery profile in light of the large effect of temperature on free volume, which enables the entropic effect to act. However, it should be noted that the 25DEG25PEG50tBA material with higher crosslink density and rubbery modulus should provide larger force during constrained recovery, although this effect was not explored here.

4.4 Summary

We have investigated the dependence of the bulk and nanomechanical properties of shape memory polymer networks on crosslink density. This research provides a foundation to understand and further explore the nanomechanical behavior of shape memory polymers. The following primary conclusions have been drawn.

The ambient temperature modulus showed a slight, but statistically insignificant dependence on the crosslinker concentration measured using both nanoindentation and tensile

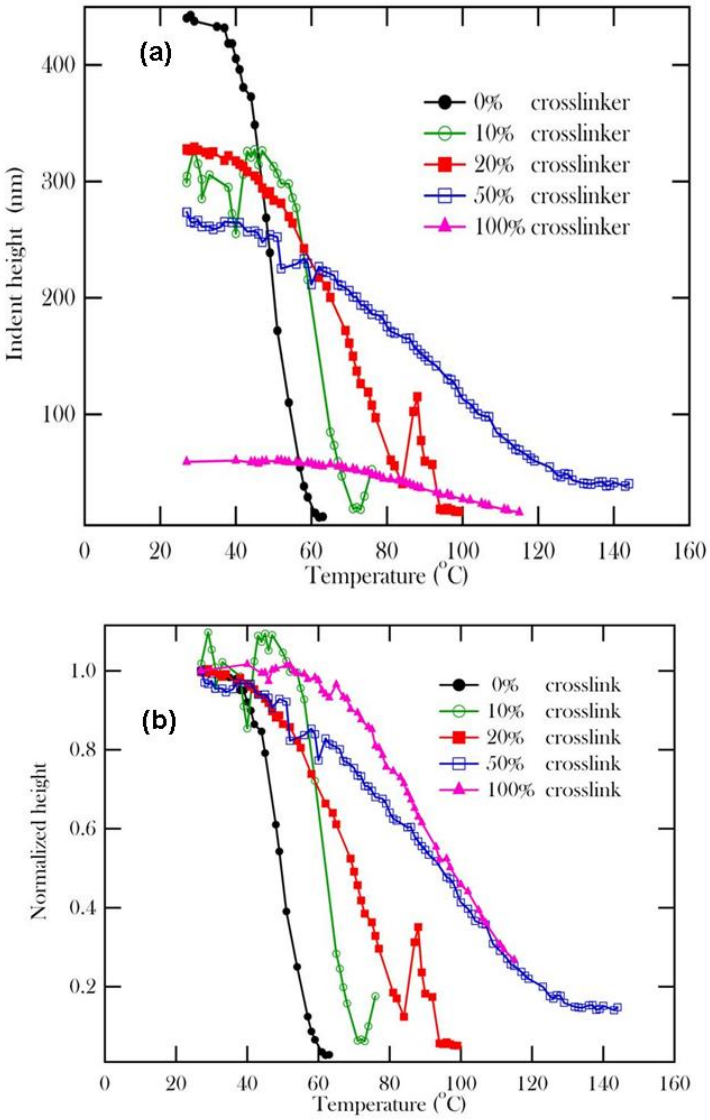

Figure 4.13: (a) Evolution of indent peak-to-peak height with temperature. (b) The normalized peak-to-peak height with respect to the peak-to-peak height at room temperature.

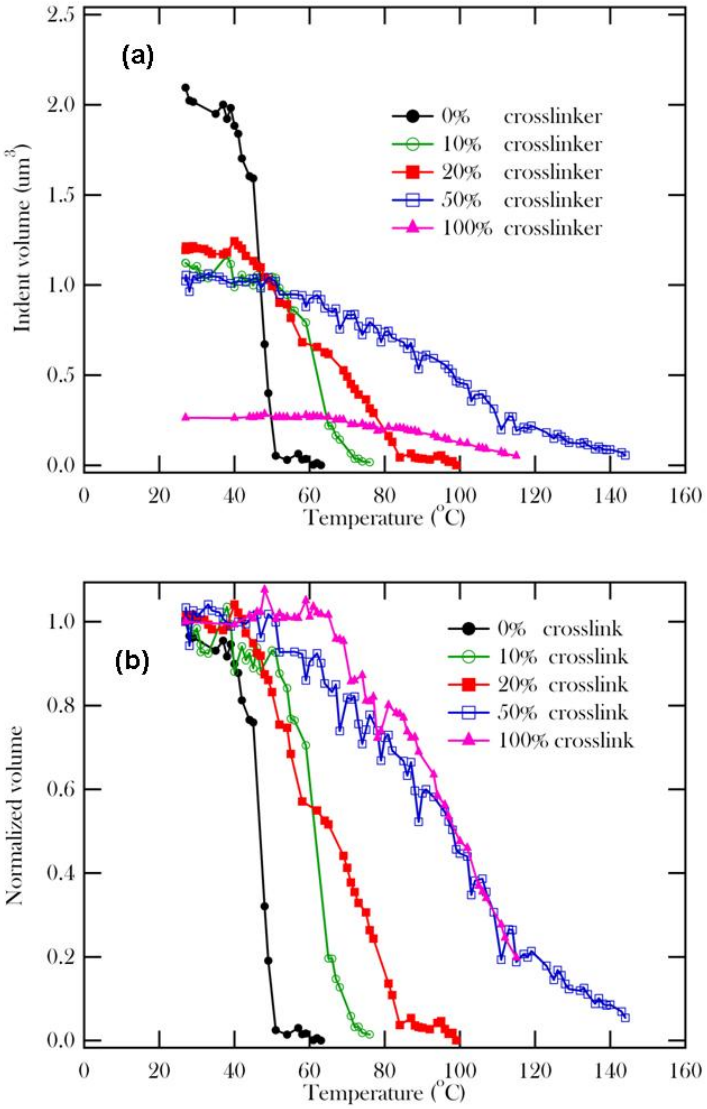

Figure 4.14: (a) Calculated indent volume based on indent height sweeps. (b) Normalized peak-to-peak volume with respect to the peak-to-peak volume at room temperature.

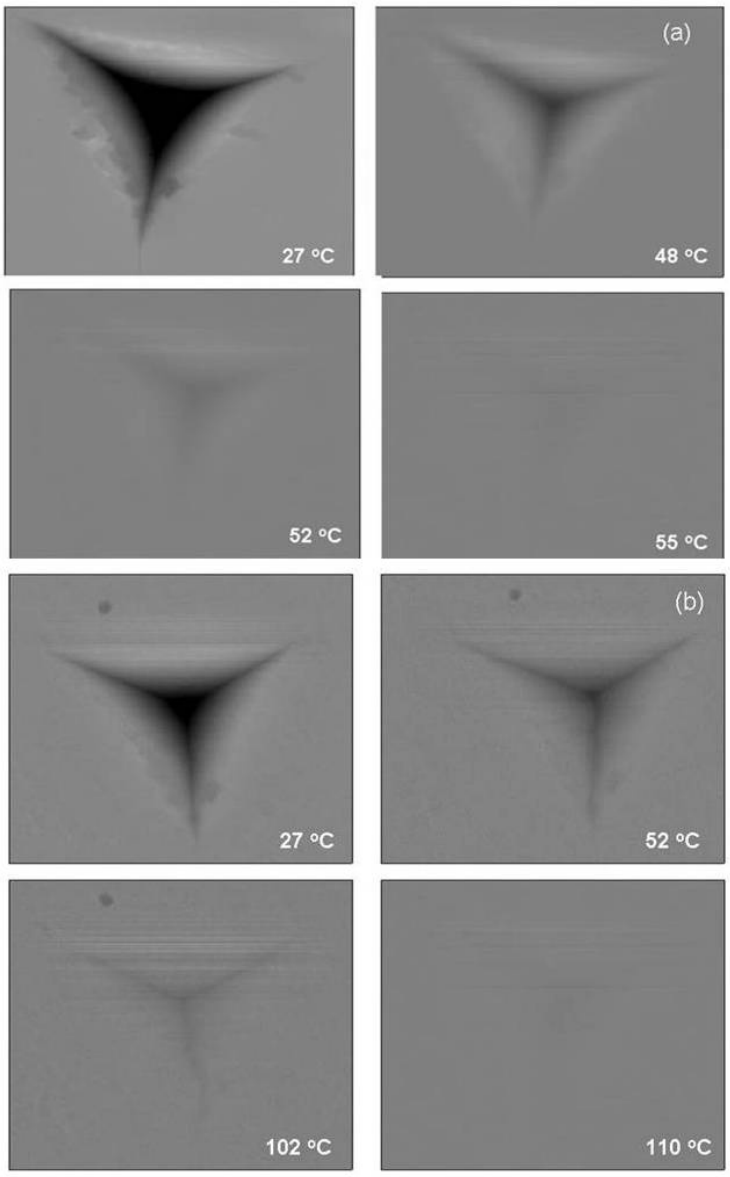

Figure 4.15: Tapping mode AFM images showing evolution of shape recovery from room temperature to the recovery temperature for (a) 100tBA, and (b) 50DEG50tBA.It is noted that the indents shrink as temperature is increased. The indents eventually diminish in the vicinity of T_g for each material.

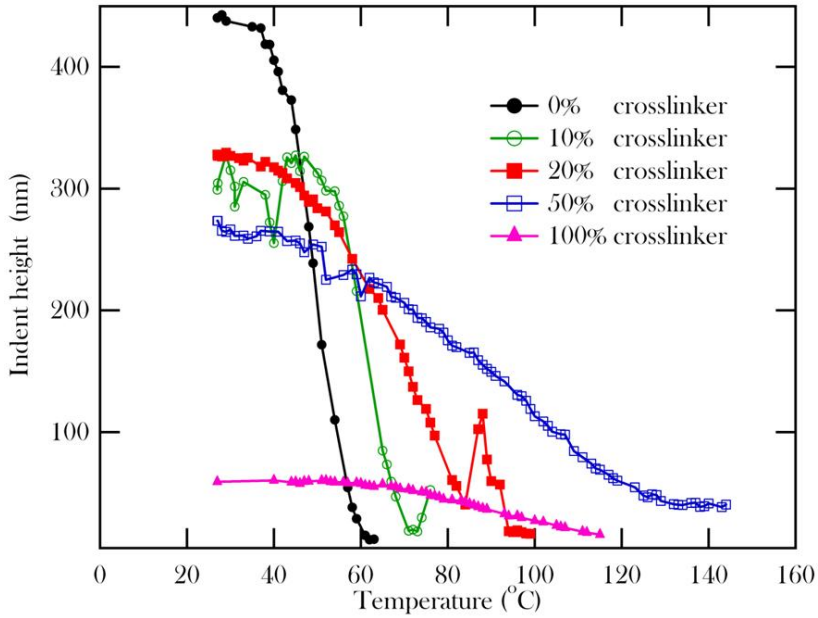

Figure 4.16: Indent height sweeps.

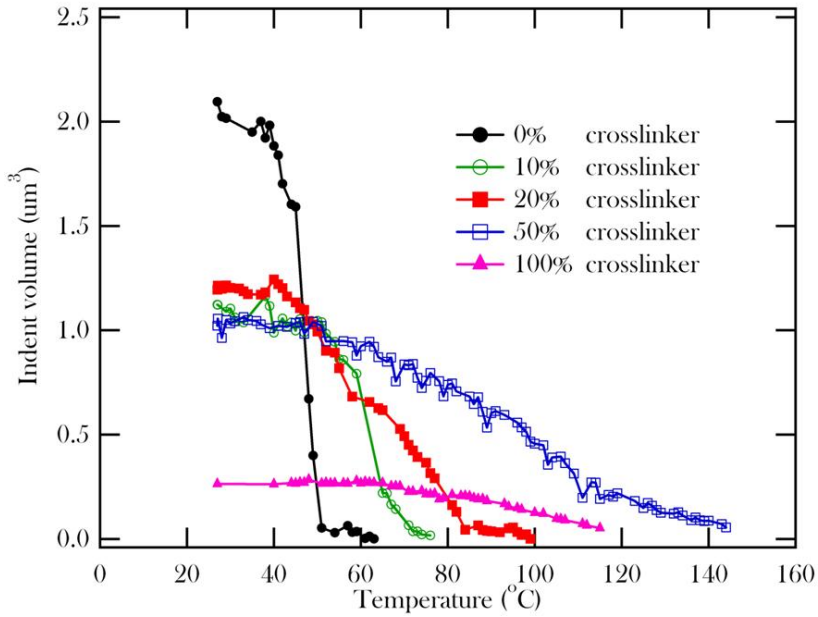

Figure 4.17: Calculated indent volume based on indent height sweeps of DEGDMA-co-tBA materials. The figure on the right is the normalized peak-to-peak volume with respect to the peak-to-peak volume at room temperature.

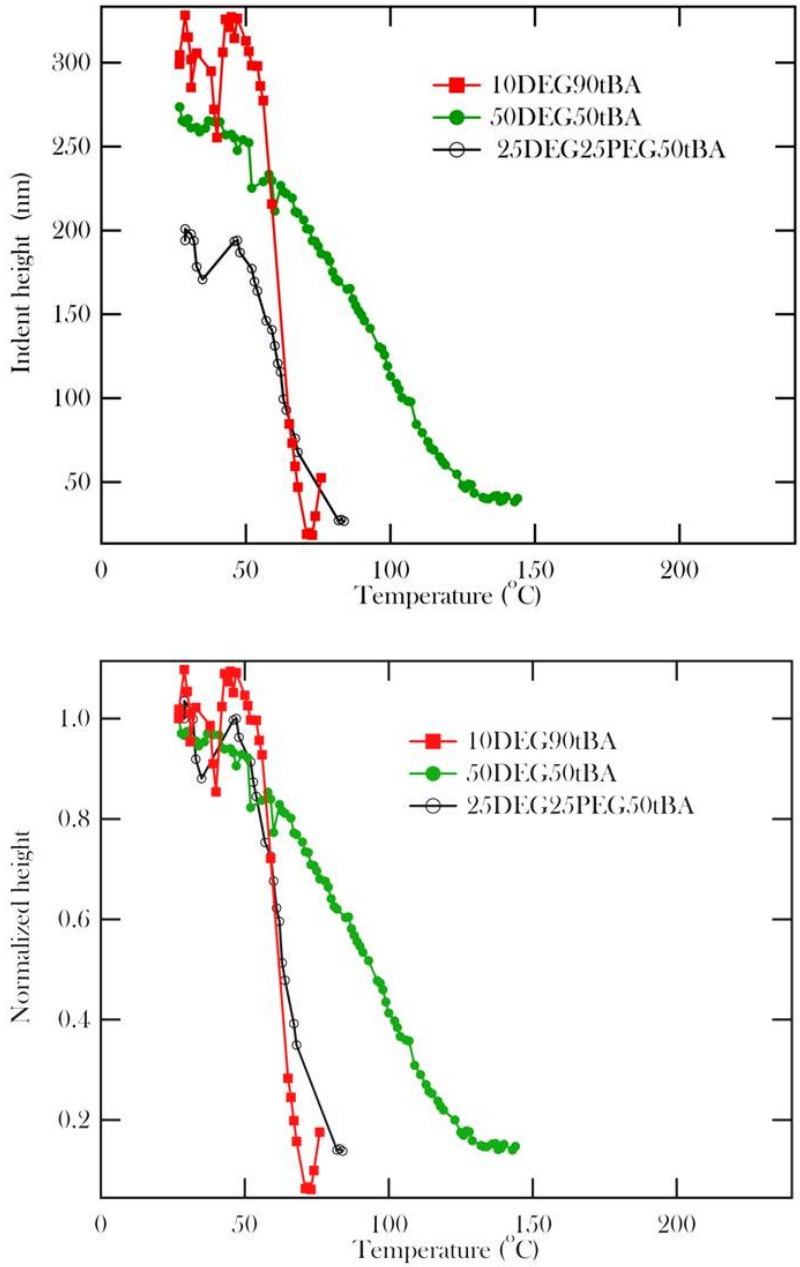

Figure 4.18: Evolution of indent peak-to-peak height with temperature for the 10DEG90tBA, 50DEG50tBA, and 25DEG25PEG50tBA. The figure on the right is the normalized peak-to-peak height wrt to the same.

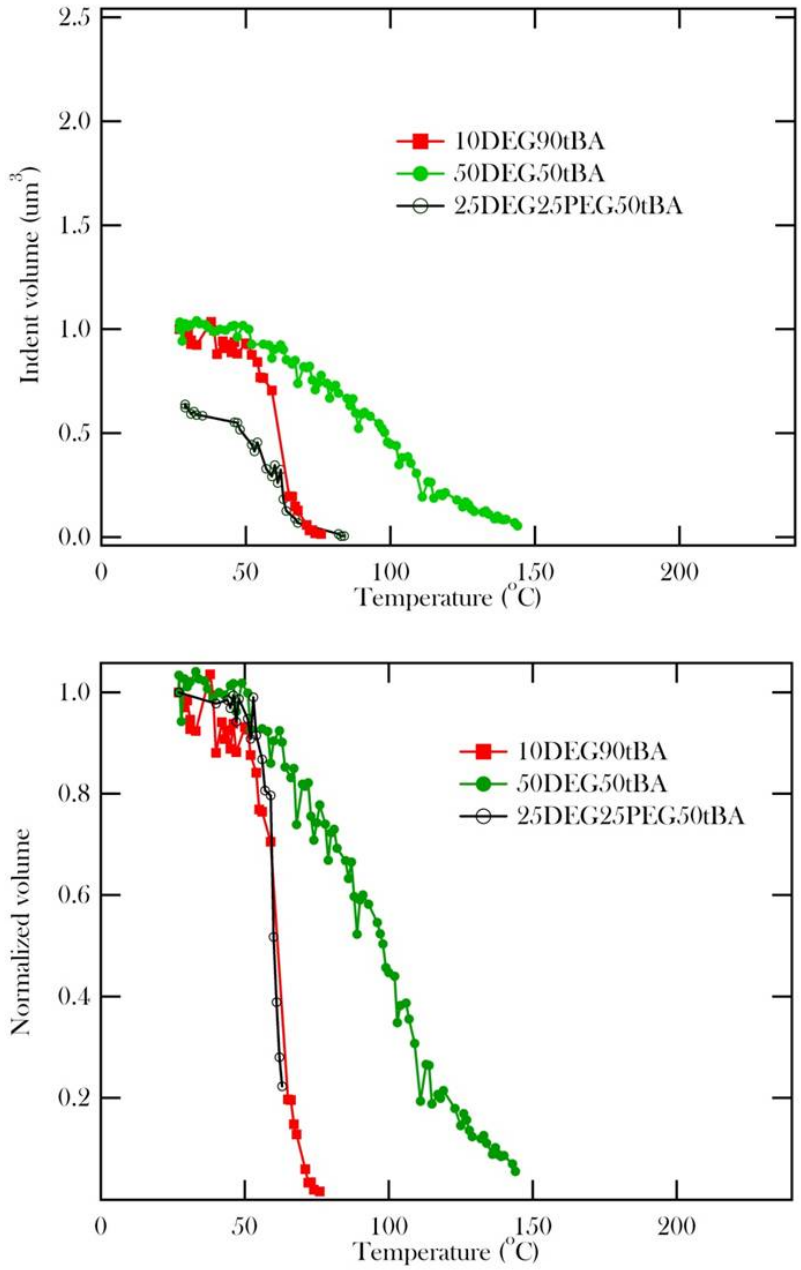

Figure 4.19: Calculated indent volume based on indent height sweeps of 10DEG90tBA, 50DEG50tBA, and 25DEG25PEG50tBA. The figure on the right is the normalized peak-to-peak volume with respect to the peak-to-peak volume at room temperature.

testing. The ambient temperature hardness showed a statistically significant increase as a function of cross linker concentration. Using a designed material, the increase was show to correlate to glass transition temperature rather than rubbery modulus. All indents showed recovery during heating above their glass transition temperature. Free strain recovery temperature was strongly influenced by crosslinker concentration through changes in glass transition temperature but not rubbery modulus.

REFERENCES

[1] Cleon, D. E. and May, G. S., "Neural network control of variable-frequency microwave processing of polymer dielectric curing," *IEEE Transactions on Electronic Packaging Manufacturing*, pp. 1521 – 334X, 2008. article.

[2] Gall, K., Kreiner, P., Turner, D., and Hulse, M., "Shape-memory polymers for microelectromechanical systems," *Microelectromechanical Systems, Journal of*, vol. 13, no. 3, pp. 472–483, 2004.

[3] Madden, J. D. and Filipozzi, L., "Web-based actuator selection tool," *Proceedings of SPIE - The International Society for Optical Engineering*, vol. 5759, pp. 9 – 15, 2005. article Dielectric elastomers;Ferroelectric polymers;SMA;Carbon nanotube actuators;Liquid crystal elastomers;IPMC;.

[4] Maitland, D. J., Wilson, T., Schumann, D. L., and Baer, G., "Laser-activated shape memory polymer microactuators for treating stroke," *Lasers and Electro-Optics Society, 2002. LEOS 2002. The 15th Annual Meeting of the IEEE*, vol. 1, pp. 359–360 vol.1, 2002. article.

[5] Wei, G. H., Bhushan, B., Ferrell, N., and Hansford, D., "Microfabrication and nanomechanical characterization of polymer microelectromechanical system for biological applications," *Journal of Vacuum Science and Technology A*, vol. 23, no. 4, pp. 811–819, 2005. article.

[6] Yu, Y. L. and Ikeda, T., "Photodeformable polymers: A new kind of promising smart material for micro- and nano-applications," *Macromolecular Chemistry and Physics*, pp. 1705–1708, 2005. article.

CHAPTER V

NANOSCALE INDENT FORMATION

5.1 Introduction

A broad range of microsystems rely on organic actuatorsto perform critical functions [2, 4, 11, 15, 18, 22, 25–27, 30, 35, 36, 43, 44]. For example, tiny amounts of therapeutic drugs may be delivered from an active reservoir on-demand via shape memory effect [11, 15, 22, 30, 35]. In tissue engineering, an implant surface made from shape memory polymers may change topography during cell growth, providing a means to understand the cell dynamics, including, orientation, proliferation and differentiation [15]. Furthermore, shape memory polymers have the potential to provide accurate actuation in surgery, which is essential in the restricted environment [29–31]. The successful development of the emerging applications calls for detailed understanding of the thermomechanical characteristics of shape memory polymers. As mentioned in Chapter 2, shape memory polymers have the capability of changing their shape upon the application of external stimulus, and a change in shape caused by a change in temperature is called a thermally induced shape memory effect [24]. The first shape memory polymer was a block copolymer formulation by Mitsubishi Heavy Industries, commercialized as heat shrink tubing [4, 37]. The hard segments in the copolymer served as physical crosslinks and the soft segments underwent a local thermal glass transition from soft to hard to facilitate shape memory. The material showed a one-way shape memory effect caused by the rubbery to glassy transition of the soft segments. Since then, researchers have characterized and developed many amorphous polymers that show good shape memory by exclusive use of a thermal glass transition (rubbery to glassy), without use of local melting, or another bond forming/breaking mechanism. Some specific materials include epoxies [2] and acrylates [18], among others. The thermomechanical response of shape memory polymers is characterized by four critical temperatures. At the deformation temperature, T_d, the polymer is deformed into its temporary shape which, in turn, is stable over a certain period of time at a storage

temperature, Ts, below or equal to Td. When heated to a recovery temperature, Tr (typically in the vicinity of the glass transition temperature T_g, the polymer recovers its original shape. From a macroscopic viewpoint, a polymer may demonstrate a useful shape memory effect when it possesses a distinct and significant glass transition, a modulus-temperature plateau in the rubbery state and a large difference between the maximum achievable strain and the plastic strain after recovery [26, 27, 36]. The microscopic structures responsible for shape recovery are the 'memorable' network structure in thermosets, or the finite fraction of hard crystalline regions serving as physical crosslinks in thermoplastics. In crosslinked thermosets, the materials studied here, the recoverable deformation is facilitated by conformational chain motion, which is enabled at temperatures above T_g and limited at temperatures below T_g. The difference between an observed shape memory response and a viscoelastic response depends upon the recovery temperature. Regarding the storage of strains at temperatures below T_g, as long as the material is not experiencing another transition below T_g, the shape will be held indefinitely considering the timeframe of any reasonable experiment or application. In fact, one typically cools the polymer to temperatures below which time–temperature superposition is a valid means to predict timescales (they are significantly longer) based on data during deformation caused in the viscoelastic regime, as the relaxation mechanisms have fundamentally changed. At these low temperatures the entropy driven strain recovery forces are simply not enough to overcome the barrier for recovery (glassy chain interactions). For this reason, it is not reasonable to state that the deformation will recover given sufficient time; rather, the activation energy cannot be overcome to facilitate recovery characteristics. The strain storage and recovery behaviour of a shape memory polymer system must be well understood in order to tailor a device or process that can exploit the polymer properties. However, relatively little information is available for the strain storage and recovery at the nanometre scale, since most published reports focus on the shape memory effect in homogeneous bulk materials [12, 13]. Recently, nanoscale shape recovery was reported by Nelson et al [32] on an epoxy-based thermoset polymer. The results indicated that the extent of shape recovery was a function of the recovery temperature,and was not a strong function of time on the 1–30 min timescale. Xu et al [43] employed nanoindentation to measure the

mechanical properties of a silicone elastomer. A decrease in hardness of the polymer was observed at an annealing temperature of 80 °C. Van Vliet and coworkers [23, 24] investigated the contact creep compliance of viscoelastic materials at various temperatures. A detailed understanding of the nanoscale properties of shape memory polymers is lacking for most polymer systems, and the chapter aims to help in understanding this topic. This chapter reports an experimental investigation on the nanoscale strain storage in a class of tert-butyl acrylate (tBA) and poly ethylene glycol dimethacrylate (PEGDMA) based polymers using heated AFM probe tips. The material system is chosen for three reasons. First, using different concentrations and molecular weights of the PEGDMA crosslinker, the structure and thermomechanical properties of the tBA/PEGDMA copolymer system may readily be tailored over a wide range [13]. Another advantage of the tBA/PEGDMA system lies in the fact that acrylates undergo rapid and well-understood photopolymerization, which allows for easy patterning of the materials using methods such as photolithography and stereolithography [3, 5]. The acrylate and ethylene glycol based polymers also have a proven history in biomedical applications [34, 40]. The heated AFM cantilever technique was initially developed for data storage, where a silicon AFM cantilever with an integrated solid-state heater is in contact with a polymer substrate to perform thermomechanical data writing [6, 9]. By operating a large array of heated cantilevers in parallel [20, 28, 38], the technique can rapidly generate enormous amount of nanoscale indents in an energy efficient manner, which are critical characteristics for large scale practical applications. Compared to the nanoscale hot embossing technique, which is another tool for making batch nanoscale features [8, 19], the heated AFM cantilever approach possesses localized heating. An integrated heater as small as a few microns near the cantilever tip supplies the processing heat, eliminating the need to heat the entire embossing tool or polymer substrate. The heated thermal cantilever technique has been used in nano-thermal analysis (nano-TA) to determine the nanoscale thermomechanochemical responses of various material systems, including nanocomposites and polycrystalline materials [14, 21]. The nano-TA greatly enhances the spatial resolution provided by the micro-thermal analysis (micro-TA) [33]. Exploiting the localized heating

feature of the heated AFM cantilever technique, the current chapter provides a novel experimental study on the nanoscale deformation of the shape memory polymer networks under thermomechanical load. The quantitative knowledge obtained on the dynamics of nanoscale strain storage provides useful information for the design of nanoscale actuators based on shape memory polymers. The strain recovery of the shape memory polymers is reported in a separate publication. The next section discusses the current experimental details on the material's synthesis and thermomechanical formation of nanoindents. The results clearly show the size evolution of the nanoindents under various heating temperatures and times for the shape memory polymers studied.

5.2 Materials and experimental methods

Shape memory polymers were synthesized using tert-butyl acrylate (tBA) monomer, poly ethylene glycol dimethacrylate (PEGDMA) crosslinker and 2,2-dimethoxy-2-phenylacetophenone photoinitiator from Sigma-Aldrich in as-received condition. A monomer solution was obtained by manually mixing 1 wt% initiator and desirable portions of tBA and PEGDMA in a glass vial. Table 1 shows the concentration and molecular weight of the PEGDMA component for the five polymers formulated in this study. Note that PEGDMA with a molecular weight of 242 is also named diethylene glycol dimethacrylate (DEGDMA), and numbers following PEGDMA in table 1 denote the molecular weight. For the comparison purpose among the polymers, table 1 also shows the average crosslink spacing, d, calculated from the theory of rubbery elasticity with the relation

$$Er = \frac{3kT}{d^3} \tag{5.1}$$

where Er denotes the rubbery modulus, and k is Boltzmann's constant. The values of Er were obtained from dynamic mechanical analysis (DMA) discussed later. The monomer solution was injected using a pipette into a glass mould of dimensions 75 mm x25 mm x 0.3 mm, which was subsequently placed under a ultraviolet (UV) lamp (Model B100AP, Blak-Ray) at an intensity of 10 mW cm^{-2} for 10 min photopolymerization. Samples with dimensions of 25 mm x 4mm x 0.3 mm were cut for DMA to determine the thermomechanical properties of the bulk materials. A DMA Q 800 machine from TA Instruments was used in

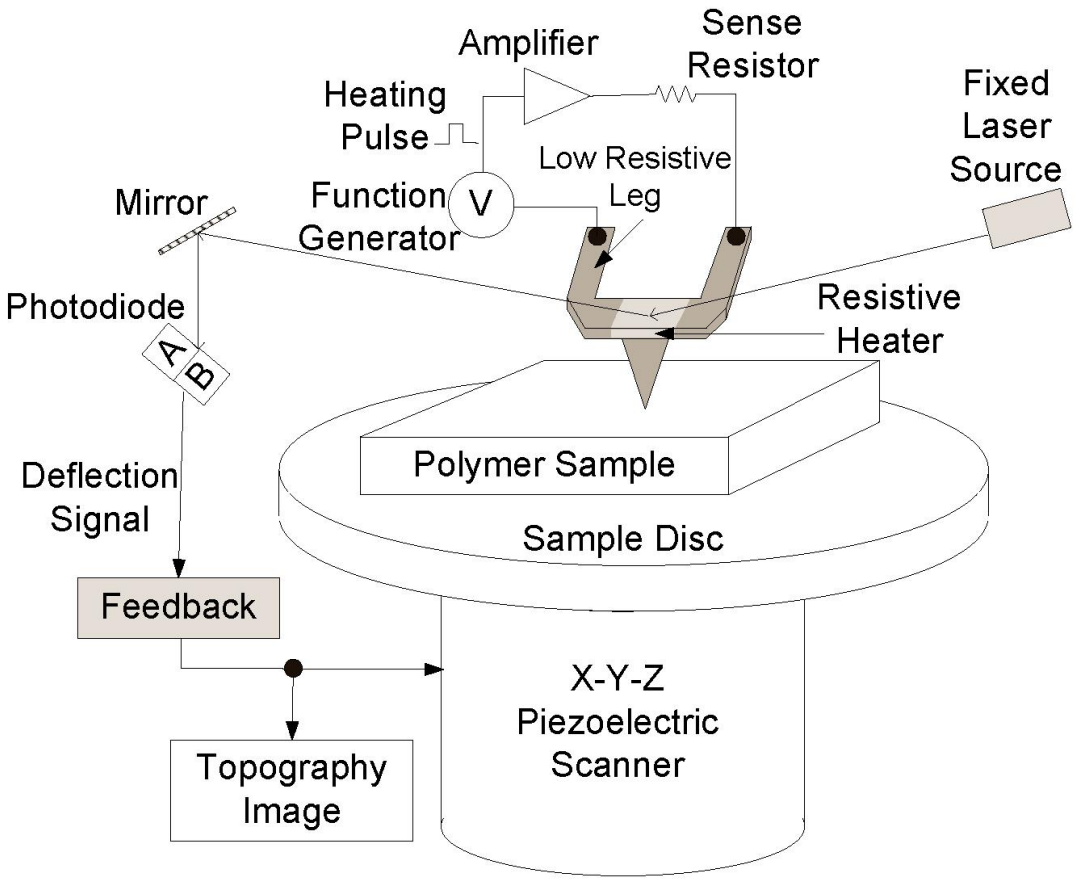

Figure 5.1: Setup of an atomic force microscopy. The diagram shows the cantilever tip and the materials.

three-point bending mode to determine the dynamic mechanical properties of the copolymers. Heating and cooling rates of 3 $^{\circ}$Cm^{-1} and a sampling rate of 1 Hz were used for the DMA tests, and a small strain lever of 0.2% was adopted to ensure the linear viscoelastic response of the polymers.

With the bulk-characterized polymer systems as a basis, samples for nanoscale strain storage studies were cut from the bulk polymers to sizes of 3 mm x 3 mm and mounted for AFM. The samples for AFM tests were prepared at a fixed time point of 24 h after the photopolymerization to avoid change of crosslink density over post-curing. Figure 5.1 shows a schematic of the multimode AFM system (from a digital instrument) adopted to manipulate the heated cantilever. The heated cantilever was fabricated by our group with a standard

silicon-on-oxide cantilever fabrication process [9, 23]. Before used in the indentation formation experiments, the thermal, mechanical and electrical properties of the cantilever were calibrated via established procedures in the literature [9, 10]. The goal of the cantilever calibration was to quantify the cantilever temperature and indentation force involved in the experiments. Two major assumptions of the cantilever temperature calibration include (1) the cantilever temperature, T_{cant}, is a function of cantilever power, P_{cant},for a fixed thermal environment, and (2) during a relatively short time period on a daily basis, the relation between T_{cant} and the cantilever resistance R_{cant} does not change. The following four steps were performed for the cantilever temperature calibration [32]:

1. Raman spectroscopy measurements were conducted to get the cantilever temperature, T_{tip}, as a function of cantilever power, P_{cant}.

2. Based on the circuit in Figure 5.1, the electrical resistances of cantilever, R_{cant}, were determined by stepping through a desirable range of cantilever power P_{cant}.In this step, the cantilever must be installed in the AFM, and kept far away from the sample surface to match the thermal environment in the Raman measurements.

3. Steps (1) and (2) were combined to relate T_{tip} to R_{cant}.

4. The cantilever temperature decreases when the cantilever approaches the sample surface at fixed cantilever power, owing to increased heat conduction from the hot tip to the cold substrate.

Using the above calibration steps, the decrease in T_{cant} was accounted for.

Figure 5.2 shows the calibration results on the cantilever resistance and temperature versus the cantilever power. The change of the resistance value at each power was less than 0.1%, and the cantilever temperature measured using Raman spectroscopy had a uncertainty of ± 5 K for the adopted temperature range [1]. A linear relationship exists between the cantilever temperature, T_{cant}, and the cantilever power, P_{cant}. The cantilever resistance, R_{cant}, however, has a peak with respect to P_{cant}, which is explained by a thermal runaway effect [23]. Furthermore, we adopted the thermal noise method to determine the spring

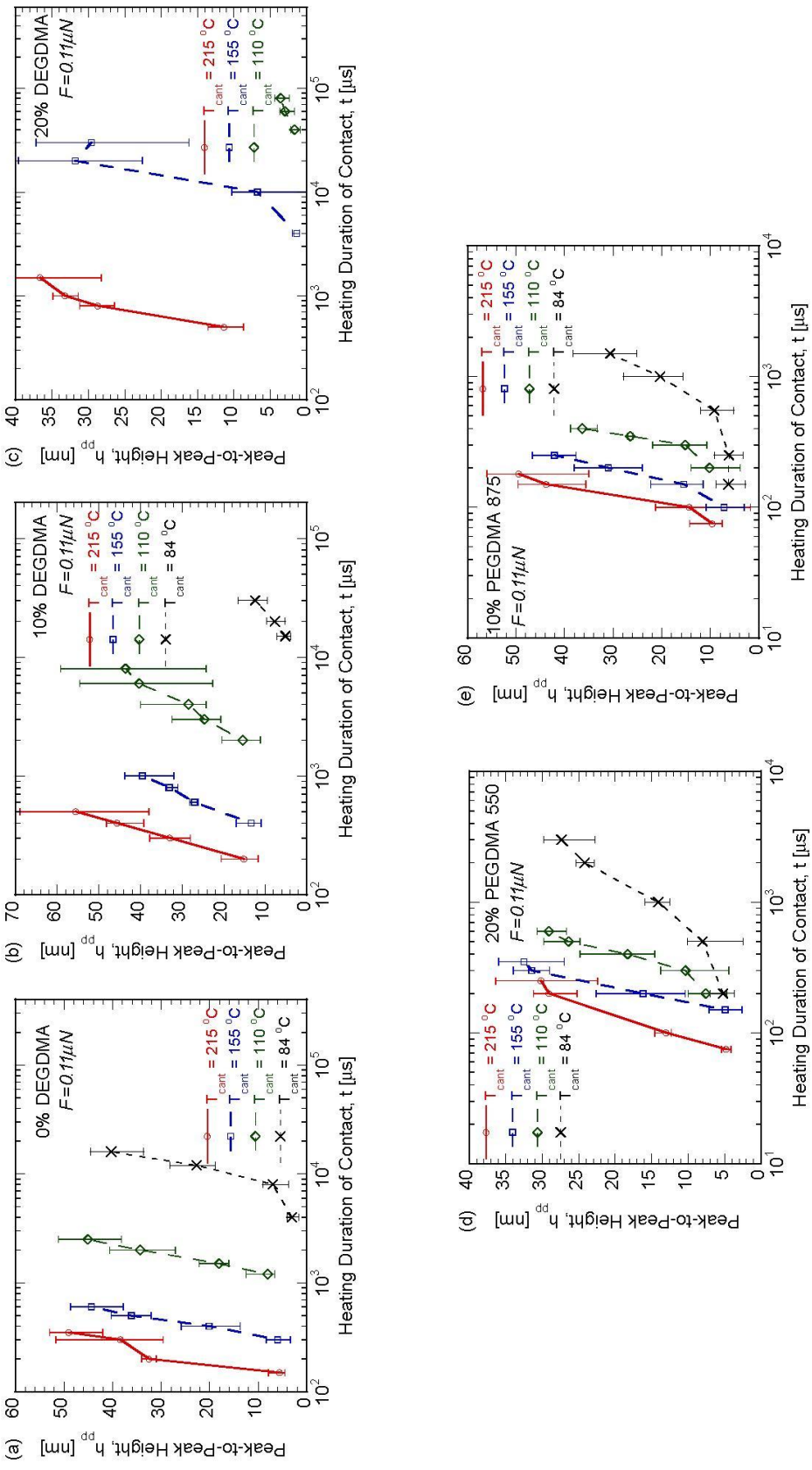

Figure 5.2: Calibration results on the cantilever resistance and temperature versus the

constant of the cantilever [17] and a value of 1.2N m^{-1} was obtained by using a MFP-3DTM AFM system from Asylum Research. The tip radius of curvature, R_{tip}, was determined by scanning the cantilever against a probe tip self-imaging calibration sample (from Aurora NanoDevices Inc.), which has a multiscale distribution of topographic features. The obtained images of the self-imaging sample were, in turn, analysed via a imaging process program, SPIP 4.3 from Image Metrology, which employs the blind reconstruction method to determine R_{tip} [39, 41]. A consistent value of $R_{tip} = 40$ nm was derived from images obtained at three different locations of the calibration sample. The tip radius of the heated cantilever is larger than that of typical commercial cantilevers, owing to the specific design considerations [9, 23].

An Agilent 830 function generator provided heating pulses, passing through an Avtech AV-110D-PS-OS high speed amplifier and a sense resistor of 9.8kΩ, to the heated cantilever (see Figure 5.1), and a detailed description on the circuit can be found in [23] . The heated cantilever was brought to contact with the polymer sample and an electrical heating pulse was subsequently triggered to raise the temperature of the cantilever and tip. The setpoint of the cantilever deflection was maintained by the feedback system of the AFM controller such that a constant loading force of F = 0.11 μN was achieved during the test. The softened polymer in direct contact with the tip was thus displaced, forming an indentation as schematically shown in Figure 5.4. The profile of the thermomechanically formed indent is characterized by two heights in Figure 5.4, namely the peak-to-peak height hpp measured between the highest and lowest points and the residual height hr measured from the original polymer surface to the lowest point. In the experiments, four cantilever temperatures, i.e. 84, 110, 155 and 215 ℃, were adopted for the five polymers shown in table 1 for a wide range of heating durations of contact. In section 3,the results for the DMA tests and the nanoscale thermomechanical indentation are presented.

5.3 Results and discussion

Figure 5.3 shows the storage modulus obtained from DMA as a function of temperature at five combinations of weight per cent PEGDMA and molecular weights. [42]

For the case of 10% PEGDMA 875, there are three distinctive regions, namely,

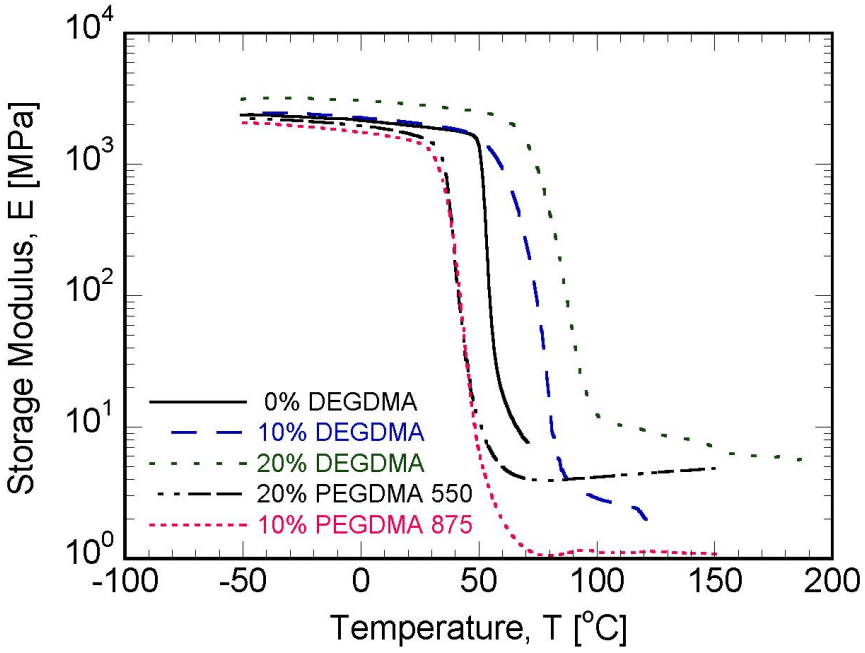

Figure 5.3: Storage modulus of tBA and PEGDMAs

1. a 'glassy' region with a relatively high modulus value of 2.0 GPa for temperature T below 50 ℃,

2. a softer 'rubber' region possessing small rubbery modulus, about Er = 1MPa, when T > 60 ℃, and

3. a glass transition region between 50 and 60 ℃ showing an orders of magnitude decrease in the modulus value.

Significant glass transition behavior is also observed for other polymer systems in Figure5.3. The 20% PEGDMA 550 has an almost identical glass transition region as that of 10% PEGDMA 875: however, the modulus in the 'rubber' region increases significantly to 4 MPa, due to increased crosslink density at higher concentration and shorter chain length of the PEGDMA component. Furthermore, the glass transition temperature, determined by the peak of the tan δ curve from DMA tests [42] , is seen to increase monotonically from 55 to 93 ℃ when the concentration of the DEGDMA crosslinker increases from 0% to 20%. Note that 0% DEGDMA contains the linear tBA species only, resulting in a thermoplastic polymer without chemical crosslinking. Consequently, the 'rubber' region is not obvious for 0% DEGDMA and the material simply melts without measurable modulus values when T > 80 ℃. Further, according to our unpublished DMA results on the three pure crosslinkers, i.e. DEGDMA, PEGDMA 550 and PEGDMA 875, the glass transition temperature of DEGDMA (PEGDMAs) is greater (less) than that of tBA. Consequently, the addition of lower molecular weight crosslinker (DEGDMA) increases T_g, while the higher molecular weight PEGDMAs tends to reduce T_g, as seen in Figure5.3, owing to a weak average effect.

Nanoscale indents were made on the surfaces of the tBA/PEGDMA polymers, with cantilever temperature in the vicinity of or above the glass transition temperatures obtained in Figure 5.3. Figures 5.5(a)–(d) present a few examples of nanoscale indents made on 10% DEGDMA and the cantilever temperature and heating duration of contact are indicated in each figure. The heating duration of contact is defined as the length of the rectangular electrical pulse sent out by the function generator in Figure 5.1. The cantilever has a heating time constant in the range of 1–20 μs and a cooling time constant of 1–50 μs [20], which are

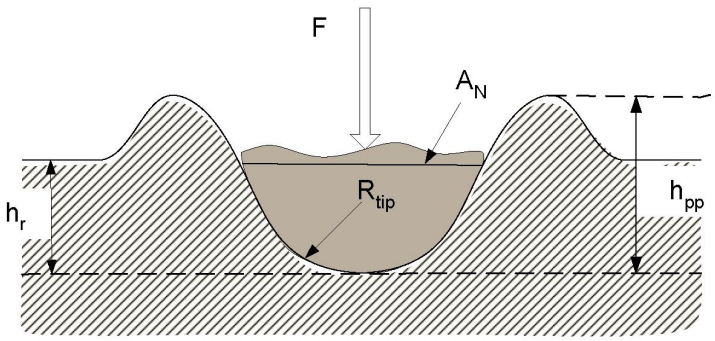

Figure 5.4: Illustration of nanoscale indent formed by a thermomechanic tip

much shorter than the heating durations of contact adopted in the study. The monotonic increase of the average indent size with increasing cantilever temperature and time is seen for all the materials tested in the study. The absolute error bars at longer heating durations are relatively larger. Counting for average indent size, however, the magnitude of relative error may be similar for all the heating durations considered.

The creeping of the viscoelastic polymers is an important contributing factor to the dependence of hpp on the heating duration of contact. Furthermore, the time dependence of hpp may also be explained by the heat transfer between the probe tip and the polymer surface. For a fixed load, the applied pressure decreases with increasing penetration, and the increase rate of h_{pp} at longer times should decrease. However, sharp increase in h_{pp} is still seen at later times in Figures 5.6–5.10,which may be explained by the fact that the increased penetration promotes the heat flow from the tip to the polymer, forming a larger volume of polymer in a rubbery state that easily deforms. It will be of great theoretical and practical interest to model the heat transfer and glass transition phenomena in the vicinity of the tip/polymer interface, and to predict the penetration height evolution with time. In

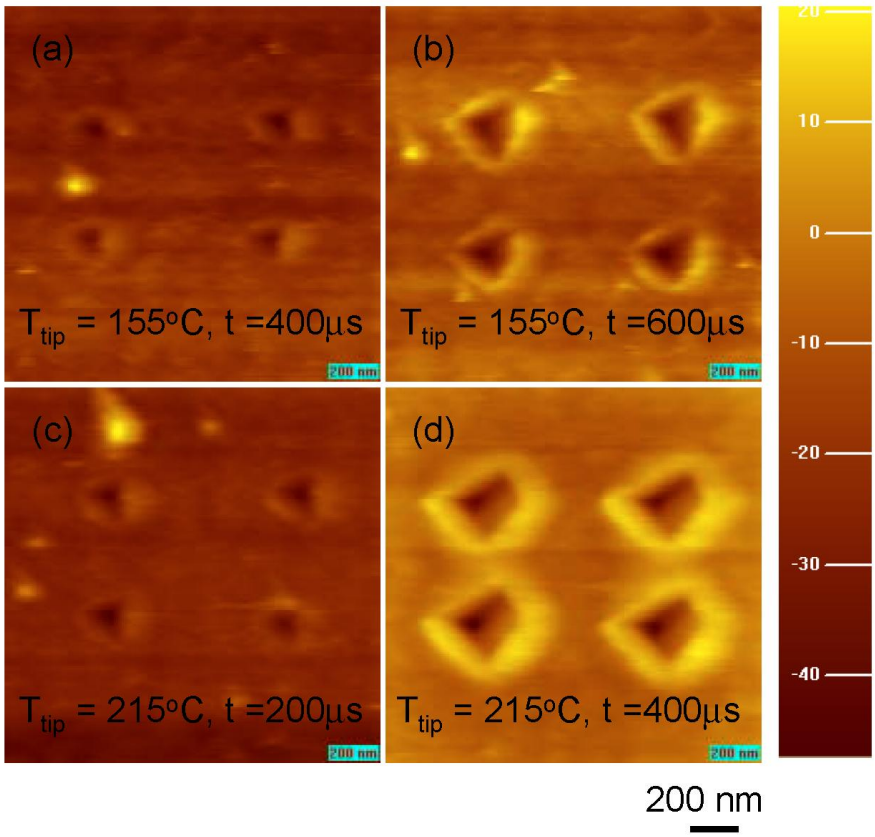

Figure 5.5: AFM images of nanoscale indents made at (a) cantilever temperature T_{cant} = 155℃ and heating duration of contact t = 400 μs, (b) T_{cant} = 155℃ and t = 600 μs, (c) T_{cant} = 215℃ and t = 200 μs, and (d) T_{cant} = 215℃ and t = 400 μs on a 10DEGDMA polymer surface at a fixed load force of 0.11 ΞÊN. The length of the scale bars in the figures represents 200 nm.

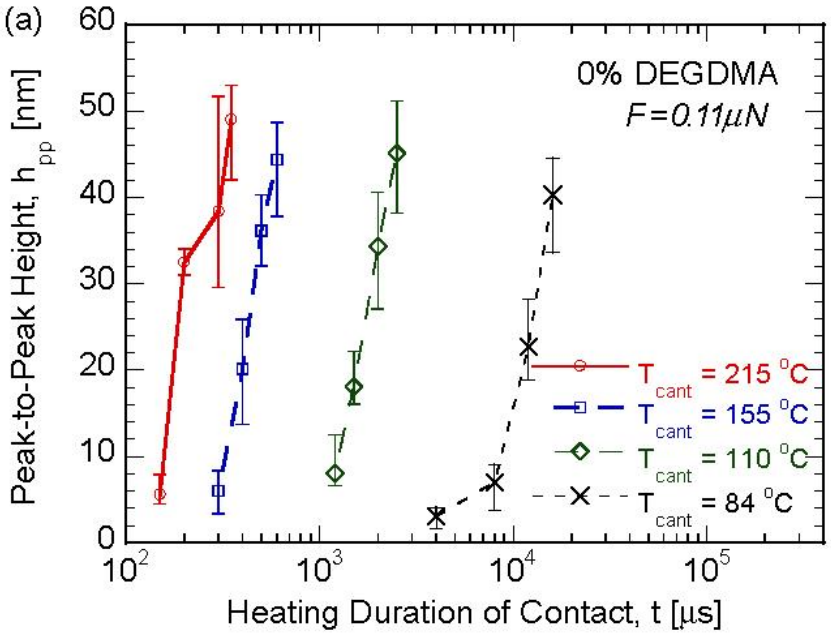

Figure 5.6: The peak-to-peak height, h_{pp}, as a function of the heating duration of contact, t, and cantilever temperature, Tcant, for (a) 0% DEGDMA

practical, the data in Figures 5.6–5.10 may be used to identify the strain storage and possible actuation for a given combination of T_{cant} and t, providing useful information for the design of nanoscale actuators.

When the concentration of the DEGDMA crosslinker increases from 0 to 20 wt% the polymers becomes 'harder' due to decreased crosslink spacing from infinity to 1.17 nm, as seen in Table 1. Consequently, Figures 5.7 and 5.8 show longer heating duration of contact to make the same size of indent in Figure 5.6 under a fixed cantilever temperature. No experimental data are reported for 20% DEGDMA at 84 ℃ since no detectable indent was made for a heating duration of contact as long as 2 min. With the increase of molecular weight in Figures 5.9 and 5.10, the crosslink spacing increases to 1.58 nm and 2.43 nm, respectively, due to longer monomer chains, resulting in 'softer' materials. For given cantilever temperature and peak-to-peak height, the heating duration of contact is seen to decrease with the increase in molecular weight.

The polymer modulus during thermomechanical nanoindentation may be estimated via the cantilever temperature and the DMA results in Figure5.3. Note that the cantilever

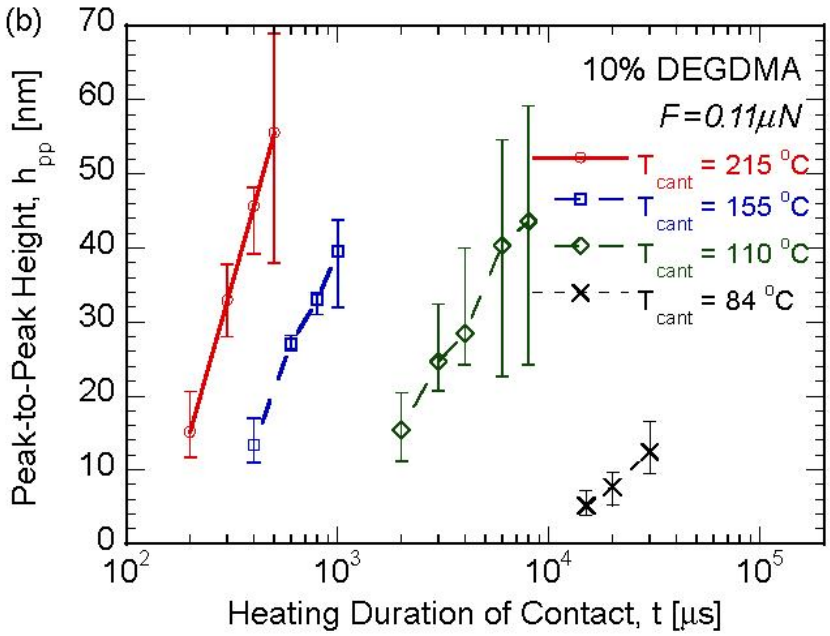

Figure 5.7: The peak-to-peak height, h_{pp}, as a function of the heating duration of contact, t, and cantilever temperature, Tcant, for (b) 10% DEGDMA

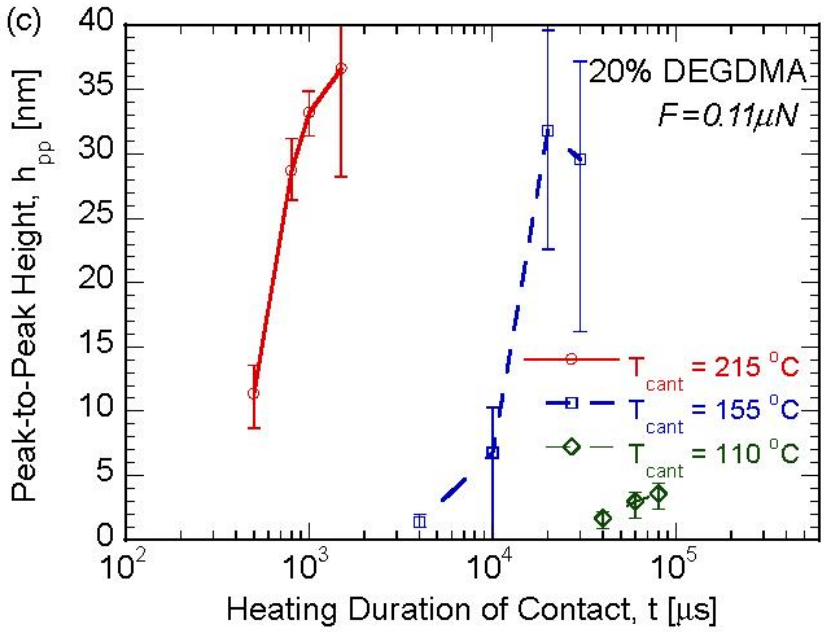

Figure 5.8: (c) 20% PEGDMA 550

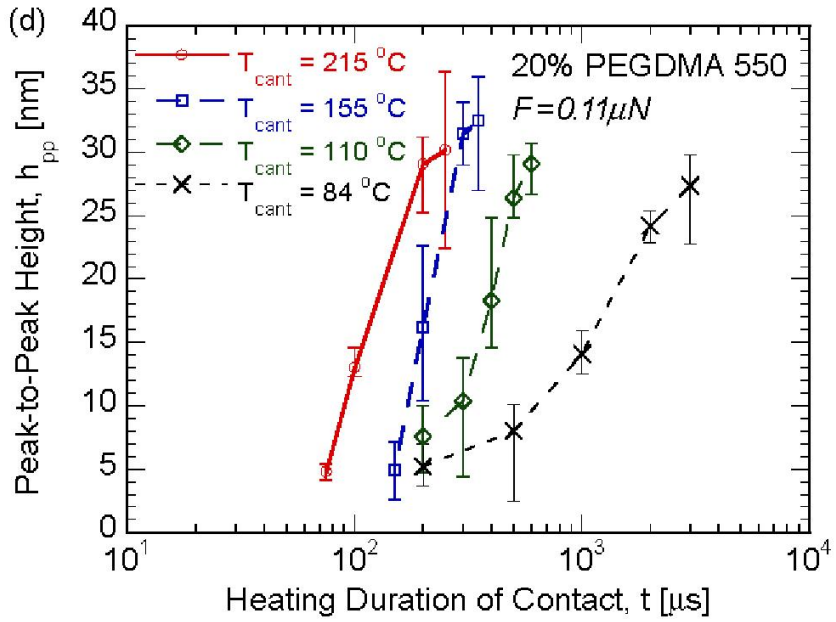

Figure 5.9: The peak-to-peak height, h_{pp}, as a function of the heating duration of contact, t, and cantilever temperature, Tcant, for (d) 10% PEGDMA 875

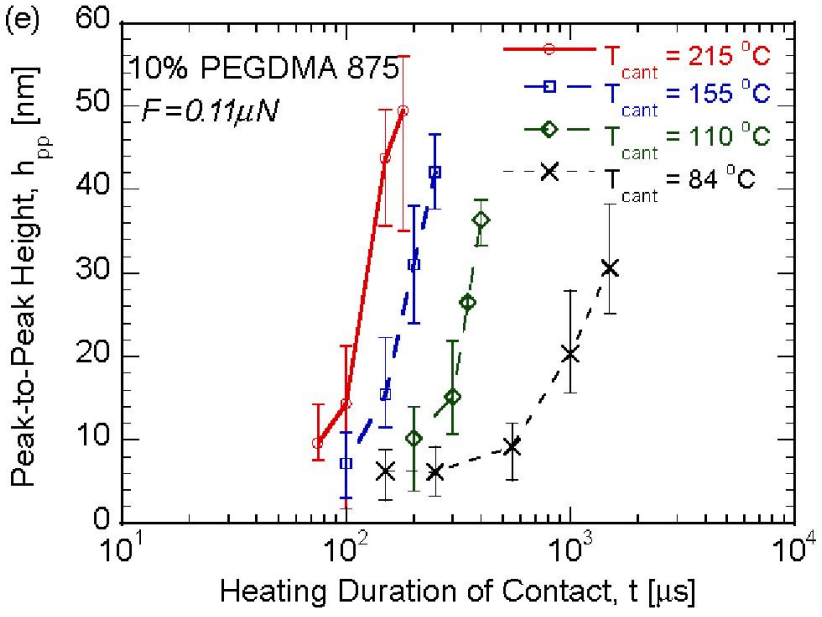

Figure 5.10: The peak-to-peak height, h_{pp}, as a function of the heating duration of contact, t, and cantilever temperature, Tcant, for 10% PEGDMA 875.The load force for the formation of the nanoindents is fixed at 0.11 μN.

temperature is used as an approximation to that of the polymer, while accurate determination of the polymer temperature requires detailed heat transfer analysis in future work. For the cases corresponding to lower modulus (an indication of softer material) during indentation, shorter heating duration of contact time is required to reach a given value of h_{pp}, as seen in Figures 5.6–5.10. Thus, the nanoindentation data are found to be qualitatively consistent with the DMA results.

The contact pressure P may be determined from the indentation height data. The contact pressure is defined as a ratio of load force, F, to normal projected contact area formed at the load, A_N, and is a transient measure of the hardness. The precise determination of the contact area requires the detailed information on both force–distance response and the area function (or exact shape) of the tip [42] , which are lacking in the current experimental set-up. It is a standard procedure to obtain a force–distance curve for nanoindentation tests using commercial tapping mode cantilevers with high spring constant [16] . The heated cantilever was a contact mode cantilever with small spring constant. Consequently, the transient heating pulses delivered to the cantilever caused large vibration of the device during the initial stage of the thermomechanical indentation process, yielding inaccurate force–distance information. Stiffer thermal cantilevers may be fabricated in our lab in a future development. However, stiffer cantilevers may not be able to accurately apply the relatively small forces studied in the chapter, and thus may not suitable for the present polymer system.

Owing to the lack of force–distance curves, we use the dimensions of the residual indents to calculation the contact area and hardness, which is a widely accepted method in the hardness measurement [7] . In this study, we approximate A_N to be the cross-sectional area of the cantilever tip at the residual height h_r (see Figure 5.4) and obtain the following equation for the contact pressure:

which is ensured in the study by choosing the appropriate combinations of the indentation conditions in Figures 5.6–5.10. In the determination of contact area A_N , the residual height h_r and the peak-to-peak height h_{pp} may constitute the lower and upper bounds, respectively, for the actual contact height. However, in the absence of precise loading/unloading data from indentation, the choice of the lower bound h_r for contact surface calculation yields consistent

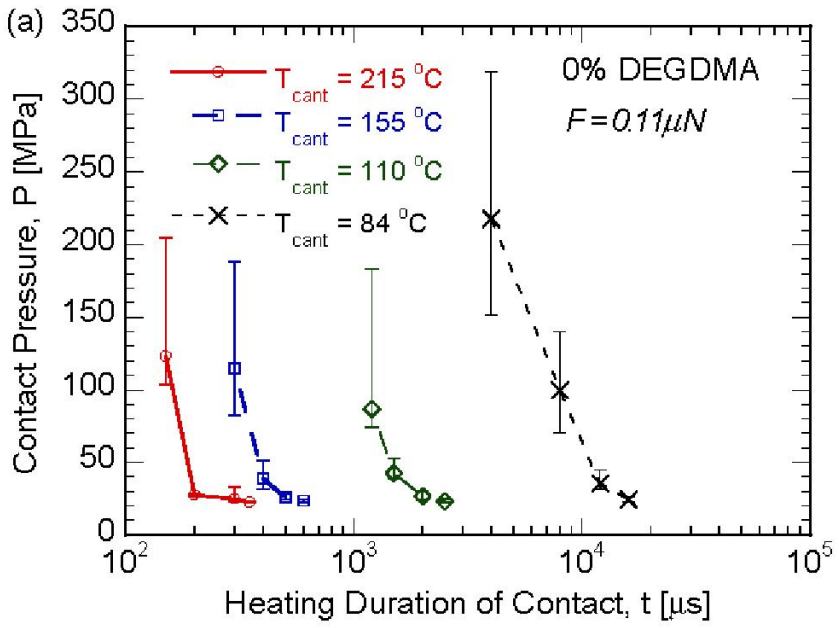

Figure 5.11: The contact pressure, P, as a function of the heating duration of contact, t, and the cantilever temperature, T_{cant}, for (a) 0% DEGDMA

results for all the experimental data. Furthermore, equation (1) has an implicit assumption that the tip shape is spherical, which is reasonable when $h_r < R_{tip}$. Using the above equation, the contact pressure is obtained as a function of heating duration of contact, t , and cantilever temperature, T_{cant} , for the polymers studied, as shown in figures 5.11–5.15. From equation (1) and the trends found for indentation height in Figures 5.6–5.10, it is evident that the contact pressure, P , increases with decreasing heating duration of contact and cantilever temperature.

The values of contact pressure determined by equation (1) are dependent on the acquisition time of the topography images, owing to the fact that the indents may experience spontaneous recovery at room temperature.In our experiments, all the images of the indents were obtained in situ using the same AFM tip, and the time lapse between the thermomechanical indentation and the acquired image was consistently about 1 min. Thus, the derived values of contact pressure have a common basis of evaluation and may be used for the purpose of comparison among different heating durations, temperatures and materials. A physical interpretation of the results in Figures 5.11–5.11 is that the polymers are 'harder' at shorter

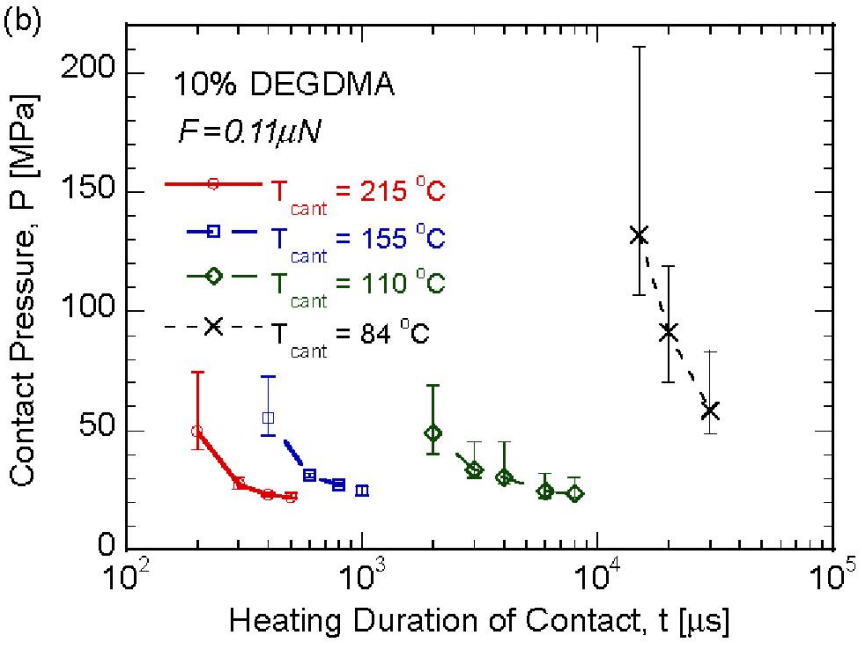

Figure 5.12: The contact pressure, P, as a function of the heating duration of contact, t, and the cantilever temperature, T_{cant}, for (b) 10% DEGDMA

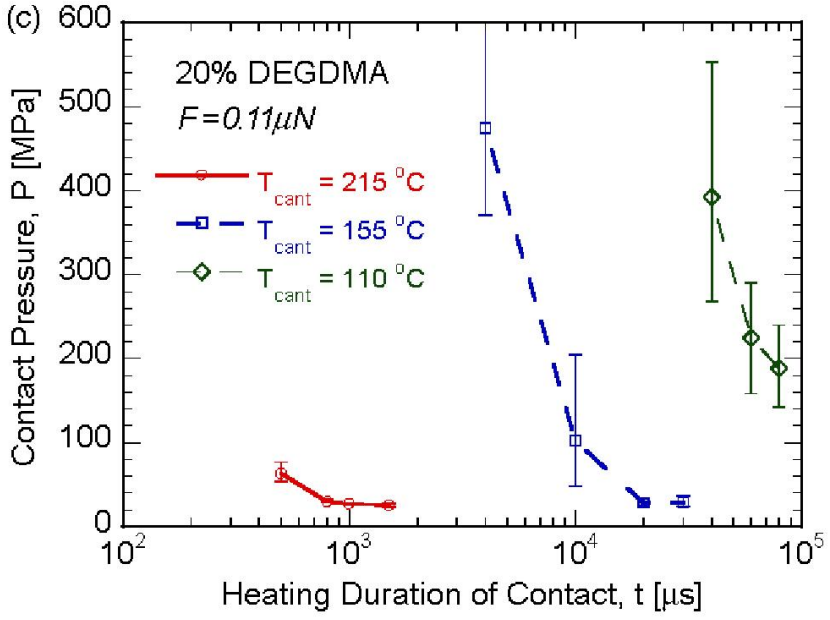

Figure 5.13: The contact pressure, P, as a function of the heating duration of contact, t, and the cantilever temperature, T_{cant}, for (c) 20% DEGDMA

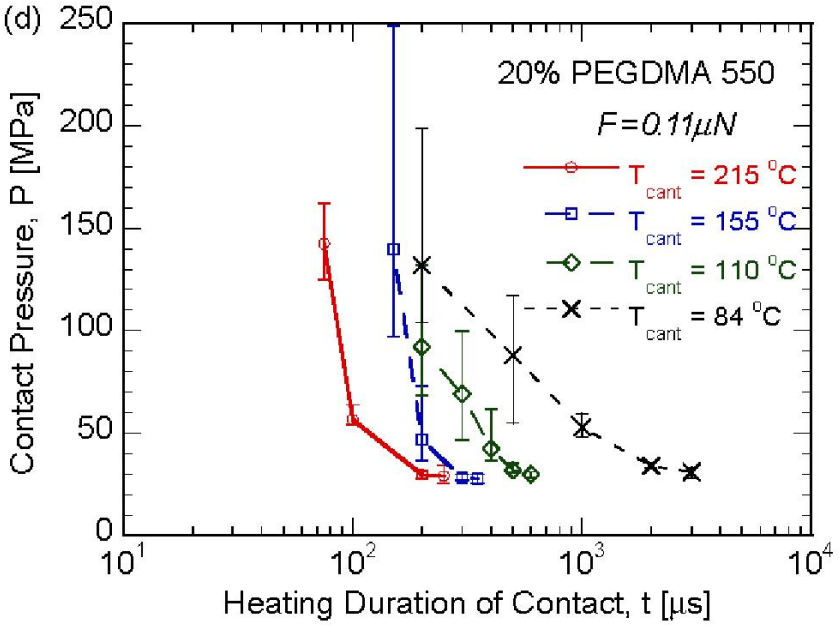

Figure 5.14: The contact pressure, P, as a function of the heating duration of contact, t, and the cantilever temperature, T_{cant}, for (d) 20% PEGDMA 550

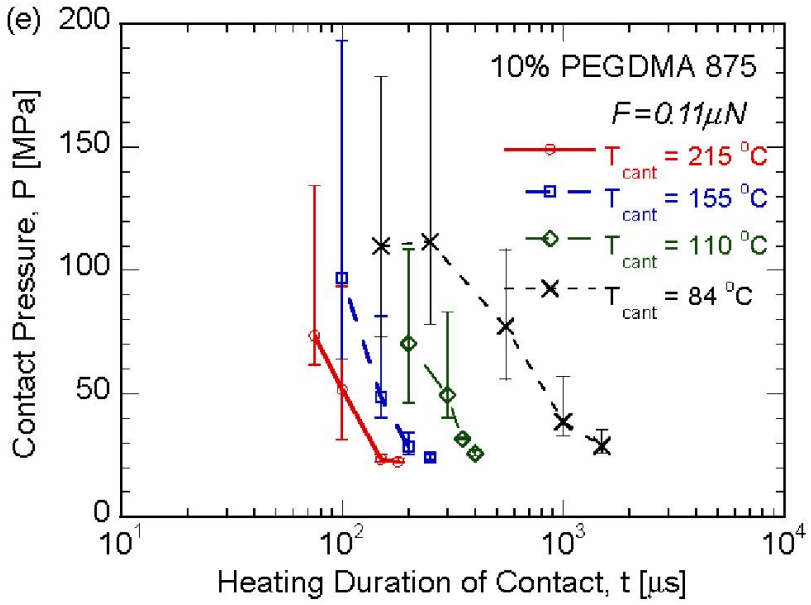

Figure 5.15: The contact pressure, P, as a function of the heating duration of contact, t, and cantilever temperature, T_{cant}, for (e) 10% PEGDMA 875.

times and lower temperatures. The measured nanoscale behaviour is consistent with the physics of viscoelastic deformation implied from bulk materials. In order to make nanoscale impressions, the local material must enter into the viscoelastic regime where polymer chains have sufficient coordinated mobility to achieve large strains at moderate forces.

The results in this chapter provide a systematic experimental study on the nanoscale indent formation for a set of acrylate and ethylene glycol polymers with controlled properties. Furthermore, the contact pressure of the polymers shows a broad range of variation between 20 and 500 MPa, indicating that the tBA/PEGDMA system could be tailored for different application requirements. Based on the current experimental results, detailed numerical simulations may be conducted in a future study to investigate the complex interaction between the hot cantilever tip and the network of polymer molecules. The investigation on the recovery dynamics of the thermomechanically formed nanoindents in the vicinity of the glass transition temperature will also be of great interest.

5.4 Summary of Chapter

The dynamics of nanoscale strain storage in a class of shape memory polymers was studied using a heated cantilever technique. The peak-to-peak height and contact pressure were obtained as functions of the heating duration of contact and cantilever temperature for five polymers with controlled structure and thermomechanical properties. The indentation height h_{pp} (or contact pressure P) increases monotonically with increasing (or decreasing) heating duration of contact and temperature. The thermomechanical nanoindentation results are consistent with the DMA data for the bulk materials. The results provide directly usable information for design of polymer actuators at small scales not only in information storage devices, but also in various biological, medical and engineering applications.

REFERENCES

[1] Abel, M., Wright, T., Sunden, E., Graham, S., King, W., and Lance, M., "Thermal metrology of silicon microstructures using raman spectroscopy," *Semiconductor Thermal Measurement and Management Symposium, 2005 IEEE Twenty First Annual IEEE*, pp. 235–242, 2005.

[2] Abrahamson, E., Lake, M., Munshi, N., and Gall, K., "Shape memory mechanics of an elastic memory composite resin," *Journal of Intelligent Material Systems and Structures*, vol. 14, no. 10, p. 623, 2003.

[3] Anseth, K. S., Wang, C. M., and Bowman, C. N., "Kinetic evidence of reaction diffusion during the polymerization of multi(meth)acrylate monomers," *Macromolecules*, vol. 27, no. 3, pp. 650–655, 1994.

[4] ASHLEY, S., "Prototyping with advanced tools," *Mechanical engineering(New York, N. Y. 1919)*, vol. 116, no. 6, pp. 48–55, 1994.

[5] Berchtold, K., Lovell, L., Nie, J., Hacioğlu, B., and Bowman, C., "The significance of chain length dependent termination in cross-linking polymerizations," *Polymer*, vol. 42, no. 11, pp. 4925–4929, 2001.

[6] Binnig, G., Despont, M., Drechsler, U., Häberle, W., Lutwyche, M., Vettiger, P., Mamin, H., Chui, B., and Kenny, T., "Ultrahigh-density atomic force microscopy data storage with erase capability," *Applied Physics Letters*, vol. 74, p. 1329, 1999.

[7] Blake, A., *Handbook of Mechanics, Materials, and Structures.* Wiley-Interscience, 1985.

[8] Chou, S., Krauss, P., and Renstrom, P., "Imprint lithography with 25-nanometer resolution," *Science*, vol. 272, no. 5258, p. 85, 1996.

[9] Chui, B., Stowe, T., Ju, Y., Goodson, K., Kenny, T., Mamin, H., Terris, B., Ried, R., and Rugar, D., "Low-stiffness silicon cantilevers with integrated heaters and piezoresistive sensors for high-density afm thermomechanical data storage," *JOURNAL OF MICROELECTROMECHANICAL SYSTEMS*, vol. 7, no. 1, p. 69, 1998.

[10] Despont, M., Brugger, J., Drechsler, U., Dürig, U., Häberle, W., Lutwyche, M., Rothuizen, H., Stutz, R., Widmer, R., Binnig, G., and others, "Vlsi-nems chip for parallel afm data storage," *Sensors & Actuators: A. Physical*, vol. 80, no. 2, pp. 100–107, 2000.

[11] El Feninat, F., Laroche, G., Fiset, M., and Mantovani, D., "Shape memory materials for biomedical applications," *Advanced Engineering Materials*, vol. 4, no. 3, p. 91, 2002.

[12] Gall, K., Kreiner, P., Turner, D., and Hulse, M., "Shape-memory polymers for microelectromechanical systems," *Journal of Microelectromechanical Systems*, vol. 13, no. 3, pp. 472–483, 2004. article.

[13] Gall, K., Yakacki, C. M., Liu, Y. P., Shandas, R., Willett, N., and Anseth, K. S., "Thermomechanics of the shape memory effect in polymers for biomedical applications," *Journal of Biomedical Materials Research Part A*, vol. 73A, no. 3, pp. 339–348, 2005. article.

[14] Gray, T., Killgore, J., Luo, J., Jen, A. K. Y., and Overney, R. M., "Molecular mobility and transitions in complex organic systems studied by shear force microscopy," *Nanotechnology*, vol. 18, no. 4, p. 044009 (9pp), 2007.

[15] Grayson, A., Choi, I., Tyler, B., Wang, P., Brem, H., Cima, M., and Langer, R., "Multi-pulse drug delivery from a resorbable polymeric microchip device," *Nature Materials*, vol. 2, no. 11, pp. 767–772, 2003.

[16] Hinz, M., Kleiner, A., Hild, S., Marti, O., Dürig, U., Gotsmann, B., Drechsler, U., Albrecht, T., and Vettiger, P., "Temperature dependent nano indentation of thin polymer films with the scanning force microscope," *European Polymer Journal*, vol. 40, no. 5, pp. 957–964, 2004.

[17] Hutter, J. and Bechhoefer, J., "Calibration of atomic-force microscope tips," *Review of Scientific Instruments*, vol. 64, p. 1868, 1993.

[18] Jeon, H., Mather, P., and Haddad, T., "Shape memory and nanostructure in poly (norbornyl-poss) copolymers," *Polymer International*, vol. 49, pp. 453–457, 2000.

[19] King, W., Kenny, T., Goodson, K., Cross, G., Despont, M., Dürig, U., Rothuizen, H., Binnig, G., and Vettiger, P., "Atomic force microscope cantilevers for combined thermomechanical data writing and reading," *Applied Physics Letters*, vol. 78, p. 1300, 2001.

[20] King, W., Kenny, T., Goodson, K., Cross, G., Despont, M., Durig, U., Rothuizen, H., Binnig, G., and Vettiger, P., "Design of atomic force microscope cantilevers for combined thermomechanical writing and thermal reading in array operation," *Microelectromechanical Systems, Journal of*, vol. 11, no. 6, pp. 765–774, 2002.

[21] King, W., Saxena, S., Nelson, B., Weeks, B., and Pitchimani, R., "Nanoscale thermal analysis of an energetic material.," *Nano Lett*, vol. 6, no. 9, pp. 2145–9, 2006.

[22] Langer, R. and Peppas, N., "Advances in biomaterials, drug delivery, and bionanotechnology," *AIChE Journal*, vol. 49, no. 12, pp. 2990–3006, 2003.

[23] Lee, J., Beechem, T., Wright, T., Nelson, B., Graham, S., and King, W., "Electrical, thermal, and mechanical characterization of silicon microcantilever heaters," *Microelectromechanical Systems, Journal of*, vol. 15, no. 6, pp. 1644–1655, 2006.

[24] Lendlein, A. and Kelch, S., "Degradable, multifunctional polymeric biomaterials with shape-memory," 2005.

[25] Lendlein, A. and Langer, R., "Biodegradable, elastic shape-memory polymers for potential biomedical applications," *Science*, vol. 296, no. 5573, p. 1673, 2002.

[26] Li, F. and Larock, R., "New soybean oil-styrene-divinylbenzene thermosetting copolymers. v. shape memory effect," *Journal of Applied Polymer Science*, vol. 84, no. 8, pp. 1533–1543, 2002.

[27] Liu, C., Chun, S., Mather, P., Zheng, L., Haley, E., and Coughlin, E., "Chemically cross-linked polycyclooctene: Synthesis, characterization, and shape memory behavior," *Macromolecules*, vol. 35, no. 27, pp. 9868–9874, 2002.

[28] Lutwyche, M., Despont, M., Drechsler, U., Dürig, U., Häberle, W., Rothuizen, H., Stutz, R., Widmer, R., Binnig, G., and Vettiger, P., "Highly parallel data storage system based on scanning probe arrays," *Applied Physics Letters*, vol. 77, p. 3299, 2000.

[29] Maitland, D. J., Wilson, T., Schumann, D. L., and Baer, G., "Laser-activated shape memory polymer microactuators for treating stroke," *Lasers and Electro-Optics Society, 2002. LEOS 2002. The 15th Annual Meeting of the IEEE*, vol. 1, pp. 359–360 vol.1, 2002. article.

[30] Metcalfe, A., Desfaits, A., Salazkin, I., Yahia, L., Sokolowski, W., and Raymond, J., "Cold hibernated elastic memory foams for endovascular interventions," *Biomaterials*, vol. 24, no. 3, pp. 491–497, 2003.

[31] Metzger, M. F., Wilson, T. S., Schumann, D., Matthews, D. L., and Maitland, D. J., "Mechanical properties of mechanical actuator for treating ischemic stroke," *Biomedical Microdevices*, vol. 4, no. 2, pp. 89–96, 2002. article.

[32] Nelson, B. A., King, W. P., and Gall, K., "Shape recovery of nanoscale imprints in a thermoset "shape memory" polymer," *Applied Physics Letters*, vol. 86, no. 10, 2005. article 103108.

[33] Reading, M., Price, D., Grandy, D., Smith, R., Bozec, L., Conroy, M., Hammiche, A., and Pollock, H., "Micro-thermal analysis of polymers: current capabilities and future prospects," *Macromolecular Symposia*, vol. 167, no. 1, pp. 45–62, 2001.

[34] Roether, J. and Deb, S., "The effect of surface treatment of hydroxyapatite on the properties of a bioactive bone cement," *Journal of Materials Science: Materials in Medicine*, vol. 15, no. 4, pp. 413–418, 2004.

[35] Santini Jr, J., Cima, M., and Langer, R., "A controlled-release microchip.," *Nature*, vol. 397, no. 6717, pp. 335–8, 1999.

[36] Sillion, B., "Shape memory polymers," *Act. Chimique*, vol. 3, pp. 182–188, 2002.

[37] Tobushi, H., Shimada, D., Hayashi, S., and Endo, M., "Shape fixity and shape recovery of polyurethane shape-memory polymer foams," *Proceedings of the Institution of Mechanical Engineers Part L-Journal of Materials-Design and Applications*, vol. 217, no. L2, pp. 135–143, 2003. article.

[38] Vettiger, P., Cross, G., Despont, M., Drechsler, U., Durig, U., Gotsmann, B., Haberle, W., Lantz, M. A., Rothuizen, H. E., Stutz, R., and Binnig, G. K., "The "millipede" - nanotechnology entering data storage," *IEEE Transactions on Nanotechnology*, vol. 1, no. 1, pp. 39–55, 2002. article.

[39] Villarrubia, J., "Algorithms for scanned probe microscope image simulation, surface reconstruction, and tip estimation," *Journal of Research of the National Institute of Standards and Technology*, vol. 102, no. 4, pp. 425–454, 1997.

[40] Wichterle, O. and Lim, D., "Hydrophilic gels for biological use," *Nature*, vol. 185, no. 4706, pp. 117–118, 1960.

[41] Williams, P., Shakesheff, K., Davies, M., Jackson, D., Roberts, C., and Tendler, S., "Blind reconstruction of scanning probe image data," *Journal of Vacuum Science & Technology B: Microelectronics and Nanometer Structures*, vol. 14, p. 1557, 1996.

[42] Wornyo, E., Gall, K., Yang, F., and King, W., "Nanoindentation of shape memory polymer networks," *Polymer*, vol. 48, no. 11, pp. 3213–3225, 2007.

[43] Xu, W., Xiao, Z., and Zhang, T., "Mechanical properties of silicone elastomer on temperature in biomaterial application," *Materials Letters*, vol. 59, no. 17, pp. 2153–2155, 2005.

[44] Yang, F., Wornyo, E., Gall, K., and King, W., "Nanoscale indent formation in shape memory polymers using a heated probe tip," *Nanotechnology*, vol. 18, no. 285302, p. 285302, 2007.

CHAPTER VI

DESIGNED EXPERIMENTS AND NEURAL NETWORKS

6.1 Process Modeling

6.1.1 Experimental Design

In order to minimize cost of production and also reduce misprocessing, designed experiments are an invaluable tool in manufacturing. Designed experiments facilitate the systematic investigation of the dependence of a set of output parameters (responses) on a set of input parameters (factors). Information on the interaction of the various input parameters is determined by a mathematical process. Statistical experimental design has been used in pharmaceutical research, food processing research, among others [1, 13, 15, 24]. In particular, the semiconductor industry, in its bid to eliminate waste and increase yield, and reliability of devices, has relied on statistical design of experiments. Experimental designs are constructed to ensure a systematic method of collecting data to build process models. In 1997, Chinoy performed designed experiments with the commercial software, RS Discover(R) to optimize processing conditions for reactive ion etching of benzo-cyclobutene (BCB) films [7]. The input variables in this research were rf power, pressure, and SF_6 concentration. The responses measured were dc bias, etch rate, via angle, uniformity, selectivity, lateral etch rate, and etch cleanliness. Chinoy deduced optimal values of various sets of input parameters for this application using designed experiments. In addition, Cecchi et al. utilized the 2^3 full-factorial design with two replicated centerpoints designed experiment to optimize spin coating conditions for polymer light emitting diode (LED) displays [6]. In this work, it was determined that the spin velocity and polymer concentration were statistically significant for film uniformity and device efficiency. Recently, Setia and May investigated the inline failure of a laser ablation process of microvias using the Dempster-Shafer (D-S) theory and a designed experiment [23]. The material used in this research was dry Kapton polyimide. Input parameters considered were laser fluence, shot frequency, number of

pulses, and helium pressure flow. The responses were the top and bottom via diameters. These researchers used the above techniques to diagnose failure of the vias. In an earlier experiment, Kim and May utilized genetic algorithms (GAs) for the study of via formation in BCB [25]. Several years ago, Wei and coworkers investigated the dependence of processing conditions on the dispersion of WO_3 nanoparticles in a polyacrylonitrile (PAN) matrix using the Taguchi experimental design methodology [27]. Among all the variables considered by these researchers, the concentration of PAN solution was found to have the most significant effect on the dispersion of the nanoparticles in the matrix. Finally, Gou et al. utilized designed experiments to investigate the effects of process parameters on the dispersion of nanotubes in bucky paper [10]. These researchers inferred from the experiment that the most significant parameters on the response, rope size distribution, were sonication time and suspension concentration. Recently, Davis and May utilized neural networks for the control of variable-frequency microwave processing of polymer dielectric curing. The neural network controller indicated an error less than 7% when compared with training [8].

A review of the current available literature shows that there is little work done in the application of designed experiments to SMPs in general, and acrylates in particular. As a result, statistical experimental design will be performed to determine the effects of various processing conditions on the thermomechanical properties of the SMPs. Multivariate methods will be utilized, as opposed to univariate methods, as the former translates into reduction of experimental time and has the potential of yielding better statistical results [21] .

Screening experiments are the initial runs of an experiment to determine relevant factors for further investigation. Some screening experiments used in this work include the Box-Behnken design, the fractional factorial design, and the full-factorial design.

The Box-Behnken method is a type of multivariate technique utilized to investigate the dependence of a variable(s) on a set of factors. The Box-Behnken design is an independent, rotatable quadratic design in which the factor combinations are at the midpoints of the edges of the process space and at the center [1]. An advantage of the Box-Behnken technique over other multivariate techniques is that all factors can not assume a maximum value at the

[1] http://www.itl.nist.gov/div898/handbook

same time.

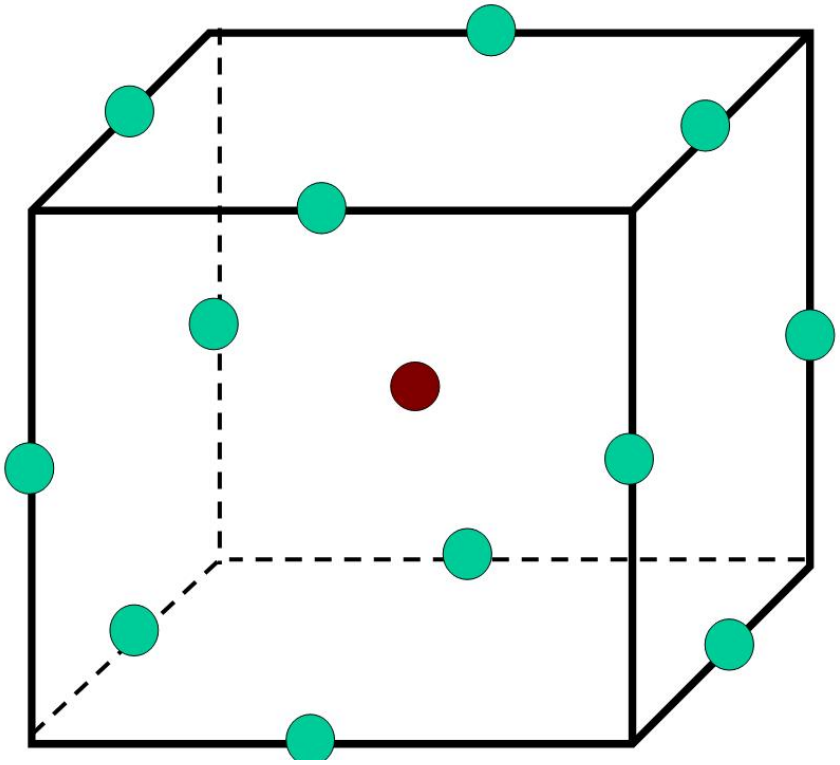

Figure 6.1: A schematic of the Box-behnken design for three factors, showing points at the center of the edges of a hyper-cube, and a point at the center of the cube.

Also, compared to design types, Box-Behnken designs have smaller number of design points and are therefore less cumbersome [14]. With the same number of factors, Box-Behnken designs require fewer numbers of levels when compared to CCC. The disadvantage of Box-Behnken designs is their limited capability for orthogonal blocking. Experimental designs provide a systematic way of collecting data to build process models.

If a fractional factorial experiment in which a few fractions of the treatment combinations of the complete factorial experiment is selected to be run. A fractional factorial experiment saves time and resources, as it helps in narrowing the number of factors required in an experiment.

The total number of experiments is expressed as l^k where l is the number of levels and k is the number of factors. For l=2, we have a two-level experiment . Most experiments in engineering belong to this class.We realize that the number of experiments required grows as the number of factors increases. Thus, using a fractional factorial experiment, we reduce

the total number of runs in an experiment by a factor. The fraction could be $\frac{1}{2}, \frac{1}{4}, \frac{1}{16}$, etc.

Full factorial experiments are based on a consideration of all runs in either the level 2 or level 3 design. Thus, these designs require more time and resources than fractional factorial designs. Fractional factorial designs can be used for screening when the number of factors is less than five (5). Response surface models may be based on full factorial designs. However, the number of runs in this case is usually high—requiring significant time and resources.

Central composite face (CCF) designs are obtained by augmenting full factorial designs with extra points at the centers of a "cube" in the design space, as shown in Figure 6.2. CCF facilitates response surface modeling and optimization [12].

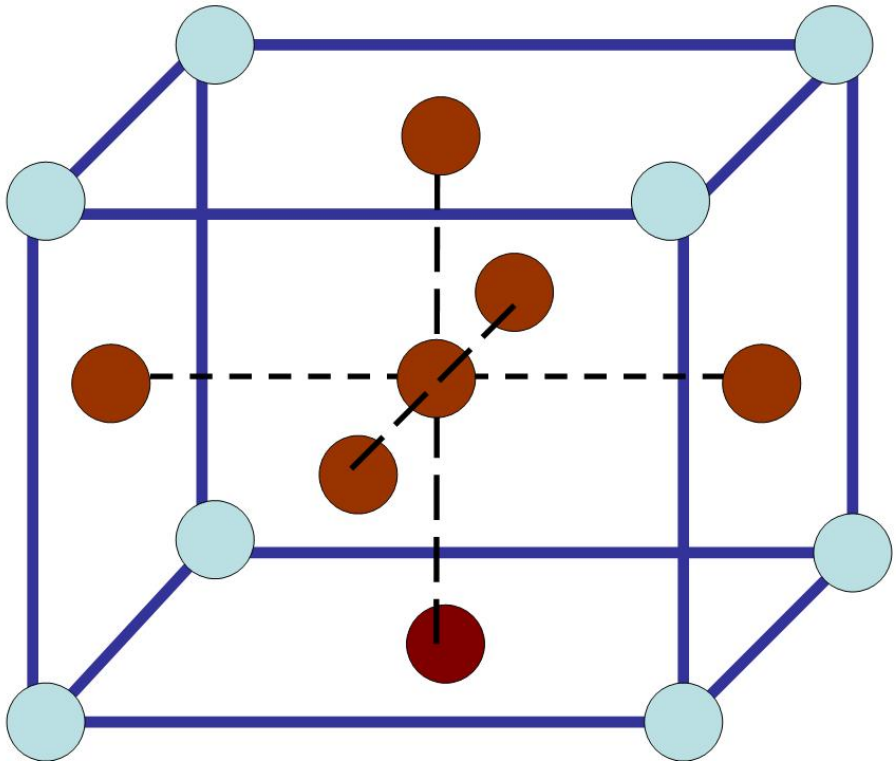

Figure 6.2: Central composite design showing the center points.

6.2 Neural Networks

Neural networks, mathematical models crudely based on neurological systems, are tools with the ability to deduce complex relationships between input and output variables in an experiment. Since their advent, neural networks have been used in many areas of research including

MEMs, biomedical engineering, etc . A neural network consists of a web of adjoining *neurons* in a network functioning in tandem to produce an output. A single neuron is shown in Figure 9.4.Neural networks are computational methods loosely based on the biological functions of the central nervous system. A neural network learns from the input provided to it and is able to remember past events by storing information in adjoining strengths called weights. Neural network models are advantageous when compared to traditional statistical regression techniques as the former offer extra degrees of freedom for generalization. Learning in a neural network may be supervised or unsupervised [8, 20] .

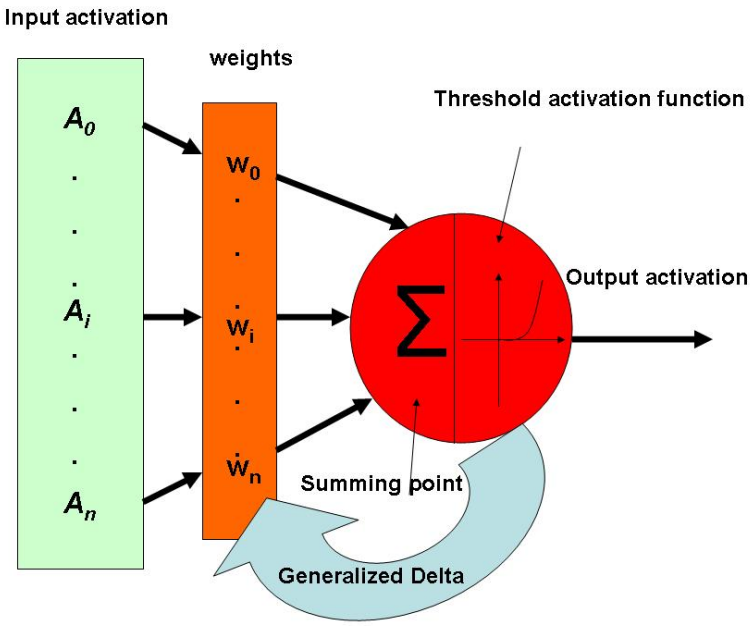

Figure 6.3: A schematic of a single neuron, showing the components of a typical artificial processing unit.

The utility of neural networks has permeated many fields of endeavor for process modeling and optimization [4, 5, 9, 16–19, 22, 26]. Recently, Kim, Bae and Lee found improvements of more than 30% in the prediction of etch microtrenching of silicon oxynitride using neural networks [11] . Al-Haik, Hussaini and Garmestani utilized neural networks for the prediction of stress relaxation in polymer composites [2] . Setia and May trained neural networks for the study of variations in a set of responses in microvia formation [23] . A hybrid neural network model was developed in [3] for the detection of phosphorus in As/P heterostructures.

6.2.1 Neural Network Theory

Figure 9.4 shows a schematic of a neuron. The activation function of the neuron may be represented as a sigmoid, such as

$$f(x) = \frac{1}{1 + e^{-x}} \tag{6.1}$$

where x is the weighted sum of the neural inputs and $f(x)$ is the output of an individual neuron.

Apart from semiconductor manufacturing, neural networks have found uses in many fields, including banking, medicine, pattern recognition, forensics, among others. As a result of the surge in demand for neural network tools, many commercial tools have being developed for neural network modeling. Commercial softwares such as MATLAB's Neural Network Toolbox [2] and Maple's Artificial Neural Network package [3] have been developed. Among them is the Object Oriented Neural Signal Simulator (ObOrNNs).

In this research, the Object-Oriented Neural Network Simulator (ObOrNNS) , a platform-independent Java-based neural network software package developed by the Intelligent Semiconductor Group at Georgia Tech, was used. The data from the designed experiment was provided to the ObOrNNS software for modeling. The data was partitioned into training and testing (validation) sets.

6.2.2 Neural Network Architecture

In neural network learning, a set of interconnection strengths, weights, are are adjusted and act as facilitators of activation of the neurons to achieve a desired state given a set of sampled patterns. Figure 9.5 illustrates a multilayer perceptron (MLP) neural network showing the input layers, hidden layers, and output layers. The first layer is the input layer, which accepts data into the network. The hidden layer then receives the weighted input and forwards it to the output through an activation function.

[2] Mathworks.http://www.mathworks.com/products/neuralnet/
[3] www.maplesoft.com/applications/appcenterview.aspx

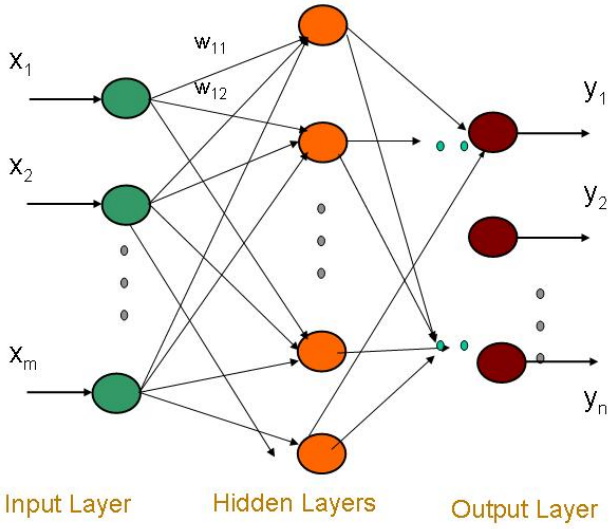

Figure 6.4: A schematic of a multilayer perceptron (MLP) neural network showing the input layers, hidden layers, and output layers.

6.2.3 Neural Network Training

Training in a neural network may be either supervised or unsupervised.In supervised training, input-output data is available, and the error between the output network and the target data is used to generate the feedback to the network for learning. Unsupervised learning is used in the absence of input-output data. In microelectronics, supervised learning is used for modeling the process data obtained during fabrication.

Supervised training involves updating weights in such a way that the error between the output of the neural network and the actual output data is minimized. The error back-propagation (BP) algorithm, a form of supervised learning, was used for network training. This algorithm seeks to minimize the mean squared error of the network output compared to a training signal. This is accomplished via the gradient descent approach [12]. During training, the input data is randomized and a learning rate is specified. Weights are updated at the last layer using weight changes for each node, and these weights are back-propagated to the input layer. The learning rate is the rate of changing the weight in the computation. The user may also specify if a part of the previous weight should be applied to the current weight. The momentum denotes the amount of the previous weight to apply to the current run. This parameter decreases the likelihood that the algorithm becomes trapped in a local minimum and increases the speed of convergence.

The weight update equation for BP training for the (n+1)th iteration is given by

$$\omega_{ijk}(n+1) = \omega_{ijk}(n) + \alpha\Delta\omega_{ijk}(n-1) + \eta\omega_{ijk}(n) \tag{6.2}$$

where ω_{ijk} is the weight between the jth neuron in layer (k-1) and the ith neuron in layer k, and Δw_{ijk} is the calculated change in the interconnection strength, that reduces the the error function of the network. η is the learning rate, and has a value between 0 and 1. α is the momentum, as defined earlier.

The network performance is measured by the metrics of network training error and prediction error. The learning ability is quantified by the root-mean-square error (RMSE)

given by

$$RMSE = \sqrt{\frac{1}{n-1}\sum_{i=1}^{n}(y_i - \widehat{y}_i)^2} \tag{6.3}$$

where n is the number of trials and y_i is the measured values of each response, and $\widehat{y}_i$ is the neural network model output. The training error is the RMSE of the data used for network training, and the prediction error is the RMSE of the data reserved for network testing.

REFERENCES

[1] Akhgari, A., Afrasiabi Garekani, H., Sadeghi, F., and Azimaie, M., "Statistical optimization of indomethacin pellets coated with ph-dependent methacrylic polymers for possible colonic drug delivery," *International Journal of Pharmaceutics*, vol. 305, no. 1-2, pp. 22–30, 2005. article.

[2] Akhgari, A., Afrasiabi Garekani, H., Sadeghi, F., Azimaie, M., Al-Haik, M. S., Hussaini, M. Y., and Garmestani, H., "Prediction of nonlinear viscoelastic behavior of polymeric composites using an artificial neural network," *International Journal of Pharmaceutics*, vol. 22, no. 7, pp. 1367–1392, 2006. Prediction of nonlinear viscoelastic behavior of polymeric composites using an artificial neural network.

[3] Brown, T. D. and May, G. S., "Hybrid neural network modeling of anion exchange at the interfaces of mixed anion iii-v heterostructures grown by molecular beam epitaxy," *Ieee Transactions on Semiconductor Manufacturing*, vol. 18, no. 4, pp. 614–621, 2005. article.

[4] Bushman, S., Edgar, T. F., and Trachtenberg, I., "Modeling of plasma etch systems using ordinary least squares, recurrent neural network, and projection to latent structure models," *Journal of the Electrochemical Society*, vol. 144, no. 4, pp. 1379–1389, 1997. article.

[5] Caffarel, J., Gibson, G. J., Harrison, J. P., Griffiths, C. J., and Drinnan, M. J., "Comparison of manual sleep staging with automated neural network-based analysis in clinical practice," *Medical & Biological Engineering & Computing*, vol. 44, no. 1-2, pp. 105–110, 2006. article.

[6] Cecchi, M., Smith, H., and Braun, D., "Method to optimize polymer film spin coating for polymer led displays," *Synthetic Metals*, vol. 121, no. 1-3, pp. 1715–1716,

2001. article.

[7] Chinoy, P. B., "Reactive ion etching of benzocyclobutene polymer films," *IEEE Transactions on Components, Packaging & Manufacturing Technology, Part C (Manufacturing)*, vol. 20, no. 3, pp. 199–206, 1997. article.

[8] Cleon, D. E. and May, G. S., "Neural network control of variable-frequency microwave processing of polymer dielectric curing," *IEEE Transactions on Electronic Packaging Manufacturing*, pp. 1521 – 334X, 2008. article.

[9] Emoto, T., Akutagawa, M., Abeyratne, U. R., Nagashino, H., and Kinouchi, Y., "Tracking the states of a nonlinear and nonstationary system in the weight-space of artificial neural networks," *Medical & Biological Engineering & Computing*, vol. 44, no. 1-2, pp. 146–159, 2006. article.

[10] Gou, J., Liang, Z., and Wang, B., "Experimental design and optimization of dispersion process for single-walled carbon nanotube bucky paper," *International Journal of Nanoscience*, vol. 3, no. 3, pp. 293–307, 2004. article.

[11] Kim, B., Bae, J., and Lee, B. T., "Modeling of silicon oxynitride etch microtrenching using genetic algorithm and neural network," *Microelectronic Engineering*, vol. 83, no. 3, pp. 513–519, 2006. article.

[12] Kowalski, S. M., Vining, G. G., Montgomery, D. C., and Borror, C. M., "Modifying a central composite design to model the process mean and variance when there are hard-to-change factors," *Journal of the Royal Statistical Society: Series C (Applied Statistics)*, vol. 55, no. 5, pp. p615 – 630, 2006. article.

[13] Kramar, A., Turk, S., and Vrecer, F., "Statistical optimisation of diclofenac sustained release pellets coated with polymethacrylic films," *International Journal of Pharmaceutics*, vol. 256, no. 1-2, pp. 43–52, 2003. article.

[14] Munasur, A., Pillay, V., Chetty, D., and Govender, T., "Statistical optimisation of the mucoadhesivity and characterisation of multipolymeric propranolol matrices for

buccal therapy," *International Journal of Pharmaceutics*, vol. 323, no. 1-2, pp. 43–51, 2006.

[15] Myers, R. H., Montgomery, D. C., Vining, G. G., Borror, C. M., and Kowalski, S. M., "Response surface methodology: A retrospective and literature survey," *Journal of Quality Technology*, vol. 36, no. 1, pp. 53–77, 2004. article.

[16] Ng, N. T., Lai, K. W., Quadir, G. A., Seetharamu, K. N., Abdul, I., and Zainal, Z. A., "Optimization of liquid cooling fins in microelectronic packaging," *Engineering Optimization*, vol. 35, no. 4, pp. 359–374, 2003. article.

[17] Ning, G. M., Su, J., Li, Y. Q., Wang, X. Y., Li, C. H., Yan, W. M., and Zheng, X. X., "Artificial neural network based model for cardiovascular risk stratification in hypertension," *Medical & Biological Engineering & Computing*, vol. 44, no. 3, pp. 202–208, 2006. article.

[18] Prange, S. J., Jahnke, A., and Klar, H., "Microelectronics for dynamic neural networks," *Annales Des Telecommunications-Annals of Telecommunications*, vol. 48, no. 7-8, pp. 368–377, 1993. article.

[19] Pratap, R. J., Staiculescu, D., Pinel, S., Laskar, J., and May, G. S., "Modeling and sensitivity analysis of circuit parameters for flip-chip interconnects using neural networks," *IEEE Transactions on Advanced Packaging*, vol. 28, no. 1, pp. 71–78, 2005. article.

[20] Pratap, R. J., Sen, P., Davis, C. E., Mukhophdhyay, R., May, G. S., and Laskar, J., "Neurogenetic design centering," *IEEE Transactions on Semiconductor Manufacturing*, vol. 19, no. 2, pp. 173 – 181, 2006. article.

[21] Ragonese, R., Macka, M., Hughes, J., and Petocz, P., "The use of the box-behnken experimental design in the optimisation and robustness testing of a capillary electrophoresis method for the analysis of ethambutol hydrochloride in a pharmaceutical formulation," *Journal of Pharmaceutical and Biomedical Analysis*, vol. 27, no. 6, pp. 995–1007, 2002. article.

[22] Robert, S. and Mure-Ravaud, A., "Control of the homogeneity of an optical grating by a neural characterization," *Optical Engineering*, vol. 44, no. 3, 2005. article 033601.

[23] Setia, R. and May, G. S., "Run-to-run failure detection and diagnosis using neural networks and dempster-shafer theory: an application to excimer laser ablation," *IEEE Transactions on Electronics Packaging Manufacturing*, vol. 29, no. 1, pp. 42–9, 2006. article.

[24] Singh, B., Dahiya, M., Saharan, P., and Ahuja, N., "Optimizing drug delivery systems using systematic "design of experiments." - part ii: Retrospect and prospects," *Critical Reviews in Therapeutic Drug Carrier Systems*, vol. 22, no. 3, pp. 215–293, 2005. article.

[25] Tae Seon, K. and May, G. S., "Optimization of via formation in photosensitive dielectric layers using neural networks and genetic algorithms," *IEEE Transactions on Electronics Packaging Manufacturing*, vol. 22, no. 2, pp. 128–36, 1999. article.

[26] Tryba, V. and Goser, K., "A modified algorithm for self-organizing maps based on the schrodinger-equation," *Lecture Notes in Computer Science*, vol. 540, pp. 33–47, 1991. article.

[27] Wei, B.-Y., Ho, S.-L., Chen, F.-Y., and Lin, H.-M., "Optimization of process parameters for preparing wo₃/polyacrylonitrile nanocomposites and the associated dispersion mechanism," *Surface and Coatings Technology*, vol. 166, no. 1, pp. 1–9, 2003. article.

CHAPTER VII

DESIGNED EXPERIMENTS

7.1 INTRODUCTION

Shape memory polymers (SMPs) [3] [4] [5] [6] have the unique property that they can recover from an imposed deformation by the application of an external stimulus such as heat, light of a specific frequency, or magnetic field. This class of polymer has received significant attention in recent years due to its prospects for applications in many areas such as nanotechnology, biomedical devices such as stents, information storage devices, and microelectromechanical systems (MEMs) [2], among others. Although shape memory polymers have found niche applications in the above areas, much work is required for the use of these polymers in MEMs in general, and information storage in particular. In this study, we considered polymer systems based on diethylene glycol dimethacrylate (DEGDMA) crosslinker and tert-butyl acrylate (tBA) monomer. These polymers were chosen since they offer many benefits including biocompatibility and ease of UV-processing. However, process optimization techniques have not been applied to fabrication using these material systems. In order to minimize cost of production and also reduce failure, statistical experimental design is an invaluable tool for modeling manufacturing processes. Designed experiments facilitate the systematic investigation of the dependence of a set of outputs (responses) on a set of process conditions (factors). Information on the interaction of the various factors is determined by a systematic mathematical process. Full factorial designs enable the exploration of input factors that are significant-this approach minimizes experimental time and helps conserve resources. Central composite face-cented (CCF) designs [14] are full factorial designs with extra points at the centers of a "cube" in the design space. CCF facilitates response surface modeling and optimization. Neural networks, mathematical models crudely based on neurological systems, are tools with the ability to deduce complex relationships between input

and output variables in an experiment. Since their advent in the early 1940s, neural networks have been used in many areas of research including MEMs, biomedical engineering, etc. [10] [7] [12] [13] [8]. A software package that enables neural network based process modeling is the Java-based Object-Oriented Neural Network Simulator (ObOrNNS) developed by the Intelligent Semiconductor Manufacturing (ISM) laboratory at the Georgia Institute of Technology [1]. A review of the current literature reveals little work in the application of designed experiments to SMPs in general, and acrylates in particular. As a result, statistical experimental designs were performed on these materials to determine the effects of various processing conditions on the thermomechanical properties of the SMPs. Subsequently, neural network process models were developed to enable the prediction of material properties from known process conditions. In this paper, Section 2 contains information on the material characterization, the designed experiments, and initial material characterization. Section 3 describes the neural network concept, while Section 4 discusses the preliminary results in the experiment. The chapter concludes with a synopsis and a brief description of future work.

7.2 EXPERIMENTAL TECHNIQUE

7.2.1 Initial material characterization

In this experiment, materials based on diethyelene glycol dimethacrylate (DEGDMA) crosslinker and a tert-butyl acrylate (tBA) monomer were investigated. The chemicals were acquired from Sigma-Aldrich and had a purity of 99%. In order to make the materials photoactive, 1 wt% of the photoinitiator dimethoxy-2-phenyl acetophenone was added to each solution in a vial. The solutions were UV-polymerized for 10 minutes each. The materials were then cut into shapes of 25mm Œ 4mm Œ 1mm. A TA Instruments dynamic mechanical analyzer (DMA) was used in tension mode to measure thermomechanical properties [11].

7.2.2 Designed experiment

Three variables were selected to explore their effect on the following responses: film thickness, film uniformity, and nanomechanical properties (hardness and modulus). The input parameters were the spin speed, spin time, and nitrogen flow rate. Prior to the selection of these variables, full factorial experiments were conducted and these variables were significant, and

thus worthy of further investigation. Previous research has shown that acrylate-based polymers are impossible to UV-polymerize in the presence of oxygen [9]. Therefore, nitrogen flow was considered in our investigation. Randomized screening experiments were performed with 23 a full factorial design having two center points. Thus, the total number of experimental trials for screening was ten. The ranges of the parameters are shown in Table 3.

Table 2: Process parameter and ranges for DEGDMA

Parameter	Abbrev.	Ranges	Units
Spin Speed	SS	500-4000	rpm
Spin Time	ST	10-100	s
Nitrogen flow	N2flow	1-5	sccm

In order to model the response surface of the materials, we augmented the full factorial design to a central composite face-centered (CCF) design. In a CCF design, the full factorial design was augmented by adding extra points at the central faces of a cube, as illustrated in Figure 6.2 of Chapter 6.1.1.

7.2.3 Material Processing and Characterization

The polymers were spin coated on diced pieces of wafers measuring approximately 2 cm square in the Microelectronics Research Center at the Georgia Institute of Technology. The spin coating was performed using a CEE coater. Curing of the films was accomplished using a SAMCO wafer stripper fitted with a nitrogen regulator.

7.2.4 Film Thickness Measurement

The film thickness of the spun and cured films were measured using the V-VASE variable angle spectroscopic ellipsometer (J.A Woolam Inc, Lincoln, NE, USA). The instrument was run from 300 nm to 1100 nm at angles of 65°C, 70°Cand 75°Cto determine the amplitude ratio, Ψ, and phase difference, Δ, ellipsometric parameters of the materials. The ellipsometric data was analyzed using the WVASE-32 analysis software. Cauchy fitting method was used to analyze the Δ and Ψ employing a film model of a polymer on a silicon substrate. The real (n) and imaginary (k) parts of the refractive index were extracted from the

generated ellipsometric data. The refractive indices were provided to the Nanospec refractometer (Nanometrics Inc, Milpitas, CA, USA) for thickness measurements. For each film, a minimum of ten individual measurements were performed to minimize measurement error. Analysis of variance (ANOVA) was used to investigate the significance of input parameters on the thickness and uniformity (Unif) of the films. The uniformity was defined as:

$$Unif = \frac{\sigma}{\mu} \tag{7.1}$$

where σ is the standard deviation of the film thickness, and the μ is the average thickness of a film.

7.3 NEURAL NETWORKS

Neural networks are computational methods loosely based on the biological functions of the central nervous system. A neural network comprises a web of adjoining neurons in a network functioning in tandem to produce an output, as illustrated in Fig.3. Neural networks are useful tools in many research and industrial applications [12]. The utility of neural networks has permeated many fields of endeavor. A neural network learns from the input provided to it and is able to remember past events by storing information in adjoining strengths called weights. Neural networks are advantageous when compared to traditional statistical regression techniques as the former offer extra degrees of freedom for generalization. Learning in a neural network may be supervised or unsupervised [7].

In this research, the error back-propagation (BP) algorithm, a form of supervised learning, was used for network training. This algorithm seeks to minimize the mean squared error of the network output compared to a training signal. This is accomplished via the gradient descent approach [12]. During training, the input data is randomized and a learning rate is specified. Weights are updated at the last layer using weight changes for each node, and these weights are back-propagated to the input layer. The learning rate is the rate of changing the weight in the computation. The user may also specify if a part of the previous weight should be applied to the current weight. The momentum denotes the amount of the previous weight to apply to the current run. This parameter decreases the likelihood that

the algorithm becomes trapped in a local minimum and increases the speed of convergence. Mathematically, the weight is updated via the generalized delta rule:

$$\omega_{jk}(n+1) = \alpha\Delta\omega_{jk}(n) + \eta\Delta\omega_{jk}(n+1) for \Delta\omega_{jk}(n+1) = \eta\delta_j(n+1)o_k(n+1) \qquad (7.2)$$

where w_{jk} is the connection strength between the output layer, k and the input layer, j, α is the momentum, n is the number of iterations and η is the learning rate [8]. Many commercial tools have being developed for neural network modeling. In this research, the Object-Oriented Neural Network Simulator (ObOrNNS) [8], a platform-independent Java-based neural network software package developed by the Intelligent Semiconductor Group at Georgia Tech, was used. The data from the designed experiment was provided to the ObOrNNS software for modeling. The data was partitioned into training and testing (validation) sets. The average RMS errors in training were less than 2% and less than 15% in testing.

7.4 RESULTS AND DISCUSSION

Response surface modeling was performed based on neural networks to establish the relationship between the outputs (thickness and uniformity) and the inputs (spin speed, spin time, and nitrogen flow). Table 1 shows the input parameters and their settings for the material, DEGDMA. Two of the input parameters were varied, while the third was held constant at its middle value. Three dimensional plots were generated using MATLAB. Figure 9.6 depicts film thickness with respect to spin speed and spin time when the nitrogen flow rate is fixed at its midpoint value of 3 sccm. It is evident from this Fig.that, the spin speed had the most prominent effect on the thickness of the films. The spin time also affected the thickness, but not as drastic as the spin speed. Uniformity variation is shown in Figure 9.7 for a midpoint flow rate of 3 sccm. Once again, the spin speed shows a drastic effect on the uniformity. The spin time shows almost no effect on uniformity except for a small parabolic small decrease in uniformity in the middle portion of the time axis.

Figure 9.8 illustrates the variation of the thickness with respect to the nitrogen flow rate and the spin speed at the midpoint spin time of 55 s. Although the thickness decreases

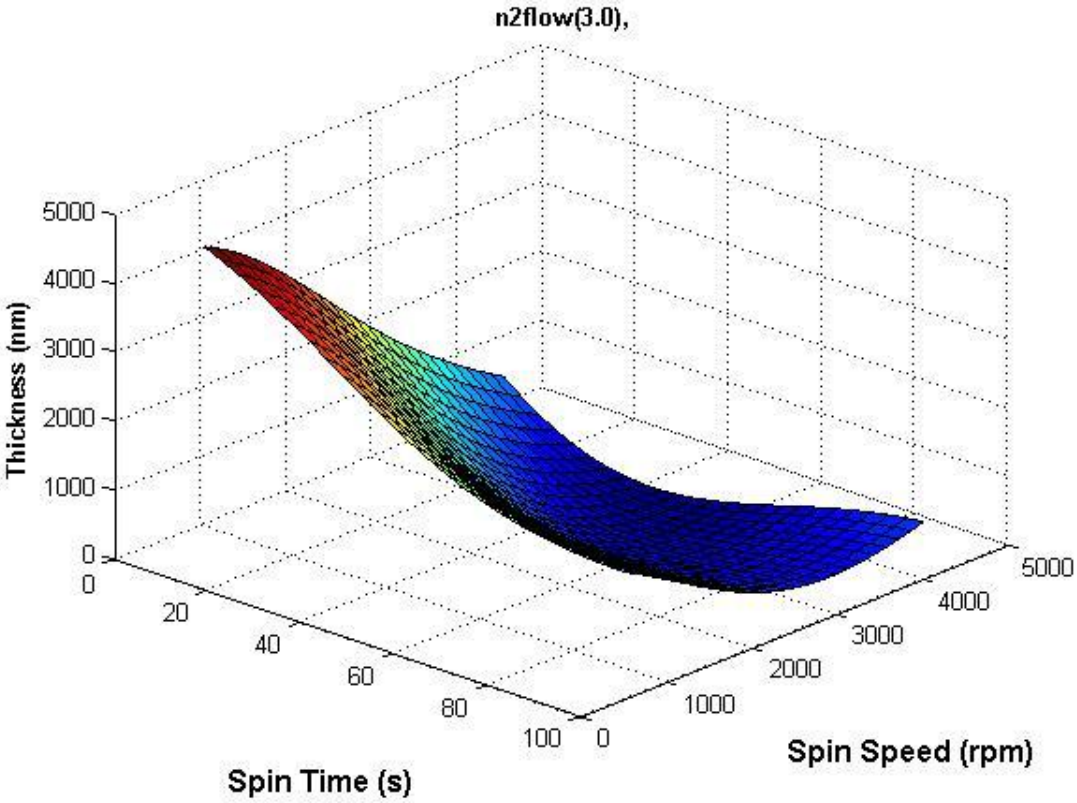

Figure 7.1: Film thickness with respect to spin speed and spin time when the nitrogen flow rate is fixed at its midpoint value of 3 sccm.

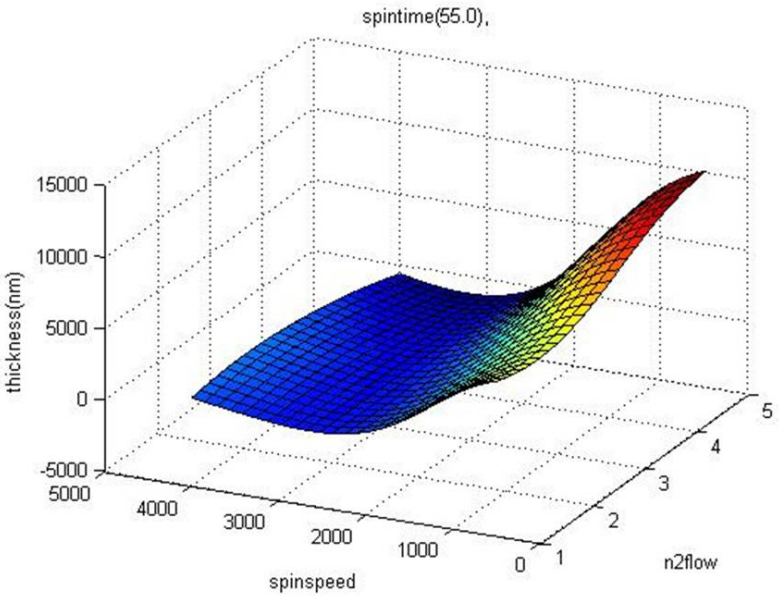

Figure 7.2: Nonuniformity for a nitrogen flow rate of 3 sccm.

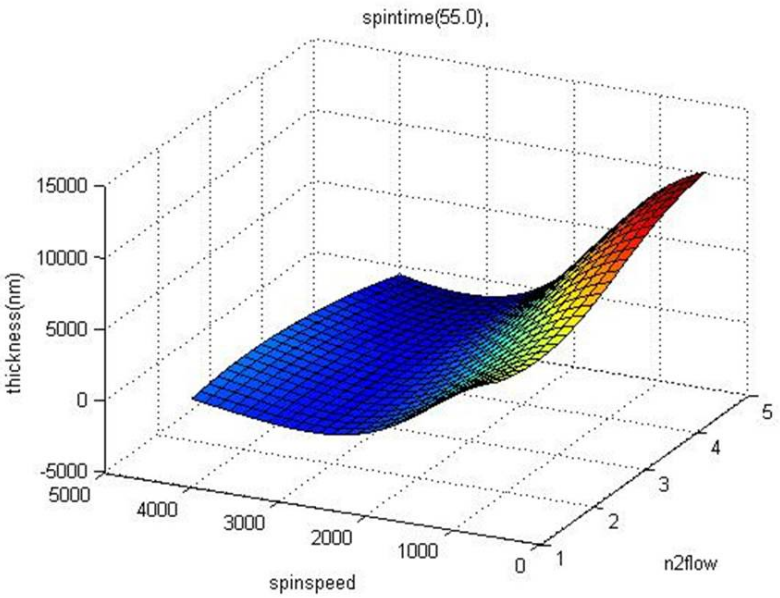

Figure 7.3: Thickness with respect to the nitrogen flow rate and the spin speed at the midpoint spin time of 55 s.

with increasing speed as expected, the nitrogen flow rate did not show any effect on the thickness. Figure 9.9 illustrates the uniformity variation on the film with respect to the nitrogen flow rate and the spin speed at the midpoint spin time of 55 s. Once again, the uniformity did not show any appreciable dependence on the spin time. However, there exists a drastic effect of spin speed on the uniformity of the films. These results reveal that a set of points can be selected for a tailored thickness and/or uniformity for a given application. For information storage using nanoindentation, a film surface devoid of imperfections (uniform) is required. Thus, these 3-D surfaces provide a baseline for the selection of process conditions for a particular application.

7.5 Summary

Three parameters were selected and full factorial screening experiments were run on spin coated polymer films of DEGDMA. Response surfaces were modeled from a neural network package. Spin speed had the most prominent effect on the both the thickness and uniformity of the spin coated films. The response surfaces are useful as a ready recipe for the processing of films based on DEGDMA. The experiment will be extended to other materials and

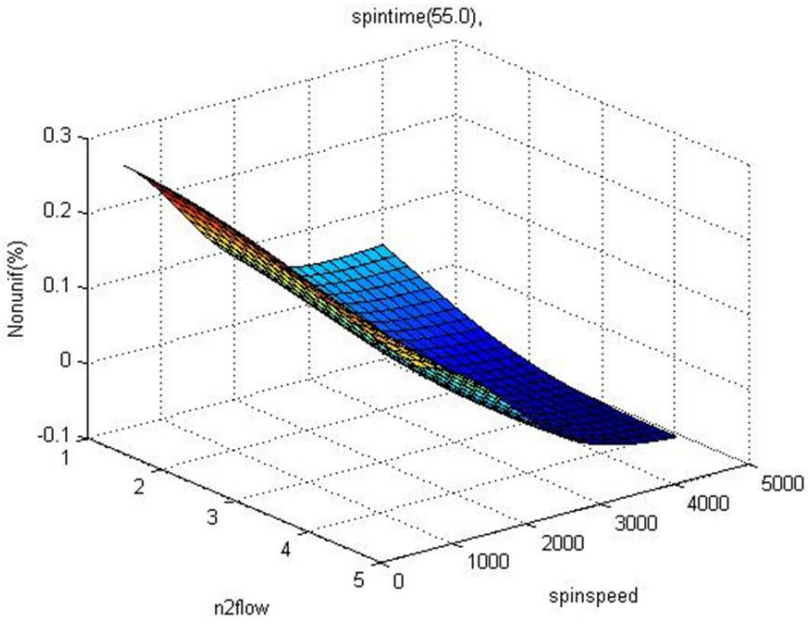

Figure 7.4: Nonuniformity for a spin time of 55 s.

investigation of the use of these materials for information storage will be performed.

The chapters that follow expand on these results using genetic optimization techniques. Thus, some figures and information from this chapter are repeated in the coming chapters.

REFERENCES

[1] Davis, C., Hong, S., Setia, R., Pratap, R., Brown, T., Ku, B., Triplett, G., and May, G., "An object-oriented neural network simulator for semiconductor manufacturing applications," *IIIS 8 thAnnual Multi-Conf. Syst. Cybern. Inform*, vol. 5, pp. 365–370, 2004.

[2] Gall, K., Kreiner, P., Turner, D., and Hulse, M., "Shape-memory polymers for microelectromechanical systems," *Microelectromechanical Systems, Journal of*, vol. 13, no. 3, pp. 472–483, 2004.

[3] Kagami, Y., Gong, J. P., and Osada, Y., "Shape memory behaviors of crosslinked copolymers containing stearyl acrylate," *Macromolecular Rapid Communications*, vol. 17, no. 8, pp. 539–543, 1996. <Go to ISI>://A1996VB88200006.

[4] Langer, R. and Tirrell, D. A., "Designing materials for biology and medicine," *Nature*, vol. 428, no. 6982, pp. 487–492, 2004. <Go to ISI>://000220540100031.

[5] Lendlein, A., Jiang, H. Y., Junger, O., and Langer, R., "Light-induced shape-memory polymers," *Nature*, vol. 434, no. 7035, pp. 879–882, 2005. <Go to ISI>://000228327600036.

[6] Lendlein, A. and Kelch, S., "Shape-memory polymers as stimuli-sensitive implant materials," *Clinical Hemorheology and Microcirculation*, vol. 32, no. 2, pp. 105–116, 2005. <Go to ISI>://000228104900004.

[7] Pratap, R. J., Sen, P., Davis, C. E., Mukhophdhyay, R., May, G. S., and Laskar, J., "Neurogenetic design centering," *IEEE Transactions on Semiconductor Manufacturing*, vol. 19, no. 2, pp. 173 – 181, 2006. article.

[8] Pulgarin, J. A. M., Bermejo, L. F. G., and Garcia, M. N. S., "Multivariate calibration applied to the time-resolved chemilumnescence for the simultaneous determination of morphine and its antagonist naloxone," *Analytica Chimica Acta*, vol. 602, no. 1, pp. 66–74, 2007. <Go to ISI>://000250629600008.

[9] Tryson, G. R. and Shultz, A. R., "A calorimetric study of acrylate photopolymerization," *Journal of Polymer Science: Polymer Physics Edition*, vol. 17, no. 12, pp. 2059–2075, 1979. General Electric Corporate Research and Development, Schenectady, New York 12345.

[10] Tseng, Y. S., Fu, H. H., Hung, T. C., and Pei, B. S., "An optimal parametric design to improve chip cooling," *Applied Thermal Engineering*, vol. 27, no. 11-12, pp. 1823–1831, 2007. <Go to ISI>://000247051700008.

[11] Wornyo, E., Gall, K., Yang, F. Z., and King, W., "Nanoindentation of shape memory polymer networks," *Polymer*, vol. 48, no. 11, pp. 3213–3225, 2007. <Go to ISI>://000246934600021.

[12] Yang, Y. K., "Optimization of a photo resists coating process for photolithography in wafer manufacturing via design of experiments method," *Microelectronics International*, vol. 23, no. 3, pp. 26–32, 2006. <Go to ISI>://000239730700005.

[13] Yang, Y. K. and Chang, T. C., "Experimental analysis and optimization of a photo resist coating process for photolithography in wafer fabrication," *Microelectronics Journal*, vol. 37, no. 8, pp. 746–751, 2006. <Go to ISI>://000238920700014.

[14] Zuazagoitia, D., Millan, E., and Garcia, R., "A screening method for polycyclic aromatic hydrocarbons determination in water by headspace spme with gc-fid," *Chromatographia*, vol. 66, no. 9-10, pp. 773–777, 2007. <Go to ISI>://000251297300021.

CHAPTER VIII

GENETIC ALGORITHMS

Genetic algorithms (GAs) are stochastic guide search techniques modeled on mechanics of evolution and natural selection. The process is based on "survival of the fittest" [1, 3–6, 8]. The search is predicated on three genetic operations in genetics (reproduction, crossover, and mutation). GAs are capable of searching through complex spaces speedily. A GA requires only an objective function value information to guide a search;it does not require derivative information, continuity, or complete knowledge of the objective function. Compared to engineering optimization, a GA takes a more global view of the search space [1]. GAs are executed through four stages:

1. Creation of a "population" of strings
2. Evaluation of each string
3. Selection of the "best" strings
4. Genetic manipulation–to create a new population

8.0.1 Creation of String Population

For a computational cycle, a new generation of possible solutions for a given problem results. The search process involves the creation of an initial population of potential solutions. These populations are then encoded into a string ("chromosome"), which is manipulated by genetic operators. Performance "fitness" of each individual in the population is evaluated based on the imposed constraints. "Mates" for the genetic manipulation process are chosen with respect to each individual string's fitness. This approach ensures that the range and precision of decision variables can be controlled. The precision (π) of the mapped encoding may be expressed as:

$$\pi = \frac{U_{max} - U_{min}}{2^l - 1} \tag{8.1}$$

8.0.2 Evaluation of Population

In order to define a chromosome, each variable must be encoded into a binary string. Alphanumeric strings may also be used. A competent method of encoding multi-parameter optimizations is concatenated, multi-parameter, mapped, and fixed-point coding.Given as a parameter of interest, number of bits of length l, there exists a linear map from to $[0, 2^l]$ a specified interval $[U_{min}, U_{max}]$.

8.0.3 Selection of the "best" strings

Concatenation of many individual parameter strings results in the multi-parameter code. Each constituent code is allowed to have its own sub-length or range. Figure 8.1 illustrates a two parameter coding, with ranges for the first and second parameters as 2-5 and 0-15, respectively.

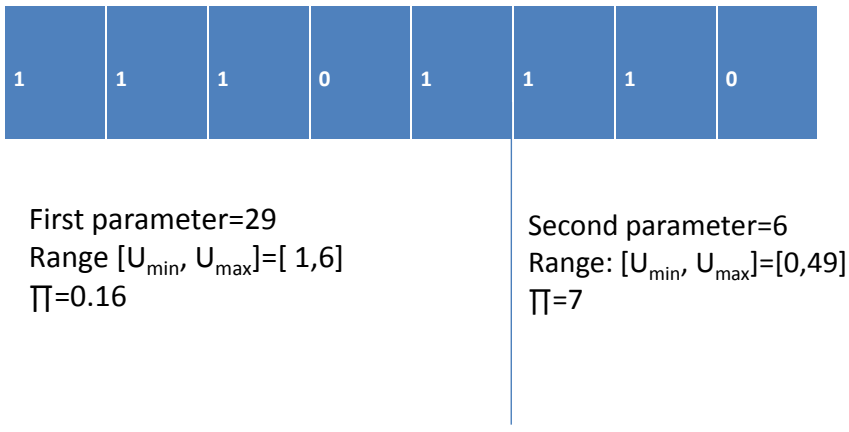

Figure 8.1: A multi-parameter coding scheme.

Manipulation of the genetic code of members ("parents") of the current population results in the creation of a new population of "offspring" via the genetic operators (reproduction, crossover, and mutation). Reproduction is the process by which strings with high fitness values–good solutions to the optimization problem under consideration–generate large number of copies in the new population. Reproduction is based on the elitist roulette wheel selection, in which strings with large fitness values F_i are assigned a proportionately higher probability of survival into the next generation. The probability distribution is expressed as:

$$P_{Select_i} = \frac{F_i}{\Sigma F} \tag{8.2}$$

The fitness function depends on the constraints imposed by the optimization problem. The value of the fitness function (F) is expressed for n number of responses as

$$F = \frac{1}{1 + \Sigma |K_n(y_d - y_o)} \tag{8.3}$$

where K_n are the weights of the responses, y_d represent the desired response, and y_d are the outputs that results from the current input parameters.

8.0.4 Crossover and Mutation

A "mating pool" stores the strings that have reproduced, awaiting actions of the crossover (Figure 8.2) and (Figure 8.3) mutation operations. The crossover operation interchanges parts of the genetic code of two parents, to produce two new chromosomes. Mutation probability is used to randomly change a fixed number of bits every generation. The mutation operation ensures that the initial population contains all the genetic information needed to solve the problem.

Typical values for probabilities of bit mutation and crossover range from 0.001 to 0.1 and 0.6 to 0.95, respectively. Higher mutation and crossover rates lead to disruption of good "building blocks". For smaller populations, sampling errors tend to nullify the predictions.Thus, for smaller population sizes, larger values for the mutation and crossover rates result in lower confinement of predicted solutions.

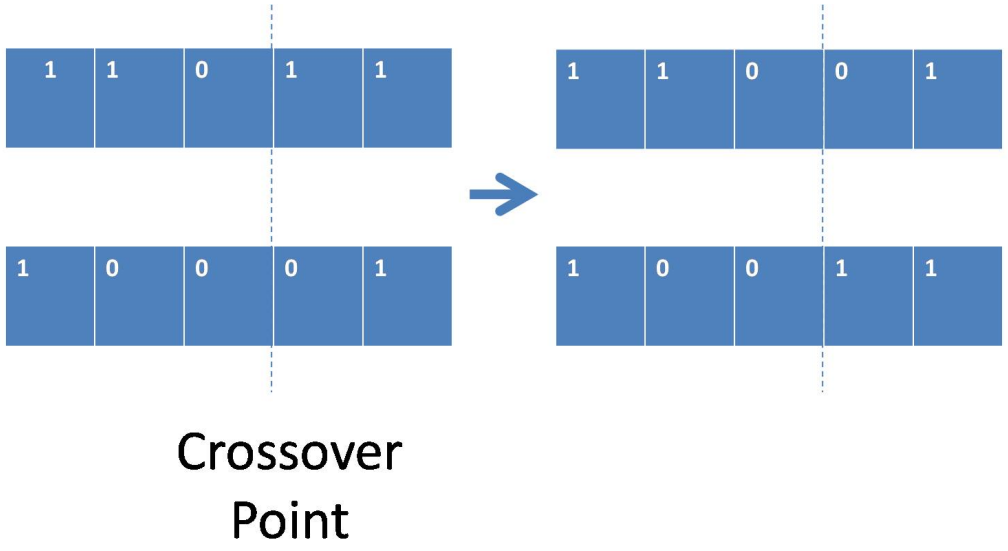

Figure 8.2: Illustration of crossover in genetic algorithms

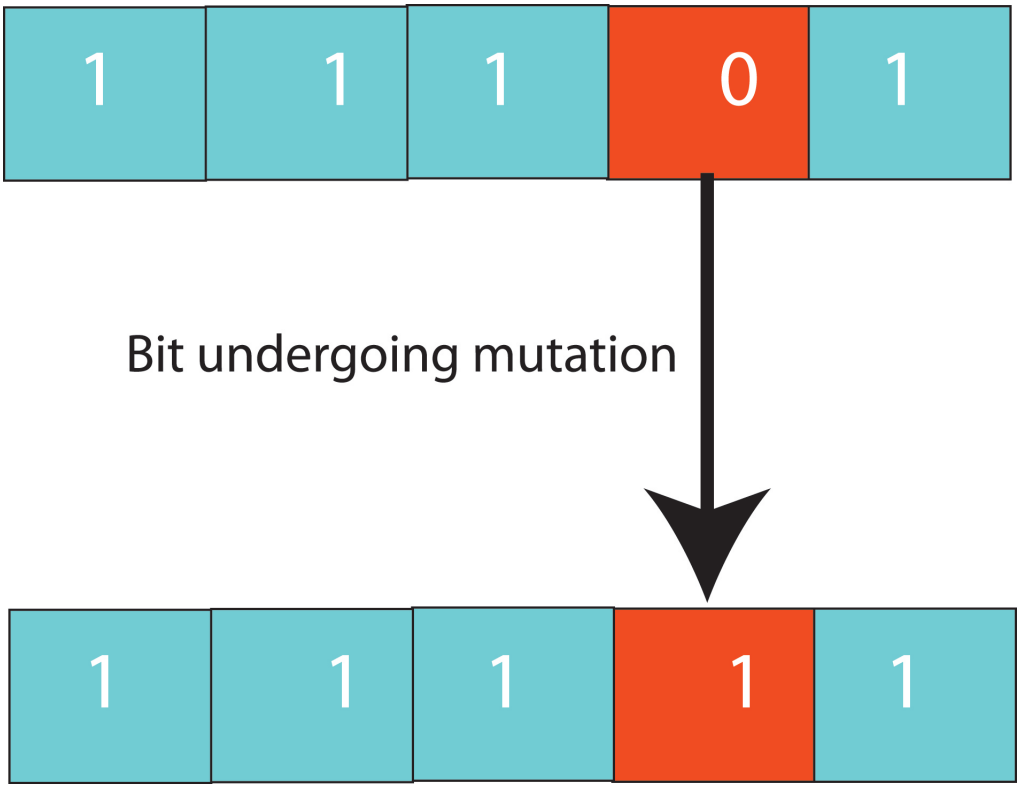

Figure 8.3: Mutation operation in genetic algorithms

8.0.5 Neuro-Genetic Manipulation

The Object Oriented Neural Network Simulator (ObOrNNs) package, a neural network modeling software developed by the Intelligent Semiconductor Manufacturing Group at Georgia Tech, was used for encoding. Process inputs are generated from the neural network model, which calculates the predicted responses. The output is fed iteratively to the genetic algorithms until a specified stopping criterion.The stopping criterion could be a user-defined maximum number of generations or a minimum error rate. The weighing coefficients for the desired outputs are also determined based on the application and the order if importance of the responses. The process optimization procedure is illustrated in Figure 8.4 [2, 4–7].

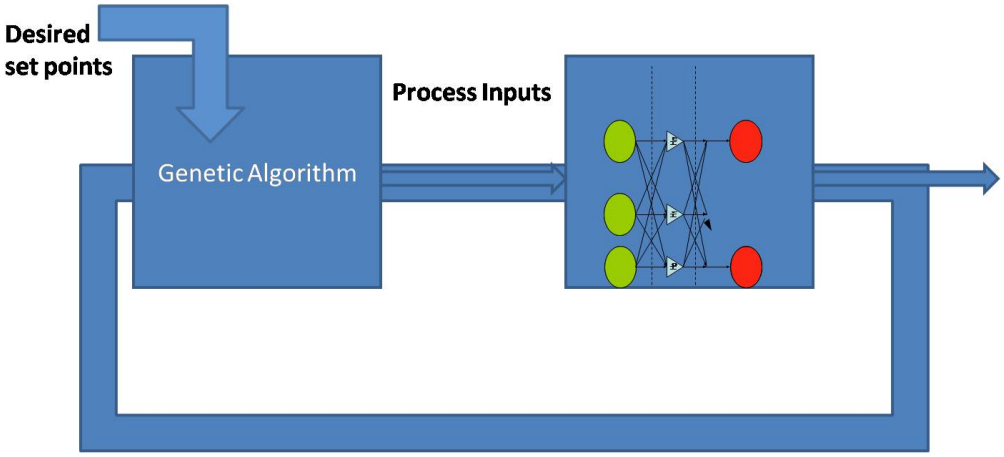

Figure 8.4: Schematic of neural network model showing the input and outputs. An iterative process continues until the stopping criterion, such as the desired error rate is achieved.

8.1 Summary

The current chapter presented a brief theory of genetic optimization techniques. It discussed the entire process from creation of a string of the initial population through the evaluation and selection of the "'best" string to the manipulation of the strings. This background is essential to the effective optimization of processes. The next chapter builds on the principles discussed here. The principles are recalled for the optimization of the thickness, uniformity, modulus, and hardness of diethylene glycol dimethacrylate (DEGDMA) and bispehenol A ethoxylate. Understanding the behavior of polymers at the nanoscale is essential to the reliability of devices in which these materials are used.

REFERENCES

[1] Han, S. S., "Modeling and optimization of plasma-enhanced chemical vapor deposition using neural networks and genetic algorithms," 1996.

[2] Kim, B., Bae, J., and Lee, B. T., "Modeling of silicon oxynitride etch microtrenching using genetic algorithm and neural network," *Microelectronic Engineering*, vol. 83, no. 3, pp. 513–519, 2006. article.

[3] Raman, S. and Domeniconi, C., "Gene expression analysis of hiv-1 linked p24-specific cd4+ t-cell responses for identifying genetic markers," *Feature Selection for Data Mining*, 2005.

[4] Setia, R. and May, G. S., "Modeling and optimization of via formation in dielectrics by laser ablation using neural networks and genetic algorithms," *Electronics Packaging Manufacturing, IEEE Transactions on [see also Components, Packaging and Manufacturing Technology, Part C: Manufacturing, IEEE Transactions on]*, vol. 27, no. 2, pp. 133–144, 2004.

[5] Setia, R., May, G. S., Sundaram, V., and Tummala, R. R., "Sensitivity analysis and optimization of excimer laser ablation for microvia formation using neural networks and genetic algorithms," *Electronics Manufacturing Technology Symposium, 2004. IEEE/CPMT/SEMI 29th International*, pp. 131–139, 2004.

[6] Tae Seon, K. and May, G. S., "Optimization of via formation in photosensitive dielectric layers using neural networks and genetic algorithms," *IEEE Transactions on Electronics Packaging Manufacturing*, vol. 22, no. 2, pp. 128–36, 1999. article.

[7] Thongvigitmanee, T. and May, G. S., "Optimization of nanocomposite integral capacitor fabrication using neural networks and genetic algorithms," *Electronics Manufacturing Technology Symposium, 2002. IEMT 2002. 27th Annual IEEE/SEMI International*, pp. 123–129, 2002.

[8] Yun, I. and May, G. S., "Passive circuit model parameter extraction using genetic algorithms," *Electronic Components and Technology Conference, 1999. 1999 Proceedings. 49th*, pp. 1021–1024, 1999.

CHAPTER IX

GENETIC OPTIMIZATION OF POLYMER PROCESSES AND NANOMECHANICAL PROPERTIES

9.1 INTRODUCTION

Shape memory polymers (SMPs) are a class of polymeric materials that have the unique property that they can recover from an imposed deformation by the application of an external stimulus such as heat, light of a specific frequency, or magnetic field. SMPs have been used in heat shrink tubing, biomedical engineering, aerospace and defense applications, among others [19] [29] [32] [18] [1] [8]. This class of polymer has received significant attention in recent years due to its prospects for additional uses in nanotechnology, information storage devices, and microelectromechanical systems (MEMs) [8]. Gall and coworkers investigated shape memory polymers based on acrylates for MEMS [7]. Kagami, Gong, and Osada prepared SMPs by copolymerizing stearyl acrylate and methyl acrylate for biological applications [13]. The principle of actuation of this SMP was based on reversible order-disorder transition of the crystalline stearyl moieties aggregates [13].Schmidt embedded nanoparticles in SMPs by applying electromagnetic fields for biomedical engineering applications [27]. Although SMPs have found niche applications in the above areas, much work is required for the use of these polymers in MEMs in general, and information storage in particular. In this study, the deposition of polymer systems based on diethylene glycol dimethacrylate (DEGDMA) and bisphenol A ethoxylate was modeled and optimized using artificial intelligence techniques. These polymers are biocompatible and lend themselves to UV processing. Statistical experimental design was applied to the spin coating process for these materials to facilitate the systematic investigation of the dependence of film properties on the process conditions. The processes were then modeled using neural networks, and genetic algorithms were applied for optimizing the process [15] [4] [10] [5] [25]. Nanoindentation was subsequently used to probe the suitability of these materials for applications such as information storage. Prior to the

present study, process optimization techniques have not been applied to these material systems. Section II of this section describes designed experimental concepts used. Section III describes process modeling using neural networks. Section IV reviews the basics of genetic algorithms for process optimization. Section V discusses the results obtained in this study.

9.2 EXPERIMENTAL DESIGN

In order to minimize cost of experimentation, statistical experimental design is an invaluable tool for modeling and controlling manufacturing processes. Designed experiments facilitate the systematic investigation of the dependence of a set of outputs (responses) on a set of process conditions (factors). Factorial designs enable the efficient exploration of input factors in a way that minimizes experimental time and conserves resources. Central composite face-centered (CCF) designs are full factorial designs with extra points at the centers of a "cube" in the design space [8]. For k factors, a CCF design consists of 2k factorial, 2k axial, and at least one center point. CCF designs facilitate response surface modeling and optimization. Figure 1 is a schematic of CCF showing the factorial and center points. Molpeceres and co-workers used central composite designs to prepare nanoparticles based on polycaprolactone by solvent displacement [23]. May et al. used composite circumscribed (CCC) design to characterize the etch rate and other variables in reactive ion etching [14]. Newnes et al. also used central composite designs for process modeling in semiconductor device manufacturing [24]. Morana et al. modeled growth rate and intensity of luminescence bands in silicon using CCF designs [23].

In this experiment, materials based on diethyelene glycol dimethacrylate (DEGDMA) and bisphenol A ethoxylate dimethacrylate were investigated. The chemicals were acquired from Sigma-Aldrich and had a purity of 99%. In order to make the materials photoactive, 1 wt% of the photoinitiator dimethoxy-2-phenyl acetophenone was added to each solution in a vial. The materials are shown in Figures 9.1 and 9.2 . The solutions were UV-polymerized for 10 minutes each. The materials were then cut into shapes of 25mm Œ 4mm Œ 1mm. A TA Instruments dynamic mechanical analyzer (DMA) was used in tension mode to measure thermomechanical properties [33].

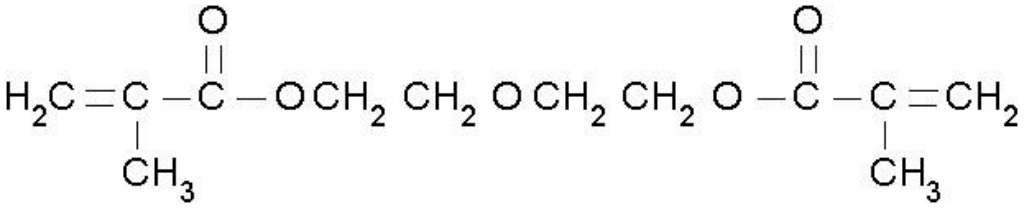

Figure 9.1: Structure of diethyelene glycol dimethacrylate (DEGDMA)

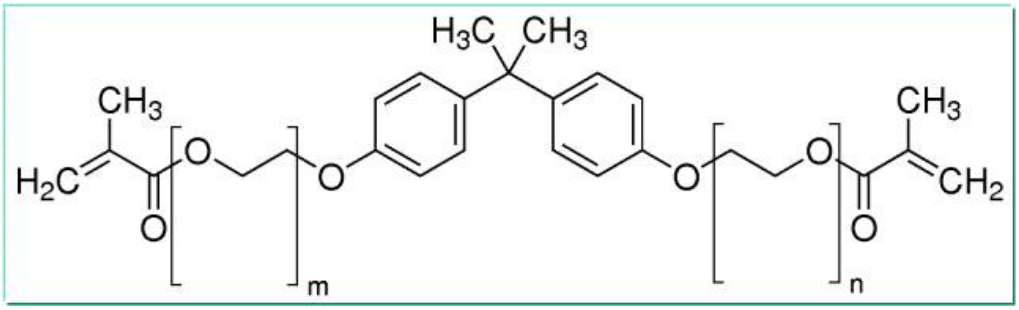

Figure 9.2: Structure of bisphenol A ethoxylate dimethacrylate

Three variables were selected to explore their effect on the following responses: film thickness, film uniformity, and nanomechanical properties (hardness and modulus). The input parameters were the spin speed, spin time, and nitrogen flow rate. Prior to the selection of these variables, full factorial experiments were conducted and these variables were significant, and thus worthy of further investigation. Previous research has shown that acrylate-based polymers are impossible to UV-polymerize in the presence of oxygen [25]. Therefore, nitrogen flow was considered in our investigation. Randomized screening experiments were performed with a full factorial design having two center points. Thus, the total number of experimental trials for screening was ten. The ranges of the parameters are shown in Table 3. The polymers were spin coated on diced wafers measuring approximately 2 cm square in the Microelectronics Research Center at the Georgia Institute of Technology. Spin coating was performed using a CEE coater. Curing of the films was accomplished using a SAMCO wafer stripper fitted with a nitrogen regulator.

Table 3: Process parameter and ranges for the materials

Parameter	Abbrev.	Ranges	Units
Spin Speed	SS	500-4000	rpm
Spin Time	ST	10-100	s
Nitrogen flow	N2flow	1-5	sccm

First, the optical parameters of the materials were characterized using the Woollam ellipsometer and curve fitting. The real (n) and imaginary (k) parts of the refractive index were extracted from the generated ellipsometric data. The refractive indices were provided to the Nanospec refractometer for thickness measurements. For each film, a minimum of ten individual measurements were performed to minimize measurement error. Analysis of variance (ANOVA) was used to investigate the significance of input parameters on the thickness and uniformity (Unif) of the films. The uniformity was defined as:

$$Unif = \frac{\sigma}{\mu} \tag{9.1}$$

where σ is the standard deviation of the film thickness, and the μ is the average thickness of a film. Modulus and hardness are important parameters for a material. These two parameters are essential to the reliability of the materials. Many studies have been conducted to probe these nanomechanical parameters [8] [32] [18] [34]. Nanoindentation was performed on the spin-coated films using the MTS Nanoindenter (MTS Systems). A minimum of 16 indents were performed on each sample. The modulus and hardness were calculated as described in [33] However, a Berkovich tip was not used for the measurements due to tip-substrate interaction effects that were observed during initial material testing (Figure 9.3). Instead, a spherical-conical tip was used to minimize these interactions. To further reduce substrate effects on the nanomechanical parameters, the maximum depth for each test was set at 10% of the thickness of each film [26]. Due to instrument limitations, the maximum depth was fixed at 2000 nm for the thicker films. The sensitivity was 40 %, and surface approach velocity 2.5 nm/s. The low surface approach velocity was used to reduce the kinetic effects of contact. The low surface velocity also helps to accurately determine the point of contact [31].

9.3 PROCESS MODELING USING NEURAL NETWORKS

Because of their learning capability, adaptability, and robustness, artificial neural networks are used to solve problems that have resisted solutions by other more traditional methods.

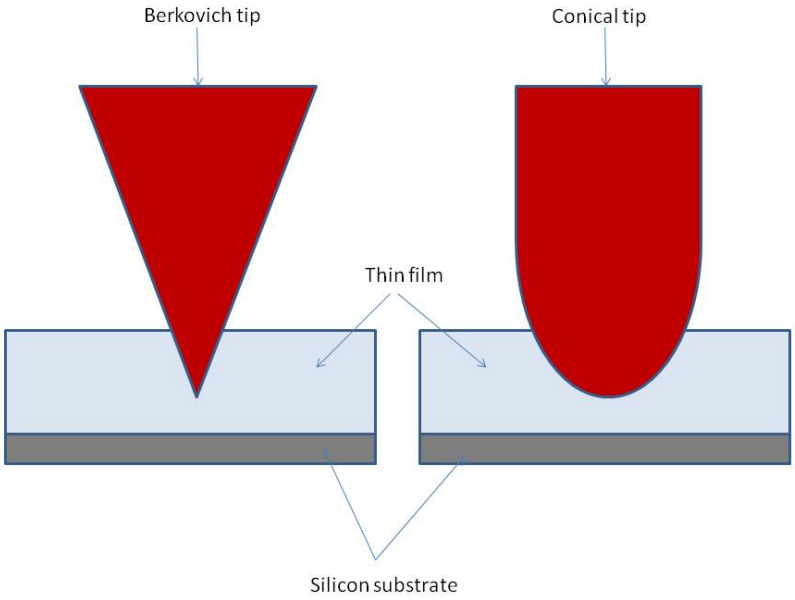

Figure 9.3: A schematic of the Berkovich tip and the conical tip. Due to the sharper end of the Berkovich, it penetrates the material to a greater depth. The likelihood of the tip touching the substrate is higher in the case of the Berkovich.

Neural networks are capable of performing highly complex mappings on noisy and/or nonlinear data, thereby inferring very subtle relationships between diverse sets of input and output parameters. Moreover, these networks can also generalize well enough to learn overall trends in functional relationships from limited training data [26]. There are several neural network architectures and training algorithms eligible for manufacturing applications. However, multilayer perceptron (MLP) networks employing the back-propagation (BP) algorithm are the most generally applicable and popular approach in semiconductor manufacturing. MLP neural networks trained by BP consist of layers of simple processing elements called "neurons". These processors are interconnected so that information relevant to input/output mappings is stored in the weight of the connections between them. Each neuron contains the weighted sum of its inputs filtered by a sigmoid transfer function. The layers of neurons in these networks receive, process, and transmit critical information about the relationships between the input parameters and corresponding responses. In addition to the input and output layers, these networks incorporate one or more "hidden" layers of neurons which do not interact with the outside world, but assist in performing nonlinear feature extraction

tasks on information provided by the input and output layers [31]. In the BP algorithm, the network begins with a random set of weights. An input vector is then presented and fed forward through the network, and the output is calculated by using this initial weight matrix. Next, the calculated output is compared to measured output data, and the squared difference between these vectors determines system error. The accumulated error for all of the input-output pairs is defined as the Euclidean distance in the weight space which the network attempts to minimize. Minimization is accomplished via the gradient descent approach, in which the network weights are adjusted in the direction of decreasing error. It has been demonstrated that if a sufficient number of hidden neurons are present, a three-layer BP network can encode any arbitrary input-output relationship [21]. In this research, the Object-Oriented Neural Network Simulator (ObOrNNS) [21], a platform-independent Java-based neural network software package developed by the Intelligent Semiconductor Group at Georgia Tech, was used for modeling. The data was partitioned into training and testing (validation) sets.

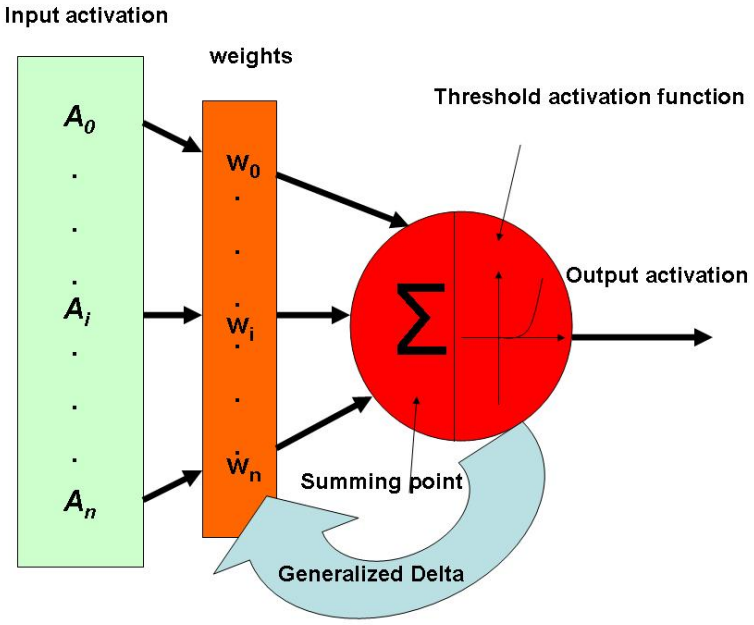

Figure 9.4: Schematic of the neuron.

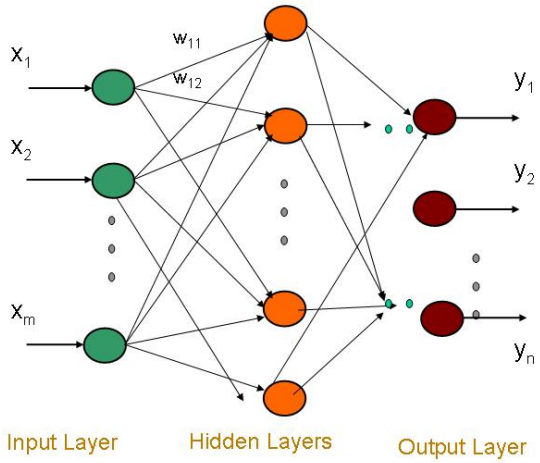

Figure 9.5: Multi-layer neural network, showing the input layer, hidden layer and output layers.

9.4 GENETIC ALGORITHMS

Neural networks are useful for defining the often complex relationships between controllable process conditions and measurable responses. However, in addition to the need to predict the output behavior of a given process given a set of input conditions, a need also exists to use such models to derive an optimum set a process conditions (or "recipe") to achieve desirable process targets. Genetic algorithms (GAs) represent computationally intelligent methods of optimizing a given process and define this reverse mapping. GAs are guided stochastic search techniques based on the principles of genetics [16, 21] [22]. Their operations are based on natural evolution for guiding their path through the search space: selection, crossover, and mutation. Using these operations, GAs search through large, irregularly shaped spaces quickly; requiring only objective function value to guide the global search. In computing terms, a GA maps a problem onto a set of binary strings. Each string represents a potential solution. Then, the GA manipulates the most promising strings in searching for improved solutions. The operation of a GA occurs in a simple four stage cycle of: 1) creation of a population of strings; 2) evaluation of each string; 3) selection of "best" strings; and 4)

genetic manipulation to create the new population of strings.

During each computational cycle, a new generation of possible solutions for a given problem is produced. At the first stage, an initial population of potential solutions is created as a starting point for the search process. Each element of the population is encoded into a string (the "chromosome"), to be manipulated by the genetic operators. In the next stage, the performance (or fitness) of each individual of the population is evaluated. Based on each individual string's fitness, a selection mechanism chooses "mates" for the genetic manipulation process. The selection policy is responsible for assuring survival of the fittest individuals [17]. Binary strings are typically used in coding genetic searches. Figure shows an example of a two-parameter coding with four bits in each parameter. The string manipulation process employs genetic operators to produce a new population of individuals ("offspring") by manipulating the genetic "code" possessed by members ("parents") of the current population. Selection is the process by which strings with high fitness values (i.e., good solutions to the optimization problem under consideration) receive larger numbers of copies in the new population. Once the strings have reproduced, they are stored in a "mating pool" awaiting the actions of crossover (Fig. 8.2) and mutation operations (8.3). The crossover operation takes two chromosomes and interchanges part of their genetic information to produce two new chromosomes. Mutation is implemented by randomly changing a fixed number of bits in every generation according to a specified mutation probability. Typical values for the probabilities of crossover and bit mutation range from 0.6 to 0.95 and 0.001 to 0.01, respectively [21].

9.5 RESULTS AND DISCUSSION

9.5.1 Process Modeling

Modeling was performed using BP neural networks to establish the relationship between process outputs (thickness and uniformity) and inputs (spin speed, spin time, and nitrogen flow). The data was separated into training (75%) and testing (25%) sets. The learning rate and momentum were varied until the training error decreased to less than 2%. On average, the testing error was less than 10%. Table 3 shows the input parameters and their settings

for DEGDMA deposition. Three dimensional response surface plots were then generated using MATLAB.

Figure 9.6 depicts film thickness with respect to spin speed and spin time when the nitrogen flow rate is fixed at its midrange value (3 sccm). It is evident from this figure that spin speed had the most prominent effect on the thickness of the films. The spin time also affected the thickness, but not as drastic as the spin speed. Uniformity variation is shown in Figure 9.7 for a nitrogen flow rate of 3 sccm. Once again, the spin speed shows a drastic effect on the uniformity. The spin time shows almost no effect on uniformity except for a small parabolic small decrease in uniformity in the middle portion of the time axis. Figure 9.8 illustrates the variation of the thickness with respect to the nitrogen flow rate and the spin speed at the midrange spin time of 55 s. Although the thickness decreases with increasing speed as expected, the nitrogen flow rate does not show any effect on the thickness. Figure 9.9 illustrates the uniformity variation on the film with respect to the nitrogen flow rate and the spin speed at the midpoint spin time of 55 s. Once again, the uniformity did not show any appreciable dependence on the spin time. Similar relationships between the input parameters and the outputs were exhibited by the bisphenol A ethoxylate dimethacrylate material as well. However, there exists a drastic effect of spin speed on the uniformity of the films. The inverse relationship between film thickness and spin speed has been explored by other researchers [30] [20]. Reduction in thickness as spin speed increases is attributed to centripetal forces that act on the solution resulting in the decreased thickness. Lima and Andrade studied poly(o-methoxyaniline) thin-films deposited by spin coating [20]. They observed a decrease in thickness as spin speed increased. At higher speeds, the solvent or photoresist undergoes Increasing spin speed also increases centripetal forces. Film uniformity was also studied by these researchers. A similar pattern of uniformity increasing with film thickness was observed. It is evident from the above figures that the spin speed and thickness follow a power-law relationship [2] [3] [6] [9]. There are several factors that comprise the curvature of the relationship. Viscosity, concentration of solution, material composition, glass transition temperature are a few material properties influencing the thickness and uniformity of thin films [9] [28] [12] [16].

The bisphenol ethoxylate, with its higher viscosity, has a considerably higher thickness than the DEGDMA at comparable spin speeds. One of the primary reasons is attributable to the higher viscosity of bisphenol ethoxylate. A high viscosity decreases the effect of the centripetal forces at a particular spin speed [30]. Likewise, the uniformity of the films exhibits a similar dependence on the input parameters.

Figures 9.12–9.15 show the variation of the nanomechanical properties (modulus and hardness) for the materials. It is clear from the figures that the modulus increases with increasing spin speed for both materials. The hardness follows a similar pattern. Since the thickness decreases with increasing spin speed, this implies that a thinner film has a higher modulus and hardness compared to a thicker film. This phenomenon has been observed by other researchers [26] [31]. Such an effect is due to substrate contributions to the nanomechanical parameters of the film [31]. Previous work has established that the modulus of bulk polymers is 3 GPa. Deviations from this value for thin films are attributed to substrate effects.

9.5.2 Genetic Algorithms for Process Optimization

The modeling results imply that a recipe can be selected for a tailored thickness and/or uniformity for a given application. For information storage using nanoindentation, a film surface devoid of imperfections (uniform) is required. Thus, these 3-D surfaces provide a baseline for the selection of process conditions for a particular application. Genetic algorithms were employed with parameters shown in Table 4. Figure 8.4 shows the link between the various stages of experimentation used in this research. The process begins with identifying the process set points [21] [16]. These set points are used for designing the experiments, modeling using neural networks, and optimization using genetic algorithms. For DEGDMA, verification runs were performed for thickness and uniformity for the set of parameters shown in Table 4. Table 5 shows a summary of the results obtained for applying the optimized recipe consisting of a spin speed of 4000 rpm, spin time of 100s, and a nitrogen flow rate of 1 sccm. Subsequent comparison between the experimental results and the results predicted by the

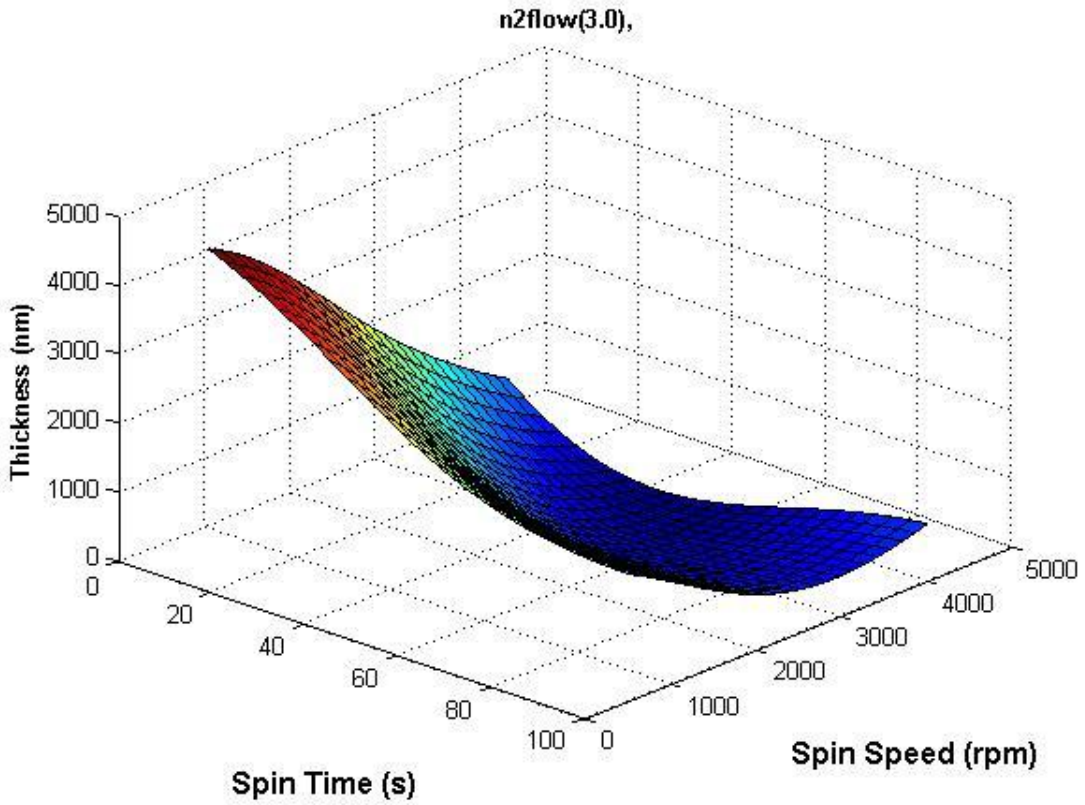

Figure 9.6: Film thickness with respect to spin speed and spin time when the nitrogen flow rate is fixed at its midpoint value of 3 sccm.

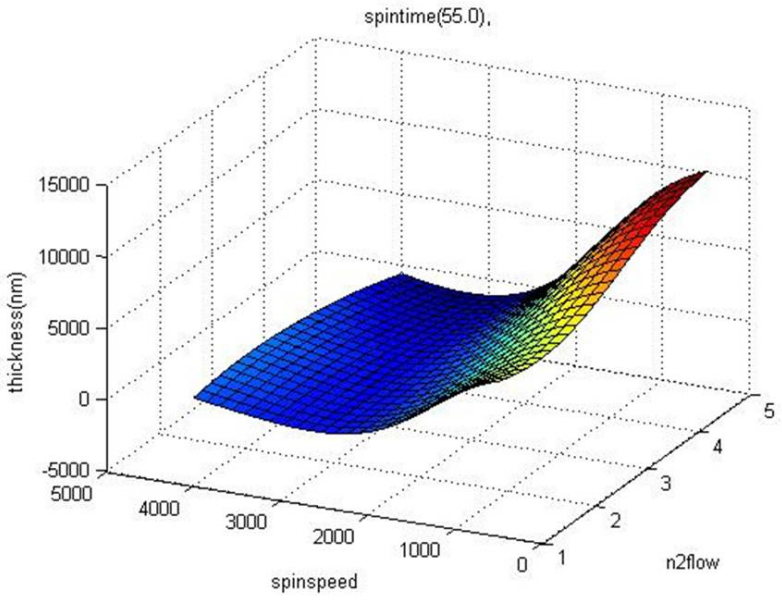

Figure 9.7: Nonuniformity for a nitrogen flow rate of 3 sccm.

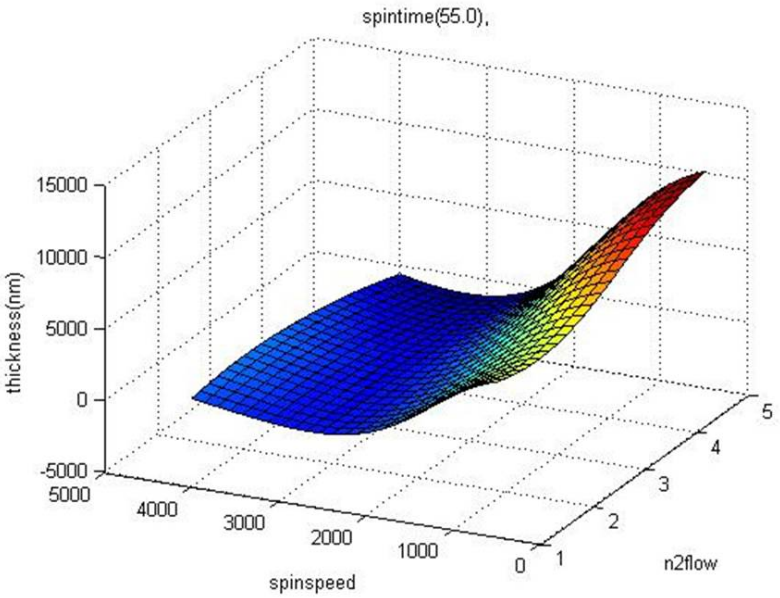

Figure 9.8: Thickness with respect to the nitrogen flow rate and the spin speed at the midpoint spin time of 55 s.

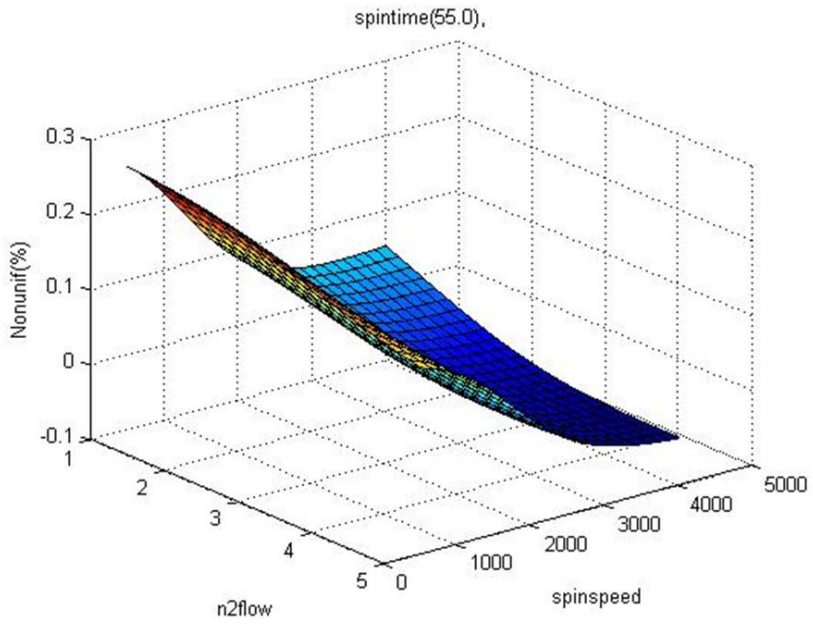

Figure 9.9: Nonuniformity for a spin time of 55 s.

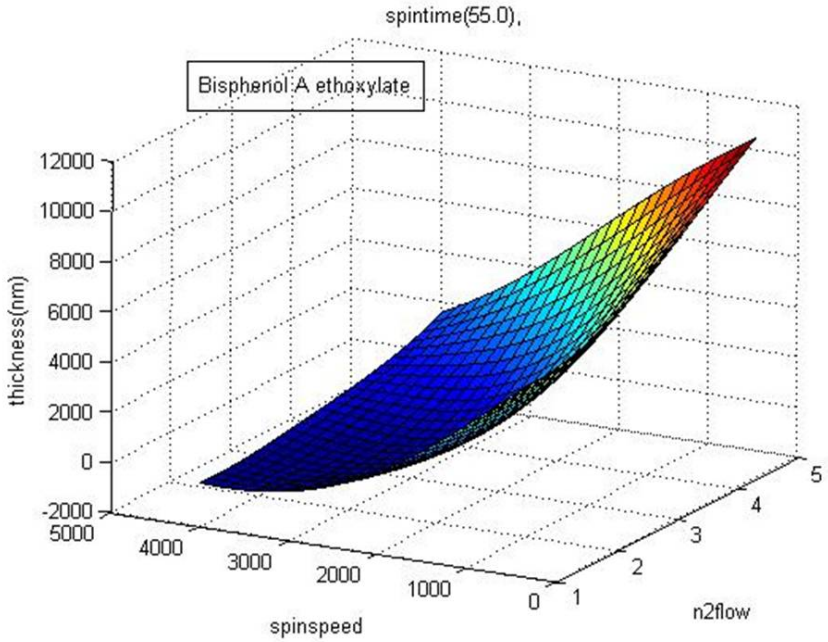

Figure 9.10: Relationship between the output film thickness, and the inputs spins peed and nitrogen flow rate at the midpoint of 55 s spin time.

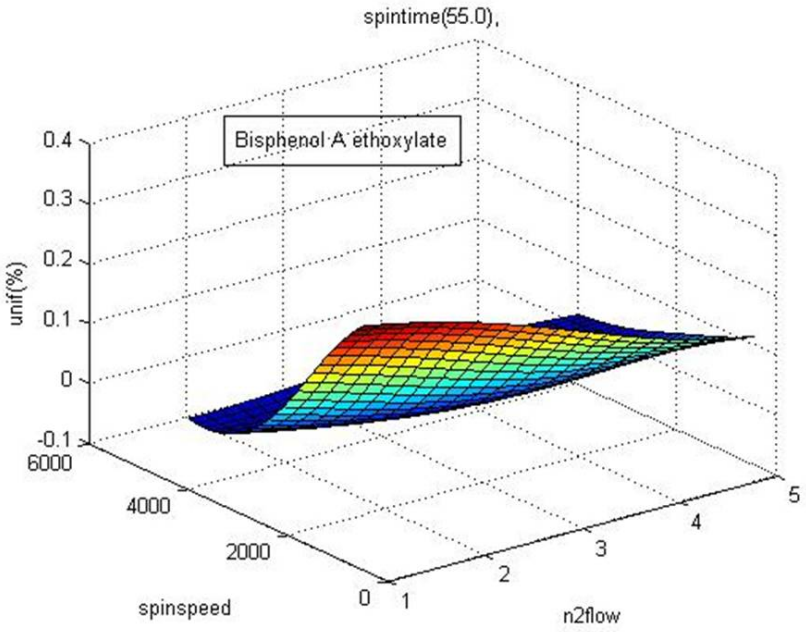

Figure 9.11: The effect of the input parameters spin speed and nitrogen flow on film uniformity of bisphenol A ethoxylate.

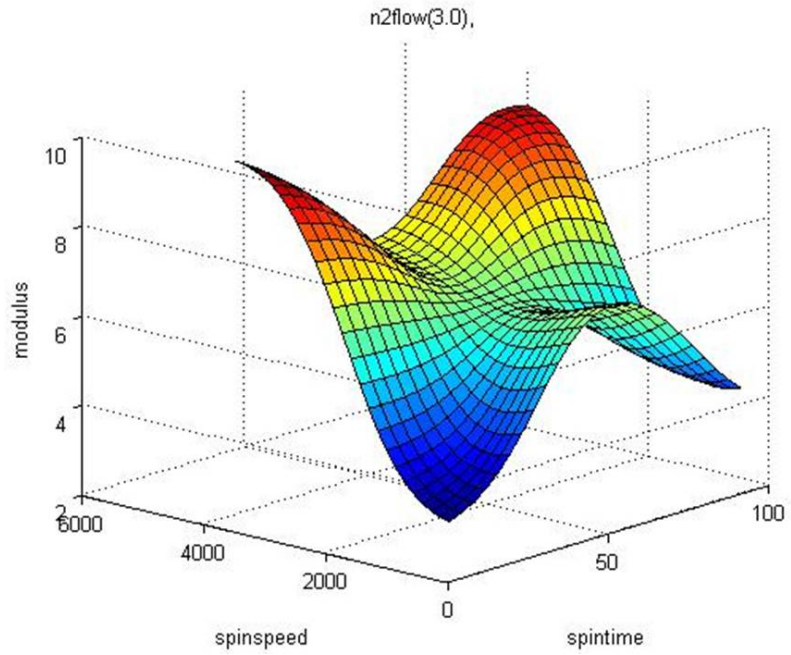

Figure 9.12: Modulus as a function of spin speed and spin time for DEGDMA. The nitrogen flow rate is held constant at the mid-value of 3 sccm.

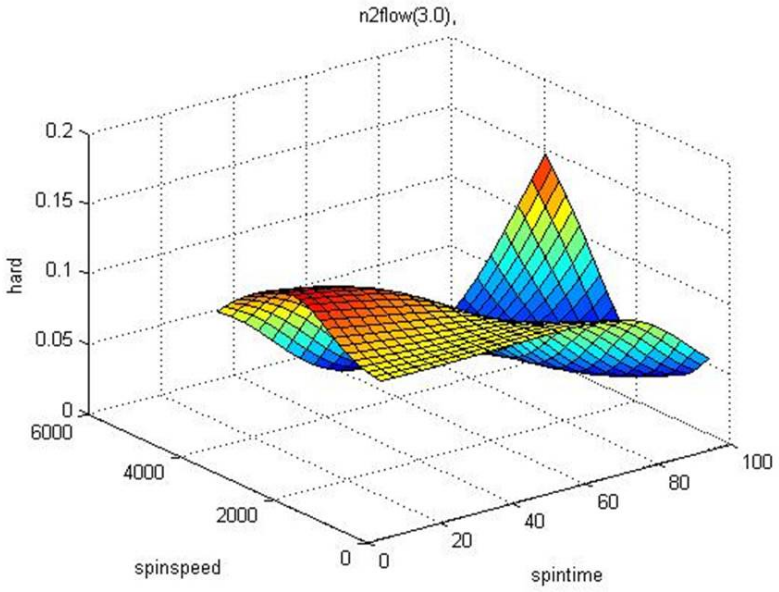

Figure 9.13: Hardness as a function of spin speed and spin time for DEGDMA. The nitrogen flow rate is held at the mid-value of 3 sccm.

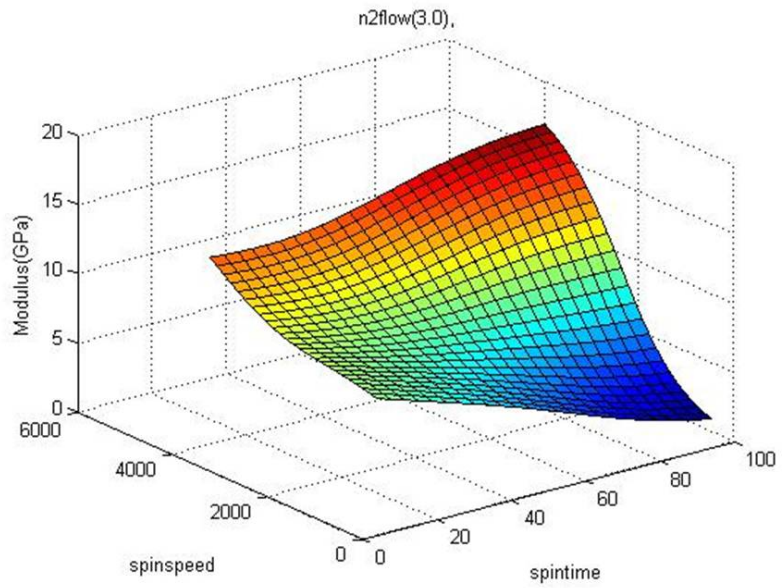

Figure 9.14: Modulus as a function of spin speed and spin time for bisphenol A. The nitrogen flow rate is held constant at 3sccm.

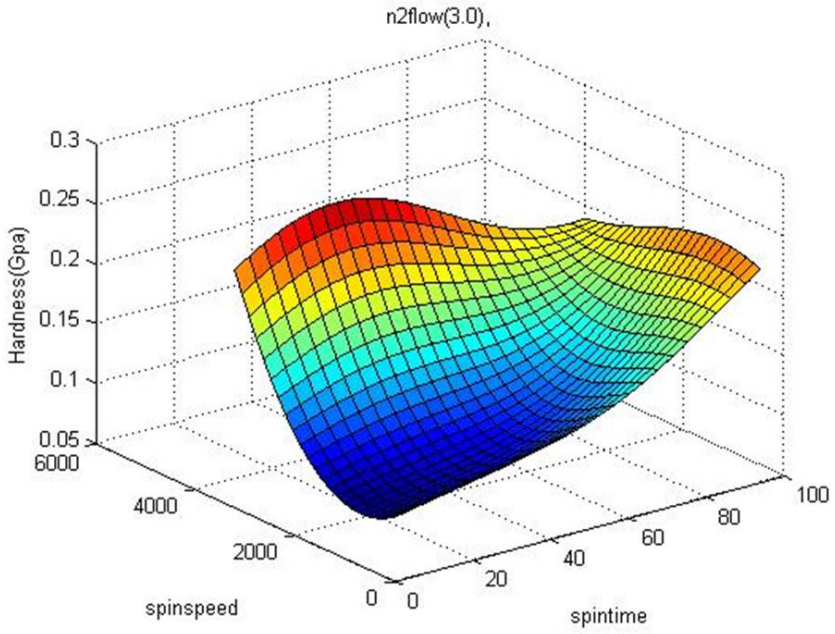

Figure 9.15: Hardness as a function of spin speed and spin time for DEGDMA. Thenitrogen flow rate is held at the mid-value of 3 sccm.

genetic algorithms yielded errors of approximately 2.9% for thickness and 5.4% for uniformity. The errors for DEGDMA modulus and hardness were 10% and 11%, respectively. A similar analysis was performed for bisphenol A ethoxylate but with the optimized recipe of 500 rpm, 100s, 3 sccm. For this material, thickness values were within 7.21%; uniformity was within 10.03%; and the modulus and hardness errors were 15.4% and 18.941%, respectively. One problem observed for the bisphenol was that there was buckling of the film. Future studies could investigate the use of adhesion aqgents such as hexamethyldisilazane (HMDS). Thus, the neuro-genetic approach provides a systematic methodology for modeling and optimizing processes. Neuro-genetic methods offer cost-saving alternatives and accuracy in manufacturing and process development [10] [11].

Table 4: Parameters of genetic algorithms used for DEGDMA

Parameter	**Value**
Population Size	100
Probability of Crossover	0.65
Probability of Mutation	0.01
Chromosome length	10
Maximum Generations	100
Weights	1

9.6 Summary

This section combined the neural network approach with genetic algorithms to model and optimize two polymers: diethylene glycol dimethacrylate and bisphenol A ethoxylate. Thickness, uniformity, modulus, and hardness were modeled, and optimum recipes were identified. Thickness and uniformity were strongly influenced by the spin speed for both materials. A similar pattern was evident for the modulus and hardness for both materials. Since these materials are finding applications in nanotechnology, this study will serve as a guide for the use of these materials at the nanoscale. Future research could use the neuro-genetic approach to optimize processing conditions for mixtures of these films. As nanotechnology and biotechnology converge, biocompability of these materials could be studied along with other input parameters.

The next chapter discusses results obtained in this research.

Table 5: Results of recipe synthesis for DEGDMA

	Recipe	4000 rpm	100 s	1 sccm	
		Thickness (nm)	**Non-Uniformity**	**Modulus (GPa)**	**Hardness (GPa)**
	Weight	1	1	1	100
	Target	200	0	3.5	0.1
Results	Simulated	203	0.3	10.2	0.16
	Actual	208.887	0.3162	11.45	0.18
Error		0.029	0.054	0.109	0.1111
%Error		2.9	5.4	10.90%	11.1

The next section discusses the contributions offered by this dissertation. It further projects future work that could be derived from this research.Projections are made for the use of the techniques and materials studied here for futuristic applications.

REFERENCES

[1] Bertmer, M., Buda, A., Blomenkamp-Hofges, I., Kelch, S., and Lendlein, A., "Biodegradable shape-memory polymer networks: characterization with solid-state nmr," *Macromolecules*, vol. 38, no. 9, pp. 3793–3799, 2005.

[2] Britten, J. and Thomas, I., "Non-newtonian flow effects during spin coating large-area optical coatings with colloidal suspensions," *Journal of Applied Physics*, vol. 71, no. 2, p. 972, 1992.

[3] Chen, B., "Investigation of the solvent-evaporation effect on spin coating of thin films," *Polymer Engineering and Science*, vol. 23, no. 7, pp. 399–403, 1983.

[4] Cleon, D. E. and May, G. S., "Neural network control of variable-frequency microwave processing of polymer dielectric curing," *IEEE Transactions on Electronic Packaging Manufacturing*, pp. 1521 – 334X, 2008. article.

[5] Dollarhide, R. L., Agah, A., and Minden, G. J., "Evolving controllers for autonomous robot search teams," *Artificial Life and Robotics*, vol. 5, no. 3, pp. 178–188, 2001.

[6] Flack, W., Soong, D., Bell, A., and Hess, D., "A mathematical model for spin coating of polymer resists," *Journal of Applied Physics*, vol. 56, p. 1199, 1984.

[7] Gall, K., Kreiner, P., Turner, D., and Hulse, M., "Shape-memory polymers for microelectromechanical systems," *Journal of Microelectromechanical Systems*, vol. 13, no. 3, pp. 472–483, 2004. <Go to ISI>://000221845700010.

[8] Gall, K., Yakacki, C. M., Liu, Y. P., Shandas, R., Willett, N., and Anseth, K. S., "Thermomechanics of the shape memory effect in polymers for biomedical applications," *Journal of Biomedical Materials Research Part A*, vol. 73A, no. 3, pp. 339–348, 2005. article.

[9] Hall, D., Underhill, P., and Torkelson, J., "Spin coating of thin and ultrathin polymer films," *POLYMER ENGINEERING AND SCIENCE*, vol. 38, no. 12, p. 2039, 1998.

[10] Han, S. S. and May, G. S., "Recipe synthesis for pecvd sio 2 films using neural-networks and genetic algorithms," *Electronic Components and Technology Conference, 1996. Proceedings., 46th*, pp. 855–860, 1996.

[11] Han, S. S. and May, G. S., "Using neural network process models to perform pecvd silicondioxide recipe synthesis via genetic algorithms," *Semiconductor Manufacturing, IEEE Transactions on*, vol. 10, no. 2, pp. 279–287, 1997.

[12] Hong, J., Kim, H., and Park, H., "The effect of sol viscosity on the sol–gel derived low density sio2 xerogel film for intermetal dielectric application," *Thin Solid Films*, vol. 332, no. 1-2, pp. 449–454, 1998.

[13] Kagami, Y., Gong, J. P., and Osada, Y., "Shape memory behaviors of crosslinked copolymers containing stearyl acrylate," *Macromolecular Rapid Communications*, vol. 17, no. 8, pp. 539–543, 1996. article.

[14] Kim, B. and May, G., "Reactive ion etch modeling using neural networks and simu-latedannealing," *Components, Packaging, and Manufacturing Technology, Part C, IEEE Transactions on [see also Components, Hybrids, and Manufacturing Technology, IEEE Transactions on]*, vol. 19, no. 1, pp. 3–8, 1996.

[15] Kim, T. S. and May, G. S., "Intelligent control of via formation by photosensitive bcb for mcm-l/d applications," *IEEE Transactions on Semiconductor Manufacturing*, vol. 9, no. 2, pp. 191–206, 1999.

[16] Kim, T. S. and May, G. S., "Intelligent control of via formation process in mcm-l/d substratesusing neural networks," *Advanced Packaging Materials: Processes, Properties and Interfaces, 1999. Proceedings. International Symposium on*, pp. 106–112, 1999.

[17] Kim, T. S. and May, G. S., "Optimization of via formation in photosensitive dielectric layersusing neural networks and genetic algorithms," *Electronics Packaging Manufacturing, IEEE Transactions on [see also Components, Packaging and Manufacturing Technology, Part C: Manufacturing, IEEE Transactions on]*, vol. 22, no. 2, pp. 128–136, 1999.

[18] Lee, B. S., Chun, B. C., Chung, Y. C., Sul, K. I., and Cho, J. W., "Structure and thermomechanical properties of polyurethane block copolymers with shape memory effect," *Macromolecules*, vol. 34, no. 18, pp. 6431–6437, 2001. article.

[19] LENDLEIN, A., SCHMIDT, A., SCHROETER, M., and LANGER, R., "Shape-memory polymer networks from oligo (-caprolactone) dimethacrylates," *Journal of Polymer Science: Part A: Polymer Chemistry*, vol. 43, pp. 1369–1381, 2005.

[20] Lima, J. and de Andrade, A., "Morphological analysis of poly (o-methoxyaniline) thin-films deposited by spin coating technique," *Journal of Materials Science: Materials in Electronics*, vol. 17, no. 8, pp. 593–596, 2006.

[21] May, G. S., "Intelligent sop manufacturing," *Advanced Packaging, IEEE Transactions on [see also Components, Packaging and Manufacturing Technology, Part B: Advanced Packaging, IEEE Transactions on]*, vol. 27, no. 2, pp. 426–437, 2004.

[22] May, G., "Manufacturing ics the neural way," *Spectrum, IEEE*, vol. 31, no. 9, pp. 47–51, 1994.

[23] Morana, B., de Sande, J., Rodríguez, A., Sangrador, J., Rodríguez, T., Avella, M., and Jiménez, J., "Optimization of the luminescence emission of si nanocrystals synthesized from non-stoichiometric si oxides using a central composite design of the deposition process," *Materials Science & Engineering B*, vol. 147, no. 2-3, pp. 195–199, 2008.

[24] Newnes, L., Mileham, T., and Doniavi, A., "A systems approach to semiconductor optimization," *Electronics Packaging Manufacturing, IEEE Transactions on [see also*

Components, Packaging and Manufacturing Technology, Part C: Manufacturing, IEEE Transactions on], vol. 24, no. 3, pp. 171–177, 2001.

[25] Painter, M. K., Erraguntla, M., Jr, G. L. H., and Beachkofski, B., "Using simulation, data mining, and knowledge discovery techniques for optimized aircraft engine fleet management," *Proceedings of the 37th conference on Winter simulation*, pp. 1253–1260, 2006.

[26] Saha, R. and Nix, W., "Effects of the substrate on the determination of thin film mechanical properties by nanoindentation," *Acta Materialia*, vol. 50, no. 1, pp. 23–38, 2002.

[27] Schmidt, A. M., "Electromagnetic activation of shape memory polymer networks containing magnetic nanoparticles," *MACROMOLECULAR RAPID COMMUNICATIONS*, vol. 27, no. 14, p. 1168, 2006.

[28] Spangler, L., Torkelson, J., and Royal, J., "Influence of solvent and molecular weight on thickness and surface topography of spin-coated polymer films," *Polymer Engineering and Science*, vol. 30, no. 11, pp. 644–653, 1990.

[29] Tao, X., *Smart Fibres, Fabrics and Clothing*. CRC Press, 2001.

[30] Vorotilov, K., Petrovsky, V., and Vasiljev, V., "Spin coating process of sol-gel silicate films deposition: Effect of spin speed and processing temperature," *Journal of Sol-Gel Science and Technology*, vol. 5, no. 3, pp. 173–183, 1995.

[31] Wang, J., Shi, F., Nieh, T., Zhao, B., Brongo, M., Qu, S., and Rosenmayer, T., "Thickness dependence of elastic modulus and hardness of on-wafer low-k ultrathin polytetrafluoroethylene films," *Scripta Materialia*, vol. 42, no. 7, pp. 687–694, 2000.

[32] Wornyo, E., Gall, K., and May, G. S., "Thickness and uniformity modeling of the deposition of shape memory polymers for information storage applications," *Advanced Semiconductor Manufacturing Conference, 2008. ASMC 2008. IEEE/SEMI*, pp. 85–89, 2008.

[33] Wornyo, E., Gall, K., Yang, F. Z., and King, W., "Nanoindentation of shape memory polymer networks," *Polymer*, vol. 48, no. 11, pp. 3213–3225, 2007. <Go to ISI>://000246934600021.

[34] Yang, F., Wornyo, E., Gall, K., and King, W. P., "Thermomechanical formation and recovery of nanoindents in a shape memory polymer studied using a heated tip.," *Scanning*, 2007.

CHAPTER X

CONCLUSION

10.1 Summary

This dissertation investigates properties of shape memory polymers for applications in nanotechnology. The materials investigated have applications in other areas as well. In order for these materials to be used for these applications, basic properties must bee clearly understood to avoid failure and increase reliability of the systems in which these materials are used. The dissertation stretches from the basic material investigation to the application of designed experimental schemes, neural networks and genetic algorithms to the optimization of these material systems. Important properties such as modulus and hardness are investigated into much detail. The origin and history of the problem is expounded in Chapter 1, with explanations of shape memory polymers, and characterization methods used in this research and general outline of the problem. Chapter 2 discusses characterization techniques used in this research. Chapter 3 addresses nanoindentation basics. Chapter 4 investigates nanoindentation of shape memory polymer networks. Chapter 5 covers nanoscale indent formation and recovery of shape memory polymer networks. Designed experiments and neural network analysis are described in Chapter 6 while neural network modeling is carried out in Chapter 7. Chapter 8 describes the theory of genetic optimization. Chapter 9 discusses experimental results obtained by using genetic algorithms. Conclusions and future work are discussed in Chapter 10. The results elucidated the potential for the use of these acrylate-based materials for applications in nanotechnology and nanoelectromechanical systems (NEMS).

10.2 Conclusions

The motivation for this research was the increasing reduction in scale of devices with the advent of nanotechnology. The status quo focused on the use of these materials at the microscale. Size reduction of devices to the nanoscale pose challenges that must be solved prior to any meaningful application of these materials. The approach in this research has

provided the nano-research environment with rudimentary understanding of these material systems for applications. The objectives of this research were:

1. Design of shape memory polymers based on diethylene glycol dimethacrylate (DEGDMA) crosslinker, and *tert*-butyl acrylate monomer (tBA).

2. Utilize dynamic mechanical analysis (DMA) to comprehend the thermomechanical properties of shape memory polymers based on DEGDMA and tBA.

3. Utilize nanoindentation to understand the nanoscale behavior of these SMPs, and explore the recovery of the polymers from a deformed state.

4. Study spin coating conditions on thin film quality with designed experiments.

5. Model and optimize spin coating conditions of these thin films using neural networks and genetic algorithms.

10.3 Contributions

The research in this dissertation investigated the basic small-scale properties of shape memory polymers based on acrylates with the aid of designed experiments, neural networks and genetic algorithms. The research has provided the fundamental, important properties of these materials. The properties investigated here also essential to other areas such as biomedical engineering, defense, and other related areas. The intellectual contributions of the research presented are as follows:

- designed and characterized novel shape memory polymers using dynamic mechanical analysis, nanoindentation and atomic force microscopy (AFM) at the nanoscale
- determined basic material properties of the polymers
- established benchmarks for using the polymers at small scales
- performed recovery of these polymers from an imposed stress
- optimized these polymers for information storage

- established relationship between bond length and shape recovery
- applied neural network and genetic algorithms to these materials

10.4 Future Work

The research performed in this thesis explored the fundamental research of applying shape memory polymers in nanosystems. It covered a few techniques for understanding the behavior of shape memory polymers at small scale. There exist many opportunities for further exploration of this class of materials for applications, not only in information storage, but in other areas biomedical, aerospace and defense applications. However, further research must be conducted to understand such areas such as the maximum number of cycles of writing, reading, erasing that these materials can endure. Tensile testing may be performed to understand this area. Material modeling techniques may also be used to explore the effect of adding functional groups to the polymers. If these polymers should be used in biological systems, research should also be performed on the toxicity and other biological properties of these polymers. Designed experiments, neural networks, and genetic optimization techniques can provide an effective and efficient method of investigating many input parameters on output factors. Future research can explore material properties using these techniques. Additives, such as nano-magnetic particles and high temperature inducing materials, may be added to these polymers to tailor their properties. Multi-parameter designs could be performed to examine the effect of these additives on shape memory and other properties of the materials. Information storage applications rely on both the medium of writing (the polymer) and the writing tool (the tip). Research in collaboration with tip makers could help extend the capacity of polymer storage media.

REFERENCES

[1] Akhgari, A., Afrasiabi Garekani, H., Sadeghi, F., and Azimaie, M., "Statistical optimization of indomethacin pellets coated with ph-dependent methacrylic polymers for possible colonic drug delivery," *International Journal of Pharmaceutics*, vol. 305, no. 1-2, pp. 22–30, 2005. article.

[2] Akhgari, A., Afrasiabi Garekani, H., Sadeghi, F., Azimaie, M., Al-Haik, M. S., Hussaini, M. Y., and Garmestani, H., "Prediction of nonlinear viscoelastic behavior of polymeric composites using an artificial neural network," *International Journal of Pharmaceutics*, vol. 22, no. 7, pp. 1367–1392, 2006. Prediction of nonlinear viscoelastic behavior of polymeric composites using an artificial neural network.

[3] Akita, S., Nakayama, Y., Mizooka, S., Takano, Y., Okawa, T., Miyatake, Y., Yamanaka, S., Tsuji, M., and Nosaka, T., "Nanotweezers consisting of carbon nanotubes operating in an atomic force microscope," *Applied Physics Letters*, vol. 79, pp. 1691–1691, 2001.

[4] Armstrong, W. D. and Lilholt, H., "The time dependant, super-viscoelastic behavior of niti shape memory alloy fiber reinforced polymer matrix composites," *Materials Science and Engineering B-Solid State Materials for Advanced Technology*, vol. 68, no. 3, pp. 149–155, 2000. The time dependant, super-viscoelastic behavior of NiTi shape memory alloy fiber reinforced polymer matrix composites.

[5] Ballandras, S., Calin, M., Zissi, S., Bertsch, A., Andre, J. C., Bourjault, A., and Hauden, D., "Miniaturized shape memory alloy actuators fabricated using microstereophotolithography," *Journal De Physique Iii*, vol. 6, no. 12, pp. 1759–1774, 1996. Miniaturized shape memory alloy actuators fabricated using microstereophotolithography.

[6] Bartels, L., Meyer, G., and Rieder, K. H., "Basic steps of lateral manipulation of single atoms and diatomic clusters with a scanning tunneling microscope tip," *Physical Review Letters*, vol. 79, no. 4, pp. 697–700, 1997.

[7] Beake, B. D., Chen, S., Hull, J. B., and Gao, F., "Nanoindentation behavior of clay/poly(ethylene oxide) nanocomposites," *Journal of Nanoscience and Nanotechnology*, vol. 2, no. 1, pp. 73–79, 2002. article.

[8] Benard, W. L., Kahn, H., Heuer, A. H., and Huff, M. A., "Thin-film shape-memory alloy actuated micropumps," *Journal of Microelectromechanical Systems*, vol. 7, no. 2, pp. 245–251, 1998. article.

[9] Berkowicz, B. D. and Peppas, N. A., "Characterization of surgical adhesives from uv-polymerized poly(peg dimethacrylate-co-2-hydroxyethyl methacrylate) copolymers," *Journal of Applied Polymer Science*, vol. 56, no. 6, pp. 715 –, 1995. article.

[10] Bertmer, M., Buda, A., Blomenkamp-Hofges, I., Kelch, S., and Lendlein, A., "Biodegradable shape-memory polymer networks: characterization with solid-state nmr," *Macromolecules*, vol. 38, no. 9, pp. 3793–3799, 2005.

[11] Bidaux, J. E., Bataillard, L., Manson, J. A., and Gotthardt, R., "Phase-transformation behavior of thin shape-memory alloy wires embedded in a polymer matrix composite," *Journal De Physique Iv*, vol. 3, no. C7, pp. 561–564, 1993. article Part 1.

[12] Bidaux, J. E., Yu, W. J., Gotthardt, R., and Manson, A. E., "Modeling of the martensitic-transformation in shape-memory alloy composites," *Journal De Physique Iv*, vol. 5, no. C2, pp. 543–548, 1995. article.

[13] Binnig, G., Quate, C. F., and Gerber, C., "Atomic force microscope," *Physical Review Letters*, vol. 56, no. 9, pp. 930–933, 1986.

[14] Binnig, G. K., "Atomic-force microscopy," *Physica Scripta*, vol. 19, pp. 53–54, 1987.

[15] Bowman, C. N., Carver, A. L., Kennett, S. N., Williams, M. M., and Peppas, N. A., "Polymers for information storage systems. iii. crosslinked structure of polydimethacrylates," *Polymer*, vol. 31, no. 1, pp. 135–9, 1990. article.

[16] Bowman, C. N. and Peppas, N. A., "Polymers for information storage systems. ii. polymerization kinetics for preparation of highly crosslinked polydimethacrylates," *Journal of Applied Polymer Science*, vol. 42, no. 7, pp. 2013–2018, 1991. article.

[17] Briscoe, B. J., Fiori, L., and Pelillo, E., "Nano-indentation of polymeric surfaces," *Journal of Physics D-Applied Physics*, vol. 31, no. 19, pp. 2395–2405, 1998. article.

[18] Britten, J. and Thomas, I., "Non-newtonian flow effects during spin coating large-area optical coatings with colloidal suspensions," *Journal of Applied Physics*, vol. 71, no. 2, p. 972, 1992.

[19] Brown, T. D. and May, G. S., "Hybrid neural network modeling of anion exchange at the interfaces of mixed anion iii-v heterostructures grown by molecular beam epitaxy," *Ieee Transactions on Semiconductor Manufacturing*, vol. 18, no. 4, pp. 614–621, 2005. article.

[20] Bushman, S., Edgar, T. F., and Trachtenberg, I., "Modeling of plasma etch systems using ordinary least squares, recurrent neural network, and projection to latent structure models," *Journal of the Electrochemical Society*, vol. 144, no. 4, pp. 1379–1389, 1997. article.

[21] Caffarel, J., Gibson, G. J., Harrison, J. P., Griffiths, C. J., and Drinnan, M. J., "Comparison of manual sleep staging with automated neural network-based analysis in clinical practice," *Medical & Biological Engineering & Computing*, vol. 44, no. 1-2, pp. 105–110, 2006. article.

[22] Cecchi, M., Smith, H., and Braun, D., "Method to optimize polymer film spin coating for polymer led displays," *Synthetic Metals*, vol. 121, no. 1-3, pp. 1715–1716, 2001. article.

[23] Chen, B., "Investigation of the solvent-evaporation effect on spin coating of thin films," *Polymer Engineering and Science*, vol. 23, no. 7, pp. 399–403, 1983.

[24] Cheung, E., Karagozler, M. E., Park, S., Kim, B., and Sitti, M., "A new endoscopic microcapsule robot using beetle inspired microfibrillar adhesives," *Proceedings, 2005 IEEE/ASME International Conference on Advanced Intelligent Mechatronics*, pp. 551 – 557, 2005. article.

[25] Chinoy, P. B., "Reactive ion etching of benzocyclobutene polymer films," *IEEE Transactions on Components, Packaging & Manufacturing Technology, Part C (Manufacturing)*, vol. 20, no. 3, pp. 199–206, 1997. article.

[26] Chou, S. Y., Krauss, P. R., and Renstrom, P. J., "Imprint of sub-25 nm vias and trenches in polymers," *Applied Physics Letters*, vol. 67, no. 21, pp. 3114–3116, 1995. article.

[27] Cleon, D. E. and May, G. S., "Neural network control of variable-frequency microwave processing of polymer dielectric curing," *IEEE Transactions on Electronic Packaging Manufacturing*, pp. 1521 – 334X, 2008. article.

[28] Clifford, C. A. and Seah, M. P., "Quantification issues in the identification of nanoscale regions of homopolymers using modulus measurement via afm nanoindentation," *Applied Surface Science*, vol. 252, no. 5, pp. 1915–1933, 2005. article.

[29] Davis, C., Hong, S., Setia, R., Pratap, R., Brown, T., Ku, B., Triplett, G., and May, G., "An object-oriented neural network simulator for semiconductor manufacturing applications," *IIIS 8 thAnnual Multi-Conf. Syst. Cybern. Inform*, vol. 5, pp. 365–370, 2004.

[30] Davis, C., Harry, J., Cupta, M., Joseph, P., Kohl, P., and May, G., "Neural network modeling of acid-catalyzed degradation of photosensitive polycarbonates," *Proceedings of the International Symposium and Exhibition on Advanced Packaging Materials Processes, Properties and Interfaces*, vol. 2007, pp. 115 –, 2007. article.

[31] Dollarhide, R. L., Agah, A., and Minden, G. J., "Evolving controllers for autonomous robot search teams," *Artificial Life and Robotics*, vol. 5, no. 3, pp. 178–188, 2001.

[32] Duncheon, C., "Robots will be of service with muscles, not motors," *Industrial Robot-an International Journal*, vol. 32, no. 6, pp. 452–455, 2005. article.

[33] Emoto, T., Akutagawa, M., Abeyratne, U. R., Nagashino, H., and Kinouchi, Y., "Tracking the states of a nonlinear and nonstationary system in the weight-space of artificial neural networks," *Medical & Biological Engineering & Computing*, vol. 44, no. 1-2, pp. 146–159, 2006. article.

[34] F. El Feninat, G. L. M. F. D. M., "Shape memory materials for biomedical applications," *Advanced Engineering Materials*, vol. 4, no. 3, pp. 91–104, 2002. article 10.1002/1527-2648(200203)4:3<91::AID-ADEM91>3.0.CO;2-B.

[35] Feng, G. and Ngan, A., "Creep and strain burst in indium and aluminium during nanoindentation," *Scripta Materialia*, vol. 45, no. 8, pp. 971–976, 2001.

[36] Feng, W., Brash, J. L., and Zhu, S., "Non-biofouling materials prepared by atom transfer radical polymerization grafting of 2-methacryloloxyethyl phosphorylcholine: Separate effects of graft density and chain length on protein repulsion," *Biomaterials*, vol. 27, no. 6, pp. 847–855, 2006. article.

[37] Fischer, H., Vogel, B., and Welle, A., "Applications of shape memory alloys in medical instruments," *Minimally Invasive Therapy & Allied Technologies*, vol. 13, no. 4, pp. 248–253, 2004. article.

[38] Flack, W., Soong, D., Bell, A., and Hess, D., "A mathematical model for spin coating of polymer resists," *Journal of Applied Physics*, vol. 56, p. 1199, 1984.

[39] Frear, D., "Materials issues in area-array microelectronic packaging," *JOM Journal of the Minerals, Metals and Materials Society*, vol. 51, no. 3, pp. 22–27, 1999.

[40] Gall, K., Kreiner, P., Turner, D., and Hulse, M., "Shape-memory polymers for microelectromechanical systems," *Journal of Microelectromechanical Systems*, vol. 13, no. 3, pp. 472–483, 2004. article.

[41] Gall, K., Kreiner, P., Turner, D., and Hulse, M., "Shape-memory polymers for microelectromechanical systems," *Microelectromechanical Systems, Journal of*, vol. 13, no. 3, pp. 472–483, 2004.

[42] Gall, K., Kreiner, P., Turner, D., and Hulse, M., "Shape-memory polymers for microelectromechanical systems," *Journal of Microelectromechanical Systems*, vol. 13, no. 3, pp. 472–483, 2004. <Go to ISI>://000221845700010.

[43] Gall, K., Yakacki, C. M., Liu, Y. P., Shandas, R., Willett, N., and Anseth, K. S., "Thermomechanics of the shape memory effect in polymers for biomedical applications," *Journal of Biomedical Materials Research Part A*, vol. 73A, no. 3, pp. 339–348, 2005. article.

[44] Gall, K., "Shape memory polymers for biomedical applications," *Advanced Materials and Processes*, vol. 163, no. 7, pp. 46 –, 2005. article Shape memory polymers;Biomedical applications;.

[45] Goto, H., Zhang, H. Q., and Yashima, E., "Chiral stimuli-responsive gels: Helicity induction in poly(phenylacetylene) gels bearing a carboxyl group with chiral amines," *Journal of the American Chemical Society*, vol. 125, no. 9, pp. 2516–2523, 2003. article.

[46] Gou, J., Liang, Z., and Wang, B., "Experimental design and optimization of dispersion process for single-walled carbon nanotube bucky paper," *International Journal of Nanoscience*, vol. 3, no. 3, pp. 293–307, 2004. article.

[47] Gregory, J. R. and Spearing, S. M., "Nanoindentation of neat and in situ polymers in polymer-matrix composites," *Composites Science and Technology*, pp. 595–607, 2005. article.

[48] Guerry, A., Gondran, C., and Miller, K., "Sidewall roughness measurement: a comparison of in- and off-line afm techniques," in *Proc. IEEE Conference and Workshop Advanced Semiconductor Manufacturing ASMC '04*, pp. 221–226, 4–6 May 2004.

[49] Hall, D., Underhill, P., and Torkelson, J., "Spin coating of thin and ultrathin polymer films," *POLYMER ENGINEERING AND SCIENCE*, vol. 38, no. 12, p. 2039, 1998.

[50] Ham-Su, R., Healey, J., Underhill, R., Farrell, S., Cheng, L., Hyatt, C., Rogge, R., and Gharghouri, M., "Fabrication of magnetic shape memory alloy/polymer composites," *Proceedings of SPIE*, vol. 5761, p. 490, 2005.

[51] Han, S. S., "Modeling and optimization of plasma-enhanced chemical vapor deposition using neural networks and genetic algorithms," 1996.

[52] Han, S. S. and May, G. S., "Recipe synthesis for pecvd sio 2 films using neural-networks and genetic algorithms," *Electronic Components and Technology Conference, 1996. Proceedings., 46th*, pp. 855–860, 1996.

[53] Han, S. S. and May, G. S., "Using neural network process models to perform pecvd silicondioxide recipe synthesis via genetic algorithms," *Semiconductor Manufacturing, IEEE Transactions on*, vol. 10, no. 2, pp. 279–287, 1997.

[54] HAN, S., CAI, L., ROHATGI, A., and MAY, G., "Optimizing the growth of pecvd silicon nitride films for solar cell applications using neural networks and genetic algorithms," *Intelligent Engineering Systems Through Artificial Neural Networks: Proceedings of the 1997 Artificial Neural Networks in Engineering Conference (Annie'97)*, 1996.

[55] Ho, E. and Marcolongo, M., "Effect of coupling agents on the local mechanical properties of bioactive dental composites by the nano-indentation technique," *Dental Materials*, vol. 21, no. 7, pp. 656–664, 2005. article.

[56] Hong, J., Kim, H., and Park, H., "The effect of sol viscosity on the sol–gel derived low density sio2 xerogel film for intermetal dielectric application," *Thin Solid Films*, vol. 332, no. 1-2, pp. 449–454, 1998.

[57] Kagami, Y., Gong, J. P., and Osada, Y., "Shape memory behaviors of crosslinked copolymers containing stearyl acrylate," *Macromolecular Rapid Communications*, vol. 17, no. 8, pp. 539–543, 1996. article.

[58] Kagami, Y., Gong, J. P., and Osada, Y., "Shape memory behaviors of crosslinked copolymers containing stearyl acrylate," *Macromolecular Rapid Communications*, vol. 17, no. 8, pp. 539–543, 1996. <Go to ISI>://A1996VB88200006.

[59] Kallrot, M., Edlund, U., and Albertsson, A. C., "Surface functionalization of degradable polymers by covalent grafting," *Biomaterials*, vol. 27, no. 9, pp. 1788–1796, 2006. article 05509548592 Compilation and indexing terms, Copyright 2005 Elsevier Engineering Information, Inc. 0142-9612 Covalent Solvent free Vapor-phase grafting.

[60] Kim, B., Bae, J., and Lee, B. T., "Modeling of silicon oxynitride etch microtrenching using genetic algorithm and neural network," *Microelectronic Engineering*, vol. 83, no. 3, pp. 513–519, 2006. article.

[61] Kim, B. and May, G., "Reactive ion etch modeling using neural networks and simulatedannealing," *Components, Packaging, and Manufacturing Technology, Part C,*

IEEE Transactions on [see also Components, Hybrids, and Manufacturing Technology, IEEE Transactions on], vol. 19, no. 1, pp. 3–8, 1996.

[62] Kim, T. S. and May, G. S., "Intelligent control of via formation by photosensitive bcb for mcm-l/d applications," *IEEE Transactions on Semiconductor Manufacturing*, vol. 9, no. 2, pp. 191–206, 1999.

[63] Kim, T. S. and May, G. S., "Intelligent control of via formation process in mcm-l/d substratesusing neural networks," *Advanced Packaging Materials: Processes, Properties and Interfaces, 1999. Proceedings. International Symposium on*, pp. 106–112, 1999.

[64] Kim, T. S. and May, G. S., "Optimization of via formation in photosensitive dielectric layersusing neural networks and genetic algorithms," *Electronics Packaging Manufacturing, IEEE Transactions on [see also Components, Packaging and Manufacturing Technology, Part C: Manufacturing, IEEE Transactions on]*, vol. 22, no. 2, pp. 128–136, 1999.

[65] Kowalski, S. M., Vining, G. G., Montgomery, D. C., and Borror, C. M., "Modifying a central composite design to model the process mean and variance when there are hard-to-change factors," *Journal of the Royal Statistical Society: Series C (Applied Statistics)*, vol. 55, no. 5, pp. p615 – 630, 2006. article.

[66] Kramar, A., Turk, S., and Vrecer, F., "Statistical optimisation of diclofenac sustained release pellets coated with polymethacrylic films," *International Journal of Pharmaceutics*, vol. 256, no. 1-2, pp. 43–52, 2003. article.

[67] Kumar, A. S., *Fundamentals of polymer engineering*. New York :: Marcel Dekker, 2003. book Plastics engineering ; 66 Plastics engineering (Marcel Dekker, Inc.) ; 66.

[68] Langer, R. and Tirrell, D. A., "Designing materials for biology and medicine," *Nature*, vol. 428, no. 6982, pp. 487–492, 2004. <Go to ISI>://000220540100031.

[69] Larraz, E., Elvira, C., and San Roman, J., "Design and properties of novel self-curing acrylic formulations for application in intervertebral disks restoration," *Biomacromolecules*, vol. 6, no. 4, pp. 2058 – 2066, 2005. article.

[70] Lee, B. S., Chun, B. C., Chung, Y. C., Sul, K. I., and Cho, J. W., "Structure and thermomechanical properties of polyurethane block copolymers with shape memory effect," *Macromolecules*, vol. 34, no. 18, pp. 6431–6437, 2001. article.

[71] Lendlein, A., Jiang, H., Junger, O., and Langer, R., "Light-induced shape-memory polymers," *Nature*, vol. 434, no. 7035, pp. 879–882, 2005.

[72] Lendlein, A., Jiang, H. Y., Junger, O., and Langer, R., "Light-induced shape-memory polymers," *Nature*, vol. 434, no. 7035, pp. 879–882, 2005. article.

[73] Lendlein, A., Jiang, H. Y., Junger, O., and Langer, R., "Light-induced shape-memory polymers," *Nature*, vol. 434, no. 7035, pp. 879–882, 2005. <Go to ISI>://000228327600036.

[74] Lendlein, A. and Kelch, S., "Degradable, multifunctional polymeric biomaterials with shape-memory," 2005.

[75] Lendlein, A. and Kelch, S., "Shape-memory polymers as stimuli-sensitive implant materials," *Clinical Hemorheology and Microcirculation*, vol. 32, no. 2, pp. 105–116, 2005. <Go to ISI>://000228104900004.

[76] LENDLEIN, A., SCHMIDT, A., SCHROETER, M., and LANGER, R., "Shape-memory polymer networks from oligo (-caprolactone) dimethacrylates," *Journal of Polymer Science: Part A: Polymer Chemistry*, vol. 43, pp. 1369–1381, 2005.

[77] Li, X. D. and Bhushan, B., "Micro/nanomechanical characterization of ceramic films for microdevices," *Thin Solid Films*, vol. 340, no. 1-2, pp. 210–217, 1999. article.

[78] Li, X. D. and Bhushan, B., "Micro/nanomechanical and tribological studies of bulk and thin-film materials used in magnetic recording heads," *Thin Solid Films*, vol. 398, pp. 313–319, 2001. article.

[79] Li, X. D., Bhushan, B., Takashima, K., Baek, C. W., and Kim, Y. K., "Mechanical characterization of micro/nanoscale structures for mems/nems applications using nanoindentation techniques," *Ultramicroscopy*, vol. 97, no. 1-4, pp. 481–494, 2003. article.

[80] Li, X. D. and Nardi, P., "Micro/nanomechanical characterization of a natural nanocomposite material - the shell of pectinidae," *Nanotechnology*, vol. 15, no. 1, pp. 211–217, 2004. article.

[81] Li, X. D., Zhang, L. M., and Gao, H. S., "Micro/nanomechanical characterization of a single decagonal alconi quasicrystal," *Journal of Physics D-Applied Physics*, vol. 37, no. 5, pp. 753–757, 2004. article.

[82] Lima, J. and de Andrade, A., "Morphological analysis of poly (o-methoxyaniline) thin-films deposited by spin coating technique," *Journal of Materials Science: Materials in Electronics*, vol. 17, no. 8, pp. 593–596, 2006.

[83] Liu, C., Qin, H., and Mather, P., "Review of progress in shape-memory polymers," *Journal of Materials Chemistry*, vol. 17, no. 16, pp. 1543–1558, 2007.

[84] Liu, Y. P., Gall, K., Dunn, M. L., Greenberg, A. R., and Diani, J., "Thermomechanics of shape memory polymers: Uniaxial experiments and constitutive modeling," *International Journal of Plasticity*, vol. 22, no. 2, pp. 279–313, 2006. article.

[85] Loubet, J. L., Georges, J. M., Marchesini, O., and Meille, G., "Vickers indentation curves of magnesium-oxide (mgo)," *Journal of Tribology-Transactions of the ASME*, vol. 106, no. 1, pp. 43–48, 1984. article.

[86] Lu, D., Liu, Z., Zhang, M., Wang, X., and Liu, Z., "Dextran-grafted-pnipaam as an artificial chaperone for protein refolding," *Biochemical Engineering Journal*, vol. 27, no. 3, pp. 336–343, 2006. article 05459460055 Compilation and indexing terms, Copyright 2005 Elsevier Engineering Information, Inc. 1369-703X Grafting ratio Cerium nitrate Protein aggregation.

[87] Madden, J. D. and Filipozzi, L., "Web-based actuator selection tool," *Proceedings of SPIE - The International Society for Optical Engineering*, vol. 5759, pp. 9 – 15, 2005. article Dielectric elastomers;Ferroelectric polymers;SMA;Carbon nanotube actuators;Liquid crystal elastomers;IPMC;.

[88] Maitland, D. J., Wilson, T., Schumann, D. L., and Baer, G., "Laser-activated shape memory polymer microactuators for treating stroke," *Lasers and Electro-Optics Society, 2002. LEOS 2002. The 15th Annual Meeting of the IEEE*, vol. 1, pp. 359–360 vol.1, 2002. article.

[89] Mallikarjuna, N. N. and Aminabhavi, T. M., "Versatile conjugated polymer actuators in biomedical applications," *Polymer News*, vol. 30, no. 6, pp. 195 – 196, 2005. article Electrical energy;Dielectric elastomers;Biomedical actuators;Nitinol;.

[90] May, G. S., "Intelligent sop manufacturing," *Advanced Packaging, IEEE Transactions on [see also Components, Packaging and Manufacturing Technology, Part B: Advanced Packaging, IEEE Transactions on]*, vol. 27, no. 2, pp. 426–437, 2004.

[91] May, G., "Manufacturing ics the neural way," *Spectrum, IEEE*, vol. 31, no. 9, pp. 47–51, 1994.

[92] Mertmann, M., "Non-medical applications of nitinol," *Minimally Invasive Therapy & Allied Technologies*, vol. 13, no. 4, pp. 254–260, 2004. article.

[93] Metzger, M. F., Wilson, T. S., Schumann, D., Matthews, D. L., and Maitland, D. J., "Mechanical properties of mechanical actuator for treating ischemic stroke," *Biomedical Microdevices*, vol. 4, no. 2, pp. 89–96, 2002. article.

[94] Mohr, R., Kratz, K., Weigel, T., Lucka-Gabor, M., Moneke, M., and Lendlein, A., "Initiation of shape-memory effect by inductive heating of magnetic nanoparticles in thermoplastic polymers," *PNAS*, vol. 103, no. 10, pp. 3540–3545, 2006. article.

[95] Morana, B., de Sande, J., Rodríguez, A., Sangrador, J., Rodríguez, T., Avella, M., and Jiménez, J., "Optimization of the luminescence emission of si nanocrystals synthesized from non-stoichiometric si oxides using a central composite design of the deposition process," *Materials Science & Engineering B*, vol. 147, no. 2-3, pp. 195–199, 2008.

[96] Morgan, N. B., "Medical shape memory alloy applications - the market and its products," *Materials Science and Engineering a-Structural Materials Properties Microstructure and Processing*, vol. 378, no. 1-2, pp. 16–23, 2004. article Sp. Iss. SI.

[97] Munasur, A., Pillay, V., Chetty, D., and Govender, T., "Statistical optimisation of the mucoadhesivity and characterisation of multipolymeric propranolol matrices for buccal therapy," *International Journal of Pharmaceutics*, vol. 323, no. 1-2, pp. 43–51, 2006.

[98] Myers, R. H., Montgomery, D. C., Vining, G. G., Borror, C. M., and Kowalski, S. M., "Response surface methodology: A retrospective and literature survey," *Journal of Quality Technology*, vol. 36, no. 1, pp. 53–77, 2004. article.

[99] Nelson, B. A., King, W. P., and Gall, K., "Shape recovery of nanoscale imprints in a thermoset "shape memory" polymer," *Applied Physics Letters*, vol. 86, no. 10, 2005. article 103108.

[100] Neubauer, G., Dass, M., and Johnson, T., "Imaging vlsi cross sections by atomic force microscopy," in *Proc. 30th Annual International Reliability Physics Symposium 1992*, pp. 299–303, 31 March–2 April 1992.

[101] Newnes, L., Mileham, T., and Doniavi, A., "A systems approach to semiconductor optimization," *Electronics Packaging Manufacturing, IEEE Transactions on [see also Components, Packaging and Manufacturing Technology, Part C: Manufacturing, IEEE Transactions on]*, vol. 24, no. 3, pp. 171–177, 2001.

[102] Ng, N. T., Lai, K. W., Quadir, G. A., Seetharamu, K. N., Abdul, I., and Zainal, Z. A., "Optimization of liquid cooling fins in microelectronic packaging," *Engineering Optimization*, vol. 35, no. 4, pp. 359–374, 2003. article.

[103] Ning, G. M., Su, J., Li, Y. Q., Wang, X. Y., Li, C. H., Yan, W. M., and Zheng, X. X., "Artificial neural network based model for cardiovascular risk stratification in hypertension," *Medical & Biological Engineering & Computing*, vol. 44, no. 3, pp. 202–208, 2006. article.

[104] Nishi, D., Arai, T., Inoue, K., and Takubo, T., "Measurement of the mechanical properties of living cell using micro hand and developed afm system," in *Proc. IEEE/RSJ International Conference on Intelligent Robots and Systems (IROS 2005)*, pp. 990–995, 2–6 Aug. 2005.

[105] Oliver, W. C. and Pharr, G. M., "An improved technique for determining hardness and elastic-modulus using load and displacement sensing indentation experiments," *Journal of Materials Research*, vol. 7, no. 6, pp. 1564–1583, 1992. article.

[106] Oyabu, N., Custance, ., Yi, I., Sugawara, Y., and Morita, S., "Mechanical vertical manipulation of selected single atoms by soft nanoindentation using near contact atomic force microscopy," *Physical Review Letters*, vol. 90, no. 17, pp. 176102–176102, 2003.

[107] Painter, M. K., Erraguntla, M., Jr, G. L. H., and Beachkofski, B., "Using simulation, data mining, and knowledge discovery techniques for optimized aircraft engine fleet management," *Proceedings of the 37th conference on Winter simulation*, pp. 1253–1260, 2006.

[108] Prange, S. J., Jahnke, A., and Klar, H., "Microelectronics for dynamic neural networks," *Annales Des Telecommunications-Annals of Telecommunications*, vol. 48, no. 7-8, pp. 368–377, 1993. article.

[109] Pratap, R. J., Lee, J. H., Pinel, S., May, G. S., Laskar, J., and Tentzeris, E. M., "Millimeter wave rf front end design using neuro-genetic algorithms," *Electronic Components and Technology, 2005. ECTC'05. Proceedings*, pp. 1802–1806.

[110] Pratap, R. J., Staiculescu, D., Pinel, S., Laskar, J., and May, G. S., "Modeling and sensitivity analysis of circuit parameters for flip-chip interconnects using neural networks," *IEEE Transactions on Advanced Packaging*, vol. 28, no. 1, pp. 71–78, 2005. article.

[111] Pratap, R. J., Sen, P., Davis, C. E., Mukhophdhyay, R., May, G. S., and Laskar, J., "Neurogenetic design centering," *IEEE Transactions on Semiconductor Manufacturing*, vol. 19, no. 2, pp. 173 – 181, 2006. article.

[112] Pulgarin, J. A. M., Bermejo, L. F. G., and Garcia, M. N. S., "Multivariate calibration applied to the time-resolved chemilumnescence for the simultaneous determination of morphine and its antagonist naloxone," *Analytica Chimica Acta*, vol. 602, no. 1, pp. 66–74, 2007. <Go to ISI>://000250629600008.

[113] Ragonese, R., Macka, M., Hughes, J., and Petocz, P., "The use of the box-behnken experimental design in the optimisation and robustness testing of a capillary electrophoresis method for the analysis of ethambutol hydrochloride in a pharmaceutical formulation," *Journal of Pharmaceutical and Biomedical Analysis*, vol. 27, no. 6, pp. 995–1007, 2002. article.

[114] Ram, A., *Fundamentals of polymer engineering.* New York :: Plenum Press, 1997. book.

[115] Raman, S. and Domeniconi, C., "Gene expression analysis of hiv-1 linked p24-specific cd4+ t-cell responses for identifying genetic markers," *Feature Selection for Data Mining*, 2005.

[116] Richardson, H., Sferrazza, M., and Keddie, J. L., "Influence of the glass transition on solvent loss from spin-cast glassy polymer thin films," *European Physical Journal E*, vol. 12, no. SUPPL 1, pp. 75 – 79, 2003. article Solvent loss;Energy barriers;Glassy thin films;.

[117] Robert, S. and Mure-Ravaud, A., "Control of the homogeneity of an optical grating by a neural characterization," *Optical Engineering*, vol. 44, no. 3, 2005. article 033601.

[118] Saha, R. and Nix, W., "Effects of the substrate on the determination of thin film mechanical properties by nanoindentation," *Acta Materialia*, vol. 50, no. 1, pp. 23–38, 2002.

[119] Schmidt, A. M., "Electromagnetic activation of shape memory polymer networks containing magnetic nanoparticles," *MACROMOLECULAR RAPID COMMUNICATIONS*, vol. 27, no. 14, p. 1168, 2006.

[120] Setia, R. and May, G. S., "Modeling and optimization of via formation in dielectrics by laser ablation using neural networks and genetic algorithms," *Electronics Packaging Manufacturing, IEEE Transactions on [see also Components, Packaging and Manufacturing Technology, Part C: Manufacturing, IEEE Transactions on]*, vol. 27, no. 2, pp. 133–144, 2004.

[121] Setia, R. and May, G. S., "Run-to-run failure detection and diagnosis using neural networks and dempster-shafer theory: an application to excimer laser ablation," *IEEE Transactions on Electronics Packaging Manufacturing*, vol. 29, no. 1, pp. 42–9, 2006. article.

[122] Setia, R. and May, G. S., "Run-to-run failure detection and diagnosis using neural networks and dempster???gshafer theory: An application to excimer laser ablation," *Electronics Packaging Manufacturing, IEEE Transactions on [see also Components, Packaging and Manufacturing Technology, Part C: Manufacturing, IEEE Transactions on]*, vol. 29, no. 1, pp. 42–49, 2006.

[123] Setia, R., May, G. S., Sundaram, V., and Tummala, R. R., "Sensitivity analysis and optimization of excimer laser ablation for microvia formation using neural networks and genetic algorithms," *Electronics Manufacturing Technology Symposium, 2004. IEEE/CPMT/SEMI 29th International*, pp. 131–139, 2004.

[124] Shaw, G., Trethewey, J., Johnson, A., Drugan, W., and Crone, W., "Thermomechanical high-density data storage in a metallic material via the shape-memory effect," *Advanced Materials*, vol. 17, no. 9, pp. 1123–1127, 2005.

[125] Shmulewitz, A., Langer, R., and Patton, J., "Convergence in biomedical technology," *Nature Biotechnology*, vol. 24, no. 3, pp. 277–280, 2006. article.

[126] Singh, B., Dahiya, M., Saharan, P., and Ahuja, N., "Optimizing drug delivery systems using systematic "design of experiments." - part ii: Retrospect and prospects," *Critical Reviews in Therapeutic Drug Carrier Systems*, vol. 22, no. 3, pp. 215–293, 2005. article.

[127] Small, W. I., Metzger, M. F., Wilson, T. S., and Maitland, D. J., "Laser-activated shape memory polymer microactuator for thrombus removal following ischemic stroke: preliminary in vitro analysis," *Selected Topics in Quantum Electronics, IEEE Journal of*, vol. 11, no. 4, pp. 892–901, 2005. article 1077-260X.

[128] Spangler, L., Torkelson, J., and Royal, J., "Influence of solvent and molecular weight on thickness and surface topography of spin-coated polymer films," *Polymer Engineering and Science*, vol. 30, no. 11, pp. 644–653, 1990.

[129] Tae Seon, K. and May, G. S., "Optimization of via formation in photosensitive dielectric layers using neural networks and genetic algorithms," *IEEE Transactions on Electronics Packaging Manufacturing*, vol. 22, no. 2, pp. 128–36, 1999. article.

[130] Tao, X., *Smart Fibres, Fabrics and Clothing*. CRC Press, 2001.

[131] Thongvigitmanee, T. and May, G. S., "Modeling and optimization of integral capacitor fabrication usingneural networks," *Electronics Manufacturing Technology Symposium, 2000. Twenty-Sixth IEEE/CPMT International*, pp. 47–54, 2000.

[132] Thongvigitmanee, T. and May, G. S., "Optimization of nanocomposite integral capacitor fabrication using neural networks and genetic algorithms," *Electronics Manufacturing Technology Symposium, 2002. IEMT 2002. 27th Annual IEEE/SEMI International*, pp. 123–129, 2002.

[133] Tobushi, H., Hashimoto, T., Ito, N., Hayashi, S., and Yamada, E., "Shape fixity and shape recovery in a film of shape memory polymer of polyurethane series," *Journal of Intelligent Material Systems and Structures*, vol. 9, no. 2, pp. 127–136, 1998. article.

[134] Tobushi, H., Ito, N., Takata, K., and Hayashi, S., "Thermomechanical constitutive modeling of polyurethane-series shape memory polymer," 2000.

[135] Tobushi, H., Shimada, D., Hayashi, S., and Endo, M., "Shape fixity and shape recovery of polyurethane shape-memory polymer foams," *Proceedings of the Institution of Mechanical Engineers Part L-Journal of Materials-Design and Applications*, vol. 217, no. L2, pp. 135–143, 2003. article.

[136] Toensmeier, P. A., "Shape memory polymers reshape product design," *Plastics Engineering*, pp. 10–11, 2005. article.

[137] Tryba, V. and Goser, K., "A modified algorithm for self-organizing maps based on the schrodinger-equation," *Lecture Notes in Computer Science*, vol. 540, pp. 33–47, 1991. article.

[138] Tryson, G. R. and Shultz, A. R., "A calorimetric study of acrylate photopolymerization," *Journal of Polymer Science: Polymer Physics Edition*, vol. 17, no. 12, pp. 2059–2075, 1979. General Electric Corporate Research and Development, Schenectady, New York 12345.

[139] Tseng, Y. S., Fu, H. H., Hung, T. C., and Pei, B. S., "An optimal parametric design to improve chip cooling," *Applied Thermal Engineering*, vol. 27, no. 11-12, pp. 1823–1831, 2007. <Go to ISI>://000247051700008.

[140] VanLandingham, M. R., Villarrubia, J. S., Guthrie, W. F., and Meyers, G. F., "Nanoindentation of polymers: An overview," *Macromolecular Symposia*, vol. 167, pp. 15–43, 2001. article.

[141] Vettiger, P., Cross, G., Despont, M., Drechsler, U., Durig, U., Gotsmann, B., Haberle, W., Lantz, M. A., Rothuizen, H. E., Stutz, R., and Binnig, G. K., "The "millipede" - nanotechnology entering data storage," *IEEE Transactions on Nanotechnology*, vol. 1, no. 1, pp. 39–55, 2002. article.

[142] Vorotilov, K., Petrovsky, V., and Vasiljev, V., "Spin coating process of sol-gel silicate films deposition: Effect of spin speed and processing temperature," *Journal of Sol-Gel Science and Technology*, vol. 5, no. 3, pp. 173–183, 1995.

[143] Wache, H. M., Tartakowska, D. J., Hentrich, A., and Wagner, M. H., "Development of a polymer stent with shape memory effect as a drug delivery system," *Journal of Materials Science: Materials in Medicine*, vol. 14, no. 2, pp. 109–112, 2003. article.

[144] Wang, J., Shi, F., Nieh, T., Zhao, B., Brongo, M., Qu, S., and Rosenmayer, T., "Thickness dependence of elastic modulus and hardness of on-wafer low-k ultrathin polytetrafluoroethylene films," *Scripta Materialia*, vol. 42, no. 7, pp. 687–694, 2000.

[145] Wei, B.-Y., Ho, S.-L., Chen, F.-Y., and Lin, H.-M., "Optimization of process parameters for preparing wo₃/polyacrylonitrile nanocomposites and the associated dispersion mechanism," *Surface and Coatings Technology*, vol. 166, no. 1, pp. 1–9, 2003. article.

[146] Wei, G. H., Bhushan, B., Ferrell, N., and Hansford, D., "Microfabrication and nanomechanical characterization of polymer microelectromechanical system for biological applications," *Journal of Vacuum Science and Technology A*, vol. 23, no. 4, pp. 811–819, 2005. article.

[147] Wei, G. H., Bhushan, B., and Torgerson, P. M., "Nanomechanical characterization of human hair using nanoindentation and sem," *Ultramicroscopy*, vol. 105, no. 1-4, pp. 248–266, 2005. article.

[148] Wei, Z. G., Sandstrom, R., and Miyazaki, S., "Shape memory materials and hybrid composites for smart systems - part ii shape-memory hybrid composites," *Journal of Materials Science*, vol. 33, no. 15, pp. 3763–3783, 1998. article.

[149] Wornyo, E., Gall, K., and May, G. S., "Thickness and uniformity modeling of the deposition of shape memory polymers for information storage applications," *Advanced Semiconductor Manufacturing Conference, 2008. ASMC 2008. IEEE/SEMI*, pp. 85–89, 2008.

[150] Wornyo, E., Gall, K., Yang, F. Z., and King, W., "Nanoindentation of shape memory polymer networks," *Polymer*, vol. 48, no. 11, pp. 3213–3225, 2007. <Go to ISI>://000246934600021.

[151] Wright-Charlesworth, D. D., Miller, D. M., Miskioglu, I., and King, J. A., "Nanoindentation of injection molded pla and self-reinforced composite pla after in vitro conditioning for three months," *Journal of Biomedical Materials Research Part A*, vol. 74A, no. 3, pp. 388–396, 2005. article.

[152] Xu, W. H., Xiao, Z. Y., and Zhang, T. Y., "Mechanical properties of silicone elastomer on temperature in biomaterial application," *Materials Letters*, vol. 59, no. 17, pp. 2153–2155, 2005. article.

[153] Yakacki, C., Lyons, M., Rech, B., Gall, K., and Shandas, R., "Cytotoxicity and thermomechanical behavior of biomedical shape-memory polymer networks cytotoxicity and thermomechanical behavior of biomedical shape-memory polymer networks post-sterilization," *Biomedical Materials*, vol. 3, p. 015010, 2008.

[154] Yang, F., Wornyo, E., Gall, K., and King, W. P., "Thermomechanical formation and recovery of nanoindents in a shape memory polymer studied using a heated tip.," *Scanning*, 2007.

[155] Yang, F., Wornyo, E., Gall, K., and King, W., "Nanoscale indent formation in shape memory polymers using a heated probe tip," *Nanotechnology*, vol. 18, no. 285302, p. 285302, 2007.

[156] Yang, L., Liu, W., Chen, W., Wang, Y., Cao, X., and Ren, X., "Electro-shape-memory effect in mn-doped (pb, sr) tio3 ceramics," *Materials Science & Engineering A*, vol. 438, pp. 176–180, 2006.

[157] Yang, Y. K., "Optimization of a photo resists coating process for photolithography in wafer manufacturing via design of experiments method," *Microelectronics International*, vol. 23, no. 3, pp. 26–32, 2006. <Go to ISI>://000239730700005.

[158] Yang, Y. K. and Chang, T. C., "Experimental analysis and optimization of a photo resist coating process for photolithography in wafer fabrication," *Microelectronics Journal*, vol. 37, no. 8, pp. 746–751, 2006. <Go to ISI>://000238920700014.

[159] Yu, S. Z., Wong, T. K. S., Hu, X., Wei, J., and Yong, M. S., "Structural, electrical and mechanical properties of templated silsesquioxane porous films," *Microelectronic Engineering*, vol. 77, no. 2, pp. 125–131, 2005. article.

[160] Yu, Y. L. and Ikeda, T., "Photodeformable polymers: A new kind of promising smart material for micro- and nano-applications," *Macromolecular Chemistry and Physics*, pp. 1705–1708, 2005. article.

[161] Yun, I. and May, G. S., "Passive circuit model parameter extraction using genetic algorithms," *Electronic Components and Technology Conference, 1999. 1999 Proceedings. 49th*, pp. 1021–1024, 1999.

[162] Zhang, S., Sun, D., Fu, Y. Q., and Du, H. J., "Recent advances of superhard nanocomposite coatings: a review," *Surface & Coatings Technology*, vol. 167, no. 2-3, pp. 113–119, 2003. article.

[163] Zuazagoitia, D., Millan, E., and Garcia, R., "A screening method for polycyclic aromatic hydrocarbons determination in water by headspace spme with gc-fid," *Chromatographia*, vol. 66, no. 9-10, pp. 773–777, 2007. <Go to ISI>://000251297300021.

INDEX

VITA

Edem Wornyo was born at Abor in the Volta Region of Ghana. He hails from Glikpome-Akatsi in Ghana. He attended Ohawu Roman Catholic Primary School, Akatsi No. 1 Junior Secondary School, and the Presbyterian Boys' Secondary School, Legon-Accra before proceeding to the Kwame Nkrumah University of Science and Technology, Kumasi. He pursued a degree in Electrical and Electronic Engineering leading to honors bachelors. He obtained a Master of Science (MS) in Electrical Engineering from the University of North Carolina at Charlotte. He then proceeded to the Georgia Institute of Technology for the PhD in Electrical and Computer Engineering. He has published and presented his research findings in many journals in Nanotechnology, Semiconductors, Telecommunications, and Developing Economies. He is a reviewer for many journals in the field. He has also filed patents on his research. He is a member of the Institute of Electrical and Electronic Engineers (IEEE); the Optical Society of America (OSA); and Eta Kappa Nu; the Electrical Engineering Honor Society. While at the Georgia Institute of Technology, he played an active leadership role in many organizations. He was elected the Graduate Senator representing Electrical and Computer Engineering in the Georgia Tech Student Government Association. He was also elected the Vice President of the GT Optical Society of America (OSA). He is a member of the Black Graduate Students Association (BGSA) and the African Students Association (ASA). He played a key role in the formation of the Georgia Tech Black Alumni Organization (GTBAO). He is one of the original founders of the GT Initiative and Education in Africa (GTIDEA). He has given many talks on technology and leadership, including a keynote address at the American Youth Foundation (AYF). He has received many awards and honors, including the IMPACT Scholarship for leadership and innovation.